Die approbierte Originalversion dieser Dissertation ist an der Hauptbibliothek der Technischen Universität Wien aufgestellt (http://www.ub.tuwien.ac.at).

The approved original version of this thesis is available at the main library of the Vienna University of Technology (http://www.ub.tuwien.ac.at/englweb/).

Geometric Contributions to Tolerance Analysis

Qinmin Yang

DISSERTATION

Geometric Contributions to Tolerance Analysis

ausgeführt zum Zwecke der Erlangung des akademischen Grades eines Doktors der technischen Wissenschaften/der Naturwissenschaften unter der Leitung von

(Betreuer): Johannes Wallner
Institut E104 für
Diskrete Mathematik und Geometrie

eingereicht an der Technischen Universität Wien,
Fakultät für Mathematik und Geoinformation

von

Qinmin Yang
Matrikelnummer 0327229
Wiedner Hauptstraße 8-10/104, A-1040 Wien

Wien, im Juli 2005

Zusammenfassung (German)

Gemetrische Toleranzanalyse befasst sich mit ungenau definierten geometrischen Objekten und den numerischen Problemen in diesem Kontext. „Geometrische Objekte“ können sein: Punkte, Gerade, Unterräume, Kurven, Flächen und so weiter. Wir betrachten geometrische Objekte, die nur ungenau gegeben sind – genauer solche, wo die Ungenauigkeit durch eine Menge spezifiziert wird, in der das Objekt liegen soll. Einer unserer Schwerpunkt liegt auf dem Rechnen mit solchen Mengen, die in diesem Zusammenhang *Toleranzzonen* heißen. Diese Dissertation bearbeitet zwei Themenkreise aus diesem Bereich.

Das erste Kapitel dieser Arbeit beschäftigt sich mit Punktwolken in der euklidischen Bewegungsgruppe, wobei eine solche Punktwolke die Toleranzzone einer Position eines starren Körpers beschreibt. Wir betrachten die Wirkung einer solchen Positions-Wolke auf starre Körper, das heißt, wir berechnen das Volumen, das von einem starren Körper überstrichen wird, wenn er alle Positionen aus der Wolke annimmt. Ein Spezialfall davon ist, daß die Wolke eine (diskrete) Kurve, also einen einparametrigen Bewegungsvorgang, repräsentiert. Hier beschäftigen wir uns mit Mengen von Positionen, deren Dimension gleich der Dimension der Bewegungsgruppe ist. Neben der Interpretation als Toleranzzone hat eine solche Punktwolke in der Bewegungsgruppe auch noch eine andere: Diese Positionen können durch Messungen oder Simulation gefunden worden sein. Wir analysieren geometrische Eigenschaften von solchen Mengen, und geben Algorithmen zum Bestimmen des überstrichenen Volumens an. Die Dimension des Problems, a priori gleich sechs, wird auf zwei reduziert. Diese Ergebnisse sind in [40] erschienen.

Das zweite Kapitel erforscht Beziehungen zwischen geometrischen Objekten im dreidimensionalen euklidischen Raum vom Standpunkt der Toleranzanalyse aus. Unsere Untersuchungen basieren auf einer Ungleichung aus [38], die den Linearisierungsfehler bei implizit gegebenen geometrischen Objekten betrifft. Durch das Sammeln von numerisch-experimentellen Daten und die Analyse von Grenzfällen untersuchen wir den Einfluss der Wahl des Koordinatensystems auf die Toleranzanalyse von quadratischen Bedingungen für die gegenseitige Lage von geometrischen Objekten. Wir untersuchen auch, wie eine geeignete Wahl von Koordinaten für geometrische Objekte die Abschätzung des Linearisierungsfehlers beeinflusst. Eine kurze Fassung dieser Arbeit findet sich in [39].

Contents

1 Swept volumes of many poses **8**

1.1 Introduction 8

§ 1.1.1 The continuous case and the discrete case 9

§ 1.1.2 The relation to tolerance analysis 10

§ 1.1.3 Applications: computing bounding volumes 10

§ 1.1.4 Overview 10

1.2 The Euclidean motion group 11

§ 1.2.1 Smooth motions and their velocities 11

§ 1.2.2 Velocities and the tangent spaces of SE_3 12

§ 1.2.3 The matrix exponential and logarithm 13

§ 1.2.4 Straightening SE_3 16

1.3 Tolerance zones 18

§ 1.3.1 Swept volumes 18

§ 1.3.2 Tangent spaces of tolerance zones 19

§ 1.3.3 Flattening tolerance zones in SE_3 19

§ 1.3.4 Envelopes 20

1.4 Point clouds and envelope computation 23

§ 1.4.1 Normal vectors of point clouds 23

§ 1.4.2 Normal vectors of pose clouds 23

§ 1.4.3 An elementary interpretation 25

§ 1.4.4 Making the result unique 26

1.5 Trimming and smoothing 27

§ 1.5.1 Smoothing 27

§ 1.5.2 Rounding off sharp edges 27

1.6 Numerical examples 29

§ 1.6.1 Pose clouds of varying smoothness 29

§ 1.6.2 Swept volumes of vibrating parts 31

1.7 Conclusion 32

2 Asymptotic analysis of implicit tolerance problems 36
2.1 Introduction 36
2.2 Preliminaries 37
§ 2.2.1 Linear and bilinear mappings: notation 37
§ 2.2.2 Taylor expansion of the constraints 38
§ 2.2.3 Computing norms of linear and bilinear mappings 38
§ 2.2.4 Norms of derivatives 39
2.3 Tolerance zones and implicit equations 39
§ 2.3.1 Local solutions 39
§ 2.3.2 Linearizing constraints 41
§ 2.3.3 Estimating the linearization error 41
§ 2.3.4 Balancing the constraint equations 44
2.4 Coordinates and relations 44
§ 2.4.1 Coordinates for geometric objects 45
§ 2.4.2 Relations between geometric objects 46
§ 2.4.3 Changing the coordinate system 46
2.5 Examples 47
§ 2.5.1 The pedal point in a plane 48
§ 2.5.2 The pedal point in a line 48
§ 2.5.3 The distance of skew lines 50
§ 2.5.4 The line spanned by two points 55
§ 2.5.5 The plane spanned by three points 59
§ 2.5.6 Intersection of line and plane 63
§ 2.5.7 Intersection of two planes 64
§ 2.5.8 Frameworks 67
§ 2.5.9 Two points determine a unit vector 69
2.6 Scalar coordinates 71
§ 2.6.1 S-coordinates of lines and planes 72
§ 2.6.2 Expressing geometric relations by S-coordinates 73
§ 2.6.3 Transformation of the scalar coordinate system 73
§ 2.6.4 Geometric constraint problems with S-coordinates 74

List of Figures

1.1 The difference between Boolean union (top) and envelope (bottom) in the case of a discrete 1-parameter motion. Differences are in the smoothness of the swept volume's boundary $\partial\mathscr{A}(X)$ and the computational cost. 9

1.2 Schematic illustration of a tolerance zone $\mathscr{A}$ in SE_3, poses (C,c) and $(E,0)$, and the matrix logarithm. 18

1.3 From left to right: The sets X, $\mathscr{A}'(X)$, and $\mathscr{A}''(X)$ for different non-smooth tolerance zones. The diameters of $\mathscr{A}'$ and $\mathscr{A}''$ are 0.2 and 0.5, respectively. 18

1.4 (a): Triangle mesh representing the boundary of an ellipsoid X. (b): The boundary of a swept volume $\mathscr{A}(X)$. 27

1.5 A vertex in the triangle mesh with its neighbours. 28

1.6 Adding edges with the purpose of rounding sharp edges. 29

1.7 Deleting vertices in rounding sharp edges. 30

1.8 rounding the sharp edges of a cube. (a) the original cube; (b) the cube after rounding sharp edges, where only a slight difference in shading is visible; (c) the offset surface of (b), where the vertices p_i with outward unit normal vector n_i are moved to $p_i + 2n_i$. 31

1.9 (a) A 3D model courtesy of Vienna University of Technology; (b)–(f) Swept volumes of the object corresponding to $\mathscr{A}_1,\ldots,\mathscr{A}_5$ of Section § 1.6.1, respectively. 32

1.10 (a) The Stanford dragon; (b)–(f) Swept volumes of the Stanford dragon corresponding to $\mathscr{A}_1,\ldots,\mathscr{A}_5$ of Section § 1.6.1, respectively. 33

1.11 (a) Car part courtesy AVL List GmbH. (b) Swept volume for a pose cloud representing vibration. (c) the mixture image of the original and the swept. (d)–(i) Part surface and the oriented envelope. Here trimming is necessary. 34

2.1 (a) Exact and (b) linearized tolerance zones. (c) Upper bound of linearization error. 41

2.2 The change of $C_{\max}$ over coordinate transformations in the constraint problem of Section § 2.5.1. (a) The pedal point in a plane. (b) Diagram of the change of $C_{\max}$ over the rotation angle ϕ while rotating the coordinate system. (c) the same for translating the coordinate system. (d) Logarithmic diagram of $\frac{C_{\max}}{s}$ over a scaling factor s. 49

2.3 (a) The pedal point in a line. (b)–(d) analogous to Figure 2.2, but for the constraint problem of Section § 2.5.2. 51

2.4 (a) A line passes through a fixed point and has fixed distance and angle to another line. (b)–(d) analogous to Figure 2.2, but for the constraint problem of Section § 2.5.3. 55

2.5 (a) A line spanned by two points. (b)–(d) analogous to Figure 2.2, but for the constraint problem of Section § 2.5.4. (e)–(g) analogous to (b)–(d) but with the second variant. 56

2.6 (a) A plane spanned by three points. (b)–(d) analogous to Figure 2.2, but for the constraint problem of Section § 2.5.5. 60

2.7 Detail of Figure 2.6.d (asymptotes). 60

2.8 (a) Intersection of a line and a plane. (b)–(d) analogous to Figure 2.2, but for the constraint problem of Section § 2.5.6. 64

2.9 (a) Intersection of two planes. (b)–(d) analogous to Figure 2.2, but for the constraint problem of Section § 2.5.7. 67

2.10 (a) A point has fixed distances from three fixed points. (b)–(d) analogous to Figure 2.2, but for the constraint problem of Section § 2.5.8. . 69

2.11 (a) An unit vector spanned by two points. (b)–(d) analogous to Figure 2.2, but for the constraint problem of Section § 2.5.9. 70

2.12 Detail of Figure 2.11.d (asymptotes). 71

2.13 The change of $C_{\max}$ over coordinate transformations in the constraint problem of Example § 2.6.4 in Section § 2.6.4. (a) Diagram of the change of $C_{\max}$ over the rotation angle ϕ while rotating the coordinate system. (b) the same for translating the coordinate system. (c) Logarithmic diagram of $\frac{C_{\max}}{s}$ over a scaling factor s. 76

2.14 (a)–(c) analogous to Figure 2.13, but for the constraint problem of Example § 2.6.4 in Section § 2.6.4. 77

2.15 (a)–(c) analogous to Figure 2.13, but for the constraint problem of Example § 2.6.4 in Section § 2.6.4. 78

Preface

Geometric tolerance analysis is concerned with imprecisely located geometric objects and the computational problems arising in this context. Here "geometric objects" may be points, lines, subspaces, curves, surfaces, and so on. We consider geometric objects which are given imprecisely, such that the amount of uncertainty is specified by a certain set (a *tolerance zone*) where the object is known to be contained in. We are interested in computations with such tolerance zones. This thesis collects work on two specific topics within the context of geometric tolerance analysis.

The first chapter considers a cloud of poses (i.e., positions of a rigid body in three-dimensional Euclidean space), which represents the tolerance zone of a pose. We consider the action of such a pose cloud on bodies in space. I.e., we investigate the volume swept by a body X if it assumes all positions represented by the cloud. A special case of this is a one-parameter motion of X, where the set of poses is curve-like. Here we consider a full- dimensional subset of the motion group. Beside the tolerance interpretation, there is also another one important for applications: The pose cloud may have been obtained by measurements or simulation. We analyze the geometric properties of such sets of poses and give algorithms for computing the swept volume. The dimension of the problem, which equals six a priori, is reduced to two. This work is published in [40].

The second chapter investigates relations between geometric objects in Euclidean $\mathbb{R}^3$ from the viewpoint of tolerance analysis. Our investigations are based on an inequality concerning the linearization error in geometric constraint solving which is given in [38]. By collecting numerical data and looking at limit cases we investigate the influence of the choice of coordinate system on analysis of a collection of quadratic constraint equations, which represent geometric problems in Euclidean space. We also investigate how modifying the coordinates used for geometric objects affect estimating the linearization error. A short version of this chapter is published in [39].

I would like to take this opportunity to express my gratitude to the supervisor of this thesis, Johannes Wallner, for his continuous support of my work. This thesis could not have been achieved without his ideas, suggestions and comments. I also want to thank all members of the Institute of Discrete Mathematics and Geometry of Vienna University of Technology. Especially I owe thanks to Stefan Leopoldseder, Shimin Hu, Hans-Peter Schröcker, Martin Peternell, Helmut Pottmann, Hellmuth Stachel, Yang

Liu, Hans Havlicek, Wolfgang Rath, Boris Odehnal, and last, but not least, Birgit Slama for their support during my stay in Vienna. I gratefully acknowledge the financial support by the Austrian Science Fund (FWF) under grant No. P15911 (*Geometric Set Operations for Tolerancing in Computer-Aided Design*), which made this research possible.

Vienna, July 2005 Qinmin Yang

Chapter 1

Swept volumes of many poses

1.1 Introduction

The volume swept by a moving rigid body is a topic of great interest and is extensively studied in the literature. We do not attempt to give an exhaustive list of references, but mention only [1] for an overview, [23] for computation, and [5] for some mathematical methods. The available literature deals mostly with one-parameter sweeps.

Speaking from a more general and abstract viewpoint, we could say that a rigid body X *moves* when it assumes any of a given set $\mathscr{A}$ of positions. We use *pose* as a synonym for position. The *swept volume* means the union of all positions $\alpha^i(X)$ of the rigid body X, as α^i runs through $\mathscr{A}$. We write $\mathscr{A}(X)$ for this swept volume.

An important special case of this concept is that X moves only by translations: The new position $\alpha(X)$ of the rigid body under consideration is the set $X+y$, where y is a translation vector taken from a set Y:

$$\mathscr{A}(X) = \{X+y \mid y \in Y\} = \{x+y \mid x \in X, y \in Y\} = X+Y. \tag{1.1}$$

We see that the swept volume coincides with the *Minkowski sum* $X+Y$ of the sets X and Y. Minkowski sums are an active area of research. The list of references given here [2, 9, 13, 20, 35, 15] is by no means exhaustive.

If $\mathscr{A}$ is a one-parameter set, either in the discrete or the continuous sense, then X undergoes a one-parameter motion, moving from one pose to the next. An example of a higher-dimensional motion is provided by the Minkowski sum case above, where X moves by translations: If Y has interior points, then it has dimension three, and X undergoes a three-dimensional motion, assuming a three-dimensional set of positions in space. We deal with a full-dimensional subset $\mathscr{A}$ of the Euclidean motion group, whose dimension equals six.

Such a set of poses can have the following two interpretations: One is that a pose α is imprecisely defined, and the amount of uncertainty is specified by a *tolerance zone* $\mathscr{A}$, which is a neighbourhood of α. The other interpretation is that X undergoes a

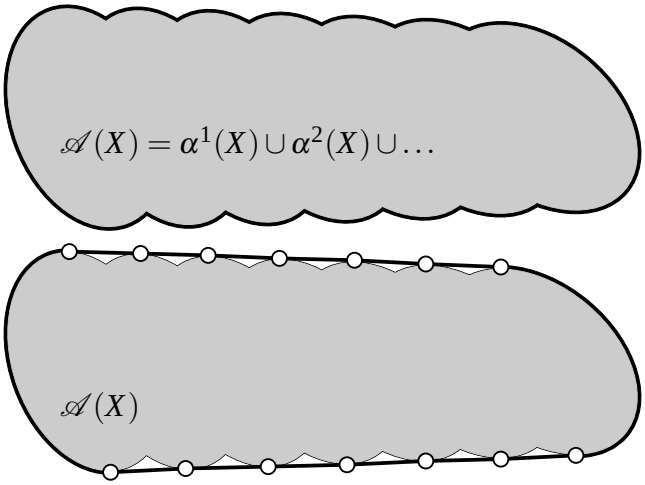

Figure 1.1: The difference between Boolean union (top) and envelope (bottom) in the case of a discrete 1-parameter motion. Differences are in the smoothness of the swept volume's boundary $\partial\mathscr{A}(X)$ and the computational cost.

small unstructured motion, and poses $\alpha^1, \alpha^2, \ldots$ have been obtained by measurements or simulation. This collection of poses then is a point cloud-like object (a *pose cloud*), whose shape is that of a 6-dimensional subset of the Euclidean motion group.

§ 1.1.1 The continuous case and the discrete case

There is a continuous version of the concepts mentioned above (rigid body, set of poses, swept volume), and also a discrete one. For computational purposes, the rigid body X is represented by its boundary as triangle mesh, and the set $\mathscr{A}$ of poses by a *pose cloud*. The swept volume will be given by a triangle mesh again. Computationally, there are two approaches to compute the swept volume, which for the 1-dimensional case are illustrated by Figure 1.1.

For given poses $\alpha^1, \alpha^2, \ldots$, we can compute the Boolean union $\alpha^1(X) \cup \alpha^2(X) \cup \ldots$. The result is an approximation (e.g., via a triangle mesh) of the volume $\mathscr{A}(X)$. As Figure 1.1 clearly shows, the smoothness of the volume computed in this way often does not adequately reproduce the smoothness of the volume $\mathscr{A}(X)$. Boolean union not only results in insufficient smoothness, also its computational cost is high. It is therefore often important to find candidates for the boundary points of $\mathscr{A}(X)$ without having to resort to Boolean set operations. Thus one is led to consider the *envelope* of a moving surface (the boundary of X) with respect to a smooth motion. This approach works well if both the body X and the set of poses $\mathscr{A}$ are at least piecewise smooth. This chapter approaches the computation of $\mathscr{A}(X)$ via envelopes.

§ 1.1.2 The relation to tolerance analysis

The concept of tolerance zone which represents an imprecisely defined object [33, 22, 21] has been used in a geometric context e.g. in [31] and [37], where geometric constructions occurring in Computer-Aided geometric design are analyzed from the tolerancing viewpoint. Tolerance zones for motions are studied in [34] from an abstract point of view. There is also related work on geometric transformations in the 2D case [10, 11, 12].

Within the tolerance analysis context, we solve the worst case tolerancing problem of computing a bounding volume for the position $\alpha(X)$ of a rigid body X, where the pose α is only known to be contained in some set $\mathscr{A}$. X itself may already be the tolerance zone of a point.

§ 1.1.3 Applications: computing bounding volumes

The sequential nature of time does not allow genuine multi-parameter motions to take place in the real world. However, there are situations where a rigid body executes a one-parameter motion of a complicated, chaotic, or unknown nature, and nevertheless one is interested in a bounding volume which contains all possible positions $\alpha(X)$.

In that case measurements or simulation may provide a collection of poses which more or less densely covers a certain subset $\mathscr{A}$ of the Euclidean motion group. The latter has dimension six, so the dimension of $\mathscr{A}$ can be any of $0,\ldots,6$. In this chapter we are not concerned with the issue of estimating that dimension. We consider the full-dimensional case and are aware of the fact that pose clouds can be "thin" and thus represent lower-dimensional shapes.

§ 1.1.4 Overview

We first present elementary Euclidean kinematics in Section 1.2: poses, velocities, and infinitesimal motions. Because we later need them for theoretical investigations, also the matrix exponential function and logarithm are introduced. Section 1.3 deals with tolerance zones $\mathscr{A}$ of poses, i.e., full-dimensional subsets of the Euclidean motion group, and with the question what happens if a rigid body X assumes all poses in $\mathscr{A}$. We consider the abstract question of outward normal vectors of tolerance zones and derive a theoretical result on the oriented envelope of a rigid body X with respect to $\mathscr{A}$. Section 1.4 deals with pose clouds, their support planes, and the actual computation of the swept volume, in part using the matrix logarithm. In Section § 1.4.3 we show how to avoid the matrix logarithm in computations. We further consider a smoothing process which takes the tolerancing side conditions into account. Numerical examples (Section 1.6) conclude this chapter. Most of the material presented here has been published in [40].

1.2 The Euclidean motion group

In Section 1.2 we present facts about kinematics and its relations to line geometry which can be found e.g. in [6] or [32].

The position of a rigid body X in 3-dimensional Euclidean space is given by an orthogonal matrix A and a translation vector a. We write $\alpha = (A,a) \in \mathbb{R}^{3\times 3+3}$ to indicate such a position. If X assumes position α, it is moved to $\alpha(X)$, which means that $x \in X$ is transformed to the point $y = Ax + a$. We do not consider orientation-reversing poses, so we forbid $\det A = -1$ and require $\det A = 1$. The Euclidean motion group is the set of such poses and denoted by SE_3:

$$\mathrm{SE}_3 = \{(A,a) \in \mathbb{R}^{3\times 3+3} \mid A^T A = E_3,\ \det A > 0\}. \tag{1.2}$$

It is a six-dimensional surface in the space $\mathbb{R}^{3\times 3+3}$ of matrix/vector pairs.

We further use the following property of skew-symmetric matrices: For any skew-symmetric 3 by 3 matrix V, there is a vector c such that $Vx = c \times x$ for all x. The corresponding notation is as follows:

$$c = (c_1,c_2,c_3),\ V = \begin{bmatrix} 0 & -c_3 & c_2 \\ c_3 & 0 & -c_1 \\ -c_2 & c_1 & 0 \end{bmatrix} \Longleftrightarrow \begin{cases} c = axis(V), \\ V = Skew(c). \end{cases} \tag{1.3}$$

§ 1.2.1 Smooth motions and their velocities

With the real parameter t as time, a smooth motion $\alpha(t) = (A(t),a(t))$ consists of a matrix-valued smooth function $A(t)$ and a vector-valued smooth function $a(t)$ such that $\alpha(t)$ is a pose in SE_3 for all t. The trajectory of the point x under this smooth motion is the curve $\alpha(t)\cdot x = A(t)x + a(t)$. The smooth motion itself can be seen as a curve lying in SE_3.

The velocity vector of the point x is the derivative

$$\dot\alpha(t)\cdot x = \frac{d}{dt}(A(t)x + a(t)) = \dot A(t)x + \dot a(t), \tag{1.4}$$

but we also employ the *velocity with respect to the coordinate system attached to X*. This means the velocity vector $v_t(x)$ such that $Av_t(x)$ equals the velocity vector of x:

$$v_t(x) = A(t)^{-1}\dot A(t)x + A(t)^{-1}\dot a(t). \tag{1.5}$$

Differentiating $A(t)^T A(t) = E_3$ with respect to the time t shows that $A(t)^T\dot A(t) + (A(t)^T\dot A(t))^T = 0$, so the matrix $A(t)^T\dot A(t)$, namely $A(t)^{-1}\dot A(t)$, is skew-symmetric, so we can define two vectors $d, \bar d$ by

$$v_t(x) = d(t)\times x + \bar d(t), \quad \text{where} \tag{1.6}$$

$$\bar d(t) = A(t)^{-1}\dot a(t),\ d(t) = axis(A(t)^{-1}\dot A(t)). \tag{1.7}$$

It is convenient to identify poses, their derivatives and the velocities with block matrices as follows:

$$\alpha(t) \equiv \begin{bmatrix} 1 & 0 \\ a(t) & A(t) \end{bmatrix}, \quad \dot{\alpha}(t) \equiv \begin{bmatrix} 0 & 0 \\ \dot{a}(t) & \dot{A}(t) \end{bmatrix}, \quad v_t \equiv \begin{bmatrix} 0 & 0 \\ \bar{d}(t) & Skew(d(t)) \end{bmatrix}. \tag{1.8}$$

Now that poses are matrices, we can multiply and invert them. It is elementary that $(A,a)\cdot(B,b) = (AB, Ab+a)$ and $(A,a)^{-1} = (A^{-1}, -A^{-1}a)$, with $A^{-1} = A^T$. Further, the vectors $d(t), \bar{d}(t)$ of (1.6) fulfill the relation

$$\begin{bmatrix} 0 & 0 \\ \bar{d}(t) & Skew(d(t)) \end{bmatrix} = \alpha(t)^{-1}\dot{\alpha}(t). \tag{1.9}$$

Observe that if α and $\dot{\alpha}$ are replaced by $\beta\alpha$ and $\beta\dot{\alpha}$ for any pose β, then

$$\begin{bmatrix} 0 & 0 \\ \bar{d}(t) & Skew(d(t)) \end{bmatrix} = (\beta\alpha)(t)^{-1}(\beta\dot{\alpha}(t)) = \alpha(t)^{-1}\dot{\alpha}(t). \tag{1.10}$$

Namely, the vectors $d, \bar{d}$ do not change in the operation of any pose.

§ 1.2.2 Velocities and the tangent spaces of SE_3

Any surface M has a tangent space in each of its points. It consists of the derivative vectors of curves in the surface which pass through that point. For the surface SE_3, points are poses, and curves are smooth motions. A time-dependent pose $\alpha(t)$, either seen as a matrix/vector pair, or as a block matrix in the sense of (1.8), has a derivative $\dot{\alpha}(t)$, which either is seen as a matrix/vector pair, or as a block matrix according to (1.8). As the derivative $\dot{\alpha} = (\dot{A}, \dot{a})$ assigns a velocity vector to points of $\mathbb{R}^3$, it is called an *infinitesimal motion* attached to the pose $\alpha = (A,a)$. For each pose $\alpha = (A,a)$, there is a six-dimensional space of infinitesimal motions

$$T_{(A,a)}\mathrm{SE}_3 = \{(\dot{A},\dot{a}) \in \mathbb{R}^{3\times 3+3} \mid (A^{-1}\dot{A})^T = -A^{-1}\dot{A}\} \tag{1.11}$$

attached to it. The space of infinitesimal motions attached to the identity pose $(E_3, 0)$ is denoted by

$$\mathrm{se}_3 = T_{(E_3,0)}\mathrm{SE}_3 = \{(\dot{A},\dot{a}) \in \mathbb{R}^{3\times 3+3} \mid \dot{A}^T = -\dot{A}\}. \tag{1.12}$$

We use the vectors $d, \bar{d}$ computed with (1.9) or (1.7) as coordinates for infinitesimal motions. According to (1.10), the six-dimensional abstract tangent space of SE_3 at any given pose is identified with se_3, as well as the space of $d, \bar{d}$'s.

Recall that a straight line parallel to the vector l which passes through the point x is assigned the Plücker coordinates $l, \bar{l}$ with $\bar{l} = x \times l$. These coordinates have the property that $\bar{l}$ does not depend on the choice of x on the line, and the line is recovered from the coordinates $l, \bar{l}$ as the solution set of the three linear equations $\bar{l} = x \times l$ in the variable

x. Any pair $l, \overline{l}$ with $\langle l, \overline{l} \rangle = 0$ and $l \neq 0$ occurs as Plücker coordinates of a line in Euclidean three-space.

If a body X in three-space has a smooth boundary, we can select a boundary point x and consider an outward normal vector n there. The line orthogonal to the boundary in the point x (the surface normal) has the Plücker coordinates $n, \overline{n}$ with $\overline{n} = x \times n$ according to the previous paragraph. Choose a pose $\alpha = (A, a)$. Then the outward normal vector of $\alpha(X)$ at the boundary point $Ax + a$ is given by An. We are interested in infinitesimal motions attached to the pose α which move x towards the inside of $\alpha(X)$.

The infinitesimal motion $\dot{\alpha}$ does not move x towards the outside of $\alpha(X)$, if and only if the velocity vector $\dot{\alpha} \cdot x$ of (1.4) does not point towards the outside of $\alpha(X)$. With the normal vector n, this relation is expressed by

$$\langle \dot{A}x + \dot{a}, An \rangle \leq 0. \tag{1.13}$$

When using coordinate vectors $d, \overline{d}$ for the infinitesimal motion, and the Plücker coordinates $n, \overline{n}$ for the surface normal, this is equivalent to

$$\langle d, \overline{n} \rangle + \langle \overline{d}, n \rangle \leq 0. \tag{1.14}$$

(as follows from $\langle \dot{A}x + \dot{a}, An \rangle = \langle A^{-1}\dot{A}x + A^{-1}a, n \rangle = \langle d \times x + \overline{d}, n \rangle$.)

Remark: The velocity vector of x is *tangent* to the boundary of $\alpha(X)$ if and only if $\langle d, \overline{n} \rangle + \langle \overline{d}, n \rangle = 0$ holds. This is the condition familiar from kinematics that the line with Plücker coordinates $n, \overline{n}$ is a path normal of the infinitesimal motion $\dot{\alpha}$.

§ 1.2.3 The matrix exponential and logarithm

The exponential function of a square matrix M is defined by the power series:

$$\exp(M) = \sum_{k \geq 0} \frac{M^k}{k!}. \tag{1.15}$$

The sum at the right hand side obviously converges, so $\exp(M)$ exists. There are two elementary properties of the matrix exponential:

1. If another square matrix N commutes with M, i.e., $MN = NM$, then $\exp(M + N) = \exp(M)\exp(N)$.
2. If t is a scalar, then $\exp(tM) = e^t \exp(M)$.

The exponential of matrix-valued curves have an interesting relation in the derivatives.

Proposition 1. *Let $M(t)$ be a matrix-valued curve such that $M(0) = 0$, then the matrix curve $\exp(M(t))$ has the same derivative as $M(t)$ at $t = 0$.*

Proof:

$$\frac{d}{dt}\exp(M(t))\Big|_{t=0} = \sum_{k\geq 0}\frac{d}{dt}\frac{(M(t))^k}{k!}\Big|_{t=0} = \frac{d}{dt}M(t)\Big|_{t=0}. \tag{1.16}$$

□

For computing $\exp(M)$, we compute $\sum_{k=0}^{s}\frac{M^k}{k!}$ instead, where s is big enough.

For measuring distortion we use the Frobenius norm of a matrix defined by $\|M\|^2 := \mathrm{tr}(M^TM)$. It is multiplicative in the sense that $\|M\cdot N\| \leq \|M\|\cdot\|N\|$ for all M and N. Then the computational error of the matrix exponential is

$$\begin{aligned}\left\|\sum_{k=s+1}^{\infty}\frac{M^k}{k!}\right\| &\leq \sum_{k=s+1}^{\infty}\frac{\|M\|^k}{k!} = \frac{\|M\|^{s+1}}{(s+1)!}\sum_{k=s+1}^{\infty}\frac{\|M\|^{k-s-1}}{(s+2)(s+3)\cdots k}\\ &\leq \frac{\|M\|^{s+1}}{(s+1)!}\sum_{j=0}^{\infty}\frac{\|M\|^j}{j!} = \frac{\|M\|^{s+1}}{(s+1)!}e^{\|M\|}.\end{aligned} \tag{1.17}$$

Thus we prefer the small magnitude of M. We have the following algorithm.

Algorithm 1. *Suppose that M is an n by n matrix and ε is a small positive value, we want to compute $R \approx \exp(M)$, such that $\|R-\exp(M)\| \leq \varepsilon$.*

1. *Let $R = N = E_n$, $k = 1$, compute $m = \|M\|$;*
2. *If $m \leq \frac{1}{2}$, let $a = m$, repeat $N = \frac{NM}{k}$, $a = \frac{am}{k+1}$, $R = R+N$ and $k = k+1$ until $ae^m < \varepsilon$.*
3. *If $m > \frac{1}{2}$, let $M = \frac{M}{2m}$ and $a = \frac{1}{2}$, repeat $N = \frac{NM}{k}$, $a = \frac{a}{2(k+1)}$, $R = R+N$ and $k = k+1$ until $ae^{\frac{4m+1}{2}} < \varepsilon$, let $R = e^{2m}R$.*

The matrix exponential provides a good mapping from se_3, as well as $\mathbb{R}^{3+3}$, to SE_3.

Proposition 2. *In the notation of* (1.8)*, the exponential of any infinitesimal motion in* se_3 *is a pose. Conversely, for any pose in* SE_3 *we can find an infinitesimal motion in* se_3 *whose exponential is the given pose.*

Proof: If $(V,\overline{v})$ is an infinitesimal motion in se_3, then $\begin{bmatrix}0 & 0\\ \overline{v} & V\end{bmatrix}^k = \begin{bmatrix}0 & 0\\ V^{k-1}\overline{v} & V^k\end{bmatrix}$ and the exponential

$$\exp\begin{bmatrix}0 & 0\\ \overline{v} & V\end{bmatrix} = \begin{bmatrix}1 & 0\\ \mathbf{f}(V)\overline{v} & \exp(V)\end{bmatrix}, \quad \text{where} \quad \mathbf{f}(V) = \sum_{k\geq 0}\frac{V^k}{(k+1)!}. \tag{1.18}$$

This is a pose, as

$$(\exp(V))^T\exp(V) = \exp(V^T)\exp(V) = \exp(-V)\exp(V) = \exp(0_{3\times 3}) = E_3$$

and $\det(\exp(V)) = 1$.
For the second part of the proof, we let

$$R = \begin{bmatrix} \cos\phi & -\sin\phi & 0 \\ \sin\phi & \cos\phi & 0 \\ 0 & 0 & 1 \end{bmatrix}, \quad q = \begin{bmatrix} 0 \\ 0 \\ p \end{bmatrix}, \quad Q = \begin{bmatrix} 0 & -\phi & 0 \\ \phi & 0 & 0 \\ 0 & 0 & 0 \end{bmatrix} \tag{1.19}$$

Through elementary computation, we know that $\exp(\begin{bmatrix} 0 & 0 \\ q & Q \end{bmatrix}) = \begin{bmatrix} 1 & 0 \\ q & R \end{bmatrix}$. For an arbitrary pose (A,a), we choose an appropriate Cartesian coordinate system $(b;b_1,b_2,b_3)$, a scalar p, and an angle $\phi \in (-\pi,\pi]$ such that (A,a) is exactly expressed as the pose (R,q) in the new coordinate system, i.e.,

$$\tilde{B}^{-1}\begin{bmatrix} 1 & 0 \\ a & A \end{bmatrix}\tilde{B} = \begin{bmatrix} 1 & 0 \\ q & R \end{bmatrix}, \qquad \text{where} \quad \tilde{B} = \begin{bmatrix} 1 & 0 \\ b & B \end{bmatrix}, \quad B = (b_1,b_2,b_3).$$

Then $\tilde{B}\begin{bmatrix} 0 & 0 \\ q & Q \end{bmatrix}\tilde{B}^{-1} = \begin{bmatrix} 0 & 0 \\ Bq - BQB^T b & BQB^T \end{bmatrix}$ and

$$\exp(\tilde{B}\begin{bmatrix} 0 & 0 \\ q & Q \end{bmatrix}\tilde{B}^{-1}) = \tilde{B}\exp(\begin{bmatrix} 0 & 0 \\ q & Q \end{bmatrix})\tilde{B}^{-1} = \tilde{B}\begin{bmatrix} 1 & 0 \\ q & R \end{bmatrix}\tilde{B}^{-1} = \begin{bmatrix} 1 & 0 \\ a & A \end{bmatrix}.$$

So, for an arbitrary pose (A,a) we have found an infinitesimal motion $(BQB^T, Bq - BQB^T b)$ in se_3 such that

$$\exp(\begin{bmatrix} 0 & 0 \\ Bq - BQB^T b & BQB^T \end{bmatrix}) = \begin{bmatrix} 1 & 0 \\ a & A \end{bmatrix}. \tag{1.20}$$

□

Especially the exponential of the zero infinitesimal motion is the identity pose. The matrix logarithm is the local inverse of the exponential such that $\log(E) = 0$. From the proof of Prop. 2 we get an algorithm to compute the logarithm of a pose.

Algorithm 2. *Suppose (A,a) is a pose, we look for* $\log(\begin{bmatrix} 1 & 0 \\ a & A \end{bmatrix})$.

1. *Compute a unit vector $b_3 \in \mathbb{R}^3$ such that $(A - I_3)b_3 = 0$;*
2. *Compute a unit vector $b_1 \in \mathbb{R}^3$ such that $(A^2 + (1 - \mathbf{tr}(A))A + I_3)b_1 = 0$;*
3. *$b_2 = b_3 \times b_1$; $p = \langle a, b_3 \rangle$;*
4. *Compute* $\sin t$ *and* $\cos t$ *in R from $R = B^T AB$ and determine the angle $t \in (-\pi,\pi]$ from the value of* $\sin t$ *and* $\cos t$*;*

5. *Compute a vector* $b \in \mathbb{R}^3$ *such that* $(A - I_3)b = pb_3 - a$;

6. $\log(\begin{bmatrix} 1 & 0 \\ a & A \end{bmatrix}) = \begin{bmatrix} 0 & 0 \\ Bq - BQB^T b & BQB^T \end{bmatrix}$.

"log" is only locally unique, just as the arcsine and arccos functions. Obviously "log" can be unambiguously defined in the neighbourhood of the identity defined by $-\pi < \phi \leq \pi$.

§ 1.2.4 Straightening SE_3

A parameterization of the surface SE_3 is given by the matrix exponential function: A pose depends on $(v, \overline{v}) \in \mathbb{R}^{3+3}$ via

$$\alpha(v, \overline{v}) = \exp \begin{bmatrix} 0 & 0 \\ \overline{v} & Skew(v) \end{bmatrix} = \begin{bmatrix} 1 & 0 \\ a(v, \overline{v}) & A(v, \overline{v}) \end{bmatrix}. \tag{1.21}$$

We use the notation $\alpha = \exp(v, \overline{v})$, $(v, \overline{v}) = \log \alpha$. For the actual computation "exp" and "log" see Algorithms 1 and 2. Moreover, according to (1.18), we can compute $\exp(v, \overline{v})$ by computing $\exp(V)$ and $\mathbf{f}(V)\overline{v}$ separately, where $V = Skew(v)$. From the definition of $\mathbf{f}$ in (1.18), we get

$$\mathbf{f}(M) = \frac{1}{2} \exp(\frac{M}{2}) \left[\mathbf{f}(\frac{M}{2}) + \mathbf{f}(-\frac{M}{2}) \right], \tag{1.22}$$

and when M is regular,

$$\mathbf{f}(M) = M^{-1}(\exp(M) - E). \tag{1.23}$$

So we have the following algorithm to compute $\mathbf{f}(M)$.

Algorithm 3. *Suppose that M is an n by n matrix and* ε *is a small positive value. We want to compute* $R \approx \mathbf{f}(M)$ *such that* $\|R - \mathbf{f}(M)\| \leq \varepsilon$.

1. *If* $\det(M) \neq 0$, *compute* $R = M^{-1}(\exp(M) - E)$.

2. *Otherwise, compute* $m = \|M\|$.

3. *If* $m < \frac{1}{2}$, *then let* $R = N = E_n$, $k = 2$, $a = \frac{m}{2}$; *repeat* $N = \frac{NM}{k}$, $a = \frac{am}{k+1}$, $R = R + N$ *and* $k = k + 1$ *until* $ae^m < \varepsilon$.

4. *Otherwise, compute*

$$R = \frac{1}{2} \exp(\frac{M}{2}) \left[\mathbf{f}(\frac{M}{2}) + \mathbf{f}(-\frac{M}{2}) \right].$$

It is well known that "exp" maps the domain defined by $\|v\| < \pi$ diffeomorphically onto the set of poses whose rotation angle is less than π.

Near the identity pose $(E,0)$, we have the approximate identity

$$\exp(v,\bar{v}) \approx (E + Skew(v),\bar{v}), \tag{1.24}$$

which is made more precise below by (1.28). This means that near the identity we may use $v,\bar{v}$ as coordinates for poses, and we may use the matrix logarithm (at least theoretically) for flattening SE_3 and analyzing small subsets of it.

The power series of the exponential function has the following easy estimate:

$$\|\exp(M) - (E_n + M)\| = \|\sum_{k\geq 2} \frac{M^k}{k!}\| \leq \sum_{k\geq 2} \frac{\|M\|^k}{k!} = g(\|M\|), \tag{1.25}$$

where $g(t) = e^t - 1 - t$. If $\alpha = (A,a)$ is a pose and $\dot{\beta}$ with coordinates $d,\bar{d}$ is an infinitesimal motion, the block matrices which represent α and β have the norms

$$\|\dot{\beta}\|^2 = \mathrm{tr}\left(\begin{bmatrix} 0 & \bar{d}^T \\ 0 & Skew(-d) \end{bmatrix}\begin{bmatrix} 0 & 0 \\ \bar{d} & Skew(d) \end{bmatrix}\right) = 2\|d\|^2 + \|\bar{d}\|^2, \tag{1.26}$$

$$\|\alpha\|^2 = \mathrm{tr}\left(\begin{bmatrix} 1 & a \\ 0 & A^T \end{bmatrix}\begin{bmatrix} 1 & 0 \\ a & A \end{bmatrix}\right) = 4 + \|a\|^2. \tag{1.27}$$

For the special case of block matrices for infinitesimal motions as in (1.8), (1.25) leads to the inequality

$$\|\exp(v,\bar{v}) - (E + Skew(v),\bar{v})\| \leq g(R), \tag{1.28}$$

where R is the norm of the infinitesimal motion with coordinates $v,\bar{v}$. Namely, $R^2 = 2\|v\|^2 + \|\bar{v}\|^2$. The function $g(t)$ has $g(0) = \dot{g}(0) = 0$, so the approximation is very good if both $v,\bar{v}$ are small. For bigger $v,\bar{v}$, this inequality gives only little information, because $g(t)$ grows rapidly.

The following well known property of the logarithm is an easy consequence of the previous inequality or Prop. :

Proposition 3. *If $\alpha(t)$ is a smooth one-parameter motion which passes through the identity pose $(E,0)$ for $t = 0$ and has the tangent vector (i.e., infinitesimal motion) with coordinates d,d there, then also the curve $\log\alpha(t)$ in $\mathbb{R}^6$ has the tangent vector $(d,\bar{d}) \in \mathbb{R}^6$ at $t = 0$.*

For straightening a piece of SE_3 around a pose α, we use

$$\log_\alpha(\beta) := \log(\alpha^{-1}\beta). \tag{1.29}$$

(1.29) is a way to represent poses near α by vectors in $\mathbb{R}^{3+3}$. A domain where $\log_\alpha$ can be unambiguously defined is e.g. the set of poses β where the rotation angle between α and β is less than π. The mapping $\log_\alpha$ is schematically illustrated by Figure 1.2.

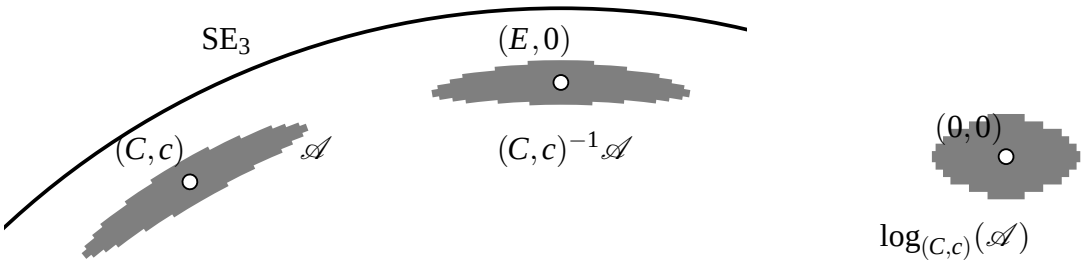

Figure 1.2: Schematic illustration of a tolerance zone $\mathscr{A}$ in SE_3, poses (C,c) and $(E,0)$, and the matrix logarithm.

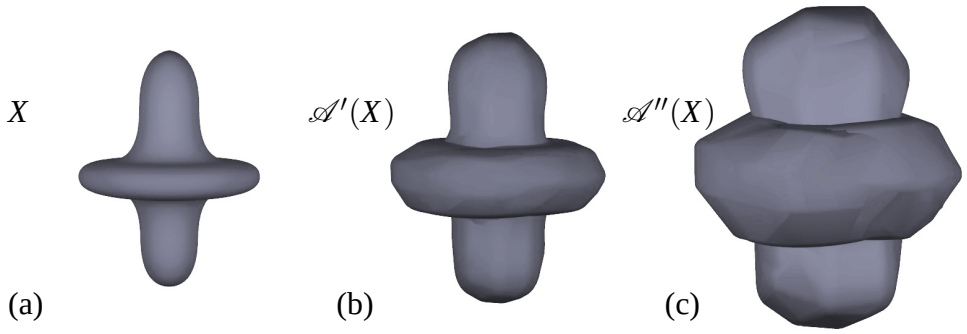

Figure 1.3: From left to right: The sets X, $\mathscr{A}'(X)$, and $\mathscr{A}''(X)$ for different non-smooth tolerance zones. The diameters of $\mathscr{A}'$ and $\mathscr{A}''$ are 0.2 and 0.5, respectively.

1.3 Tolerance zones

It is an aim of this chapter to deal with discrete "pose clouds". Like in the case of $\mathbb{R}^3$, where point clouds represent solids or surfaces, pose clouds represent six-dimensional solids in SE_3. We first have a look at the continuous case, i.e., the case of a domain with smooth boundary inside SE_3. Later we consider pose clouds which represent such solids.

Suppose that $\mathscr{A}$ is such a set of poses in SE_3. We assume that $\mathscr{A}$ is the closure of its interior (topological properties refer to the manifold SE_3, not to ambient space $\mathbb{R}^{3\times 3+3}$) and is compact. The diameter of $\mathscr{A}$ could be expressed in terms of the Frobenius norm.

§ 1.3.1 Swept volumes

The swept volume $\mathscr{A}(X)$ of a rigid body X which assumes every pose in the set $\mathscr{A}$ is defined as the union of all $\alpha(X)$ as α ranges in $\mathscr{A}$. Such volumes are illustrated in Figure 1.3. We are interested in the boundary $\partial\mathscr{A}(X)$. The following elementary statement, which is a first step in this direction, uses the boundaries ∂X and $\partial\mathscr{A}$ of the bodies X and $\mathscr{A}$.

Proposition 4. *For a point $x \in X$ and a pose $\alpha \in \mathscr{A}$, the point $\alpha \cdot x$ is contained in the boundary $\partial\mathscr{A}(X)$ of the swept volume only if x is a boundary point of X and the pose α is a boundary pose of $\mathscr{A}$.*

As has been remarked in the introduction, the computing of Minkowski sums could be seen as a special case of this chapter, if all motions are translations. Prop. 4 has a counterpart in the Minkowski sum context: If $x \in X$ and $y \in Y$, then $x+y$ is a boundary point of $X+Y$ only if both $x \in \partial X$ and $y \in \partial Y$.

Proof: (i) If x is not a boundary point of X, then neither is $\alpha \cdot x$ a boundary point of $\alpha(X)$. It follows that $\alpha \cdot x$ is no boundary point of $\mathscr{A}(X)$. (ii) If α is in $\mathscr{A}$, but not in the boundary, then small translations in all directions will change α such that it is still contained in $\mathscr{A}$. It follows that for any x, $\alpha \cdot x$ can still be translated in all directions without leaving $\alpha(X)$. Thus it is no boundary point of the swept volume. □

§ 1.3.2 Tangent spaces of tolerance zones

The boundary surface $\partial\mathscr{A}$ of the tolerance zone $\mathscr{A}$ has five-dimensional tangent spaces. The tangent space at the pose α is a subspace of the six-dimensional space of infinitesimal motions attached to α. Fortunately our introduction of coordinates $d, \bar{d}$ for infinitesimal motions by (1.6) identifies the space of infinitesimal motions attached to a pose α with the vector space $\mathbb{R}^{3+3}$ of pairs $d, \bar{d}$, so a five-dimensional subspace is determined by *one* linear relation between the six coordinates of $d, \bar{d}$: We are numbering the coordinates of $d, \bar{d}$ such that $d = (d_1, d_2, d_3)$ and $\bar{d} = (d_4, d_5, d_6)$. The *coefficients* in the linear relation are numbered in an unorthodox way:

$$n_4 d_1 + n_5 d_2 + n_6 d_3 + n_1 d_4 + n_2 d_5 + n_3 d_6 = 0. \tag{1.30}$$

We collect the coefficients n_i in two vectors $n, \bar{n}$ such that $n = (n_1, n_2, n_3)$ and $\bar{n} = (n_4, n_5, n_6)$. Then (1.30) reads

$$\langle \bar{n}, d \rangle + \langle n, \bar{d} \rangle = 0. \tag{1.31}$$

§ 1.3.3 Flattening tolerance zones in SE_3

The reason why we apply mappings like the logarithm to poses is that a vector space is a friendly environment with regard to computing tangent spaces and their linear equations. Moreover, the logarithm has the following nice property:

Proposition 5. *The equation of the boundary's tangent space is the same for α in $\mathscr{A}$ and for 0 in $\log_\alpha(\mathscr{A})$.*

Proof: The coordinates $d, \bar{d}$ for an infinitesimal motion $\dot{\beta}$ attached to α do not change if we multiply both $\dot{\beta}$ and α with the same pose from the left. Thus $\mathscr{A}$ has at α the same tangent space equation as $\mathscr{B} := \alpha^{-1} \cdot \mathscr{A}$ has at $\alpha^{-1} \cdot \alpha$.

By Prop. 3, taking the logarithm does not change the coordinates of tangent vectors. So if the identity pose happens to be a boundary pose of $\mathscr{B}$, then $\log_\alpha(\mathscr{A}) = \log(\mathscr{B})$ has in $(0,0)$ the same tangent vectors as $\mathscr{B}$ has in $(E,0)$. □

§ 1.3.4 Envelopes

§ 1.3.4 contains the main theoretical results of this chapter. We extend the concept of *normal vector pointing outwards* which is well known in the context of smoothly bounded solids to tolerance zones. We define the *oriented envelope* of a rigid body with respect to a tolerance zone and show that the boundary of the swept volume is contained in this envelope. By the passage to so-called *outer part*, equality is achieved. This is the basis of our algorithms given later — we compute the boundary of the swept volume via computing the oriented envelope.

The well known Minkowski sum case

If X and Y are bodies in $\mathbb{R}^3$ with a smooth boundary, then boundary points $x \in \partial X$ and $y \in \partial Y$ can contribute to a boundary point $x+y$ of the Minkowski sum $X+Y$ only if the tangent spaces of X at x and of Y at y are parallel. This is the so-called *envelope condition*. If it is possible to query Y for boundary points whose tangent plane has a given orientation, computation of the Minkowski sum's boundary is two-dimensional in nature: For a sample of boundary points $x^1, x^2, \ldots$ of X, we search for corresponding points in Y and thus get a surface-shaped collection of points. It is called the *envelope* of the boundary ∂X with respect to the translations defined by the boundary ∂Y. The actual boundary of $X+Y$ is contained in that surface. Another name for the envelope is *convolution surface* of the boundaries ∂X and ∂Y.

Without much effort it is possible to refine the envelope condition: Each boundary point of either X or Y is given a normal vector which points towards the outside. Then $x+y$ is a boundary point of $X+Y$ only if the outward normal vectors associated with the points x and y coincide. Again, for a sample $x^1, x^2, \ldots$ of boundary points in X we can query the boundary of Y for points $y^{i,j}$ such that x^i and $y^{i,j}$ has the same normal vector. The boundary of the Minkowski sum is contained in the *oriented envelope* of X with respect to Y, which is the surface which contains all sums $x^i + y^{i,j}$. The envelope usually is twice as big as the oriented envelope.

It is the purpose of the following sections to generalize these concepts to sets of poses.

Outward normal vectors

In general, the vector n is an *outward normal vector* of a solid in a boundary point, if for all vectors v which do *not* point toward the outside of X in that point, we have $\langle n, x \rangle \leq 0$. For a tolerance zone $\mathscr{A}$ (which is not a solid in a vector space) we do the

following: In view of Prop. 5, the tangent space of $\mathscr{A}$ at a boundary pose α occurs also as tangent space of $\log_\alpha \mathscr{A}$. When grouping the coefficients in the linear equation of this tangent space as in (1.31), $(\bar{n}, n)$ is a normal vector of $\log_\alpha \mathscr{A}$. By multiplying both n and $\bar{n}$ with -1 if necessary, we can make the vector $(\bar{n}, n)$ point outward, and we say it is an *outward normal vector* of $\mathscr{A}$. The fact that $(\bar{n}, n)$ points outward means that for all vectors $(d, \bar{d})$ pointing inwards, we have

$$d_1 n_3 + d_2 n_4 + d_3 n_5 + d_4 n_1 + d_5 n_2 + d_6 n_3 \leq 0. \tag{1.32}$$

As the boundary of the swept volume is two-dimensional, and the boundary of a tolerance zone has dimension five, only a small part (in fact, a two-dimensional one) can be expected to contribute to the boundary of the swept volume. With the solid X, this is different: Its boundary already has the right dimension, so we can expect that a substantial part of ∂X contributes to $\partial \mathscr{A}(X)$. Below follows a nice geometric relation between normal vectors of $\mathscr{A}$ and those poses which contribute to the swept volume's boundary.

Oriented Envelopes Def. 1 defines the concept of oriented envelope of a solid with respect to a full-dimensional set $\mathscr{A}$ of poses (its computation is the topic of Section 1.4). The purpose of this definition is to find a set which is not much larger than the boundary of the swept volume we are looking for.

Definition 1. *Suppose that x is a boundary point of X with outward normal vector n. If $(\bar{n}, n)$ with $\bar{n} = x \times n$ is an outward normal vector of the tolerance zone $\mathscr{A}$ at the boundary pose β, then $\beta \cdot x$ is a point of the oriented envelope of X with respect to $\mathscr{A}$.*

Proposition 6. *The boundary of the swept volume $\mathscr{A}(X)$ is contained in the oriented envelope of X with respect to $\mathscr{A}$.*

Proof: We assume that x, n and β are as in Def. 1. The solid $\beta(X)$ is contained in the swept volume $\mathscr{A}(X)$ and touches $\partial \mathscr{A}(X)$ from the inside in the point $\beta \cdot x$. Any smooth one-parameter motion $\alpha(t)$ which starts with $\alpha(0) = \beta$ and has $\alpha(t) \in \mathscr{A}$ for all t moves X inside the swept volume. So the velocity vector $\dot{\alpha} \cdot x$ at $t = 0$ points towards the inside of $\mathscr{A}(X)$, and therefore towards the inside of $\beta(X)$. If we use coordinate vectors $d, \bar{d}$ for the infinitesimal motion $\dot{\alpha}$, this fact is expressed by the inequality (1.14). This is the same inequality as (1.32) which says that $(\bar{n}, n)$ is an outward normal vector. □

The outer boundary of a solid In the context of this chapter we are not interested in any interior holes the compact solids X and $\mathscr{A}(X)$ may have. We therefore employ the concept of *outer boundary*: For any compact set Y, the difference set $\mathbb{R}^n \setminus Y$ has exactly one unbounded component (the *outside* of Y). The part of the boundary of Y which is adjacent to the outside of Y is called the *outer boundary* of Y. If Y is a

surface, then $\partial^{\text{out}}Y$ exists, but we call it *outer part* of Y in order not to apply the word "boundary" to something which is boundary-shaped already.

The operation of computing the outer part of a surface is e.g. built in software which handles triangle meshes. It consists of the trimming away of interior surface components.

Proposition 7. *If X is a solid and $\mathscr{A}$ is a tolerance zone, then the outer boundary of the swept volume is the same as the outer part of the oriented envelope.*

Proof: The implication $\partial X \subset Y \subset X \implies \partial^{\text{out}}X = \partial^{\text{out}}Y$ is obvious from the definition of ∂^{out}. With Y as the oriented envelope, the result follows from Prop. 6. □

If we specialize this result to the case of Minkowski sums, we get the statement that $\partial^{\text{out}}(X+Y)$ is the same as the outer part of of the convolution surface of ∂X and ∂Y.

All normal vectors occur If M is a compact smooth surface in Euclidean space, it is easy to show that every unit vector n occurs as an outward normal vector in some point x (choose the point x in M where $\langle x,n\rangle$ is maximal). With tolerance zones in SE_3, such simple arguments are not available, as the meaning of 'normal vector' is different and depends on the coordinates we have introduced for infinitesimal motions. There is however the following property of tolerance zones of simple shape, whose proof uses a topological argument.

Proposition 8. *Assume that the tolerance zone $\mathscr{A}$ is smooth, has the topology of a ball, and is contained in a subset of* SE_3 *where the mapping* $\log_\alpha$ *is well defined, for some α. Then for every unit vector $(\overline{n},n) \in \mathbb{R}^{3+3}$ there is $\beta \in \partial\mathscr{A}$ such that $(\overline{n},n)$ is an outward normal vector at the pose β.*

The proof uses the concept of Brouwer degree of a mapping, its homotopy invariance and the following facts: the degree of a diffeomorphism equals ± 1, and the degree of a mapping which is not onto equals zero [30].

Proof: Normal vectors of $\mathscr{A}$ do not change if we multiply $\mathscr{A}$ with a pose β from the left. Thus we can without loss of generality assume that $\alpha = (E,0)$ and $\log_\alpha = \log$. We consider the mapping ν_0 which assigns to a pose its outward unit normal vector. It is well known that there is a smooth isotopy of $\log(\partial\mathscr{A})$ to a sphere, which without loss of generality can be made arbitrarily small and close to $(0,0) \in \mathbb{R}^{3+3}$. By applying "exp" we get a smooth isotopy from $\partial\mathscr{A}$ to a surface M_1, which is the exponential of a small sphere. With (1.28) the normal vectors of M_1 are arbitrarily close to the normal vectors of a sphere, so the mapping ν_1 which assigns to each pose in M_1 the outward unit normal vector is 1-1 and onto. It follows that $\deg(\nu_1) = \deg(\nu_0) = \pm 1$, so ν_0 is onto. □

1.4 Point clouds and envelope computation

We now consider pose clouds in SE_3, which are still denoted by $\mathscr{A}$. The poses contained in $\mathscr{A}$ are denoted by the symbols α^1, α^2 and so on. Algorithm 6 given below employs the matrix logarithm, which means higher computational complexity than necessary. Section § 1.4.3 shows how to get rid of logarithms.

§ 1.4.1 Normal vectors of point clouds

We define outward normal vectors as below.

Definition 2. *The vector n is called an outward normal vector of a* convex *point cloud $x^1,\dots,x^r$ in a vertex x^{i_0}, if $\langle x^{i_0},n\rangle \geq \langle x^i,n\rangle$ for all i.*

It means that the entire cloud is contained in the halfspace with equation $\langle n,x\rangle \leq \langle n,x^{i_0}\rangle$. This halfspace is bounded by a *support plane* of the cloud. Of course, if the point cloud is dense and approximates a smooth surface, a normal vector defined in this way approximates the normal vector in the sense of differential geometry. For a given point cloud and normal vector n, there is always a vertex where this vector is an outward normal vector.

For a non-convex point cloud $\mathscr{A}$, this definition of outward normal vector is no longer useful. However, if we choose n from a uniform sample of points in the unit sphere and compute corresponding half-spaces which contain $\mathscr{A}$, then the intersection of those half-spaces approximates $\mathscr{A}$'s convex hull. The domain associated with the cloud in this way is not smaller than the domain represented by the cloud itself, and it is close to it if $\mathscr{A}$ happens to have convex shape. We collect the instructions for computing this *approximate convex hull* together with the points where given vectors are outward normal vectors in the following algorithm:

Algorithm 4. *Suppose $x^1,\dots,x^r$ is a point cloud, and $n^1,\dots,n^s$ is a point cloud representing the surface of the unit sphere. Compute all values $\langle x^j,n^i\rangle$ and for each i, choose an index $j(i)$ such that $\langle x^{j(i)},n^i\rangle \geq \langle x^j,n^i\rangle$ for all j. Then the vertex $x^{j(i)}$ has n^i as an outward normal vector, and the intersection of the half-spaces $\langle x,n^i\rangle \leq \langle x^{j(i)},n^i\rangle$ is an approximate convex hull of the point cloud.* $\diamondsuit$

§ 1.4.2 Normal vectors of pose clouds

We cannot apply Algorithm 4 to a pose cloud $\mathscr{A}$ directly. But by definition, $(\bar{n},n)$ is an outward normal vector at the boundary pose α, if it is an outward normal vector of $\log_\alpha \mathscr{A}$ at the origin of the coordinate system. This property can be used for *testing* if given $\bar{n},n$ and α fulfill the normal vector condition. Searching for α when only $\bar{n},n$ are given, is done in a way similar to Algorithm 4, using the fact that the matrix logarithm has low distortion for small pose clouds.

Suppose that a rigid body is triangulated, with vertices x^i and outward normal vectors n^i at x^i. We compute Plücker coordinates $n^i, \vec{n}^i$ with $\vec{n}^i = x^i \times n^i$. For each i, we want to find a pose $\alpha^{j(i)}$ of the given pose cloud where $(\vec{n}^i, n^i)$ is an outward normal vector. Similar to Algorithm 4, we do not search the entire pose cloud, but a convex hull-like object associated with the pose cloud. If $\mathscr{A}$ represents a tolerance zone, this operation means convexification and thus enlarging the tolerance zone, i.e., an error on the safe side.

Algorithm 5. *Suppose a pose cloud $\alpha^1, \ldots, \alpha^r$ and vectors $\bar{n}, n$ are given. Compute poses where $(\bar{n}, n)$ is an outward normal vector of the pose cloud as follows:*

1. *For each index i in $1, \ldots, r$, compute the point cloud $\mathscr{V} = \log_{\alpha^i}(\mathscr{A})$, which consists of $((v^1, \vec{v}^1), \ldots (v^r, \vec{v}^r))$. By construction, $(v^i, \vec{v}^i) = 0$. If $\langle n, \vec{v}^j \rangle + \langle \bar{n}, v^j \rangle \leq 0$ holds for all index j, then α^i is a pose we are looking for.*

2. *Collect all such index i in a sequence $i_{N-k}, \ldots, i_{N-1}$.* ♢

This procedure is rather slow, as its computational complexity grows with $O(N^2)$, where N is the number of poses in the cloud. A faster algorithm is proposed below, which does the following: We take any logarithm of $\mathscr{A}$ and look for a pose where the given vector is a normal vector. This is only an approximate answer, however. So we now take the logarithm with respect to the pose thus found, and repeat the process until it becomes stationary.

Algorithm 6. *Suppose a pose cloud $\alpha^1, \ldots, \alpha^r$ and vectors $\bar{n}, n$ are given. Compute poses where $(\bar{n}, n)$ is an outward normal vector of the pose cloud as follows:*

1. *Let $N = 0$ and choose an index i_0 with $1 \leq i_0 \leq r$.*

2. *Compute the point cloud $\mathscr{V} = \log_{\alpha^{i_N}}(\mathscr{A})$, which consists of $((v^1, \vec{v}^1), \ldots (v^r, \vec{v}^r))$. By construction, $(v^{i_N}, \vec{v}^{i_N}) = 0$.*

3. *Find i_{max} such that $\langle n, \vec{v}^i \rangle + \langle \bar{n}, v^i \rangle$ is maximal for $i = i_{max}$.*

4. *Let $i_{N+1} = i_{max}$, increment N.*

5. *If the sequence of indices computed has become periodic with period k (i.e., $i_N = i_{N-k}$), terminate with the output $i_{N-k}, \ldots, i_{N-1}$. Otherwise continue with 2.* ♢

If Algorithms 5 or 6 terminate with a unique index i_N, we have found a pose α^{i_N} where $(\bar{n}, n)$ is an outward normal vector. Otherwise there are $k > 1$ candidates for that pose. Which to choose, is the topic of Section § 1.4.4 below. Before that, we give an elementary interpretation of Algorithms 5 and 6.

§ 1.4.3 An elementary interpretation

In the proof of Prop. 6 we encountered the following situation: A pose β in $\mathscr{A}$ and a boundary point x of X with outward normal vector n have the property that $\beta \cdot x$ is a boundary point of the swept volume $\mathscr{A}(X)$. Then necessarily $\beta(X)$ touches the boundary of $\mathscr{A}(X)$ from the inside. Any velocity vector $\dot{\alpha} \cdot x$ attached to β which points towards the inside of $\mathscr{A}$ must fulfill

$$\langle \dot{\alpha} \cdot x, Bn \rangle \leq 0 \quad (\beta = (B,b)). \tag{1.33}$$

As explained in that proof, this expresses the fact that any one-parameter motion inside $\mathscr{A}$ which starts in β assigns a velocity vector to x which points towards the inside of the swept volume. The inequality (1.33) also expresses the fact that $(n \times x, n)$ is an outward normal vector of $\mathscr{A}$.

Now $\mathscr{A} = \alpha^1, \ldots, \alpha^r$ is a pose cloud. Assume that $\beta = \alpha^{i_0}$. All difference vectors $\alpha^i - \beta$ are vectors attached to β pointing towards the inside of $\mathscr{A}$. The denser $\mathscr{A}$, the better the set of difference vectors approximates the set of vectors pointing towards the inside.

It is easy to set up an algorithm which for given x and n finds a boundary pose β such that (1.33) is fulfilled. In view of the discussion above, this is in principle the same as Algorithms 5 or 6, which find poses where $(x \times n, n)$ is an outward normal vector of $\mathscr{A}$. It goes as follows: First, (1.33) is rewritten as

$$\langle Bn, (A^i - B)x + (a^i - b) \rangle \leq 0 \quad (i = 1, \ldots, r). \tag{1.34}$$

This is equivalent to

$$\langle n, B^{-1}(A^i - B)x + B^{-1}(a^i - b) \rangle \leq 0,$$

and in view of $\beta^{-1}\alpha^i = (B^{-1}A^i, B^{-1}(a^i - b))$ also equivalent to

$$\langle n, \beta^{-1}\alpha^i \cdot x \rangle \leq \langle n, x \rangle \quad (i = 1, \ldots, r). \tag{1.35}$$

Thus we have the following Algorithms 7 and 8, which are corresponding to Algorithms 5 and 6 respectively, for finding poses which for a given boundary point of X contribute to the oriented envelope:

Algorithm 7. *Suppose that a pose cloud $\alpha^1, \ldots, \alpha^r$ and a boundary point $x \in \partial X$ with an outward normal vector n are given. Compute poses where $(\overline{n}, n)$ is an outward normal vector of the pose cloud as follows:*

1. *For each index i in $1, \ldots, r$, if $\langle (\alpha^i)^{-1}\alpha^j \cdot x, n \rangle \leq \langle x, n \rangle$ holds for all index j, then α^i is a pose we are looking for.*
2. *Collect all such indices i in a sequence $i_{N-k}, \ldots, i_{N-1}$.* $\diamondsuit$

Algorithm 8. *Suppose a pose cloud $\alpha^1, \ldots, \alpha^r$ and a boundary point $x \in \partial X$ with an outward normal vector n are given. Compute poses where $(\bar{n}, n)$ is an outward normal vector of the pose cloud as follows:*

1. *Let $N = 0$ and choose an index i_0 with $1 \leq i_0 \leq r$.*
2. *Find i_{max} such that $i \mapsto \langle (\alpha^{i_N})^{-1} \alpha^i \cdot x, n \rangle$ attains its maximum for $i = i_{max}$.*
3. *Let $i_{N+1} = i_{max}$ and increment N. Terminate if the sequence of i_N's becomes constant or periodic, otherwise start again with 2.* ♢

Algorithms 7 and 8 can be used as substitutes for Algorithms 5 and 6 respectively in the later Algorithms 9 and 10. They are an entire order of magnitude faster and numerical experience shows that they indeed find the same indices as Algorithms 5 and 6.

§ 1.4.4 Making the result unique

As the purpose of Algorithms 5, 6, 7, and 8 is to compute, for a given point $x \in \partial X$ with an outward normal vector n, a pose α such that $\alpha \cdot x$ is a boundary point of the swept volume, it is not difficult to decide which of the k candidates suggested by Algorithms 5, 6, 7, or 8 is the right one:

Algorithm 9. *Suppose a pose cloud $\alpha^1, \ldots, \alpha^r$ and vectors $n, \bar{n} = x \times n$ are given. We want to compute a pose α^i where $(\bar{n}, n)$ is an outward normal vector of $\mathscr{A}$.*

1. *Compute indices $i_{N-k}, \ldots, i_{N-1}$ with Algorithms 5, 6, 7, or 8.*
2. *Compute a mean normal vector of the bodies $\alpha^{i_{N-j}}(X)$ in the points $\alpha^{i_{N-j}} \cdot x$ by letting $n^{\text{mean}} = \sum_{j=1}^{k} A^{i_{N-j}} n$.*
3. *Choose $i \in \{i_{N-k}, \ldots, i_{N-1}\}$ such that $\langle \alpha^i \cdot x, n^{\text{mean}} \rangle$ is maximal, i.e., x is moved as far as possible in direction n^{mean}.* ♢

The following algorithm computes a discrete version of the oriented envelope of a triangulated rigid body X with respect to a pose cloud $\mathscr{A}$.

Algorithm 10. *Suppose that ∂X is given as a triangle mesh with vertices x^j and outward normal vectors n^j. Further, a pose cloud $\mathscr{A}$ is given. For all x^j, use Algorithm 9 to compute an index $i(j)$ from x^j, n^j and $\mathscr{A}$. Then the point $\alpha^{i(j)} \cdot x^j$ is a vertex of the oriented envelope of X with respect to $\mathscr{A}$. The connectivity of the triangulation of the oriented envelope is the same as the one of ∂X.* ♢

According to Prop. 7, the outer part of the oriented envelope equals the boundary of the swept volume. A tame example, where the swept volume is bounded by the oriented envelope, is illustrated in Figure 1.4.

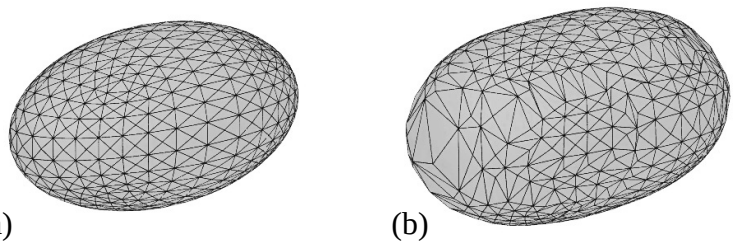

(a) (b)

Figure 1.4: (a): Triangle mesh representing the boundary of an ellipsoid X. (b): The boundary of a swept volume $\mathscr{A}(X)$.

1.5 Trimming and smoothing

The result of the algorithms above usually has self-intersections, especially if the rigid body X we started with is not convex (cf. Figure 1.11.e). Fortunately computing the outer part of a surface is a built in feature of various software packages, and we will not consider that problem here.

§ 1.5.1 Smoothing

Another topic is smoothness of the swept volume's boundary. High-dimensional point clouds must have much more points in order to represent a smooth object faithfully. We cannot expect that pose clouds have this property. Numerical experience shows that smoothing $\partial\mathscr{A}(X)$ is often necessary. In the spirit of tolerance analysis, we must not make $\mathscr{A}(X)$ smaller by smoothing, so we suggest the simple procedure below. It depends on the fact that the normal vectors in a boundary point $Ax+a$ of the swept volume is given by An, if n is the normal vector of X at x:

Algorithm 11. *Assume a triangle mesh with vertices y_i and normal vectors $\widetilde{n}_i$ in the vertices.*

1. *For all i store the neighbours of the vertex y_i in the set C_i (cf. Figure 1.5).*
2. *Consider the forces $F_i = \sum_{j\in C_i} \frac{y_j-y_i}{\|y_j-y_i\|}$ exerted on y_i from its neighbours.*
3. *Vertices y_i where $\langle F_i, \widetilde{n}_i\rangle > 0$ are moved into an equilibrium position: Consider F_i as a function of y_i and choose d such that $\langle F_i(y_i + d\widetilde{n}_i), \widetilde{n}_i\rangle = 0$. Move y_i to $y_i + d\widetilde{n}_i$.* ♢

§ 1.5.2 Rounding off sharp edges

Rounding off sharp edges in a triangulated data set X with tubular surfaces of very small radius or even zero radius has the effect that the normal vector does not abruptly

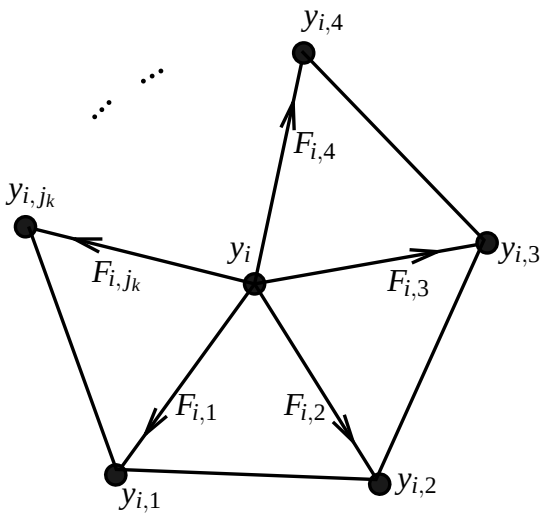

Figure 1.5: A vertex in the triangle mesh with its neighbours.

change from one face to the next. This rounding procedure (Algorithm 12) has been applied to the car part X in Section § 1.6.2.

Algorithm 12. *Assume a triangle mesh with vertex set P, face set F and normal vectors set N of the vertices, and a given threshold angle ω (i.e. the biggest angle) of the sharp edge, we want to modify the triangulation such that there is no sharp edge.*

1. *Look for all the sharp edges. (a) Compute the normal vectors of all faces according to the positions of their vertices; (b) For each pair of adjacent faces, compute the angle between them using the normal vectors in (a). If the angle is less than ω, then the edge connecting the two faces is a sharp edge.*

2. *Introduce new edges along each sharp edge. Suppose that p_1p_2 is a sharp edge connecting faces $p_1p_4p_2$ and $p_1p_2p_3$, (cf. Figure 1.6). Suppose the unit normal vectors of the faces $p_1p_4p_2$ and $p_1p_2p_3$ are n_1 and n_2, respectively. Choose a number n (e.g. $n = 5$). Introduce new vertices*

$$p_{1,1} = p_{1,2} = \cdots = p_{1,n} = p_1$$

and

$$p_{2,1} = p_{2,2} = \ldots, = p_{2,n} = p_2.$$

The normal vectors at both new vertices $p_{1,k}$ and $p_{2,k}$ are given by

$$(1 - \frac{i-1}{n-1})n_1 + \frac{i-1}{n-1}n_2 \quad (i = 1, \ldots, n).$$

Delete the faces $p_1p_4p_2$ and $p_1p_2p_3$ from the face set. Introduce new faces:

$$p_1p_4p_{1,1}, \quad p_{1,1}p_4p_{2,1}, \quad p_{2,1}p_4p_2, p_2p_3p_{2,n}, \quad p_3p_{1,n}p_{2,n}, \quad p_{1,n}p_3p_1,$$
$$p_1p_{1,i}p_{1,i+1}, \quad p_2p_{2,i+1}p_{2,i}, \quad p_{1,i}p_{2,i}p_{1,i+1}, \quad p_{2,i}p_{1,i+1}p_{2,i+1}, (i = 1, \ldots, n-1).$$

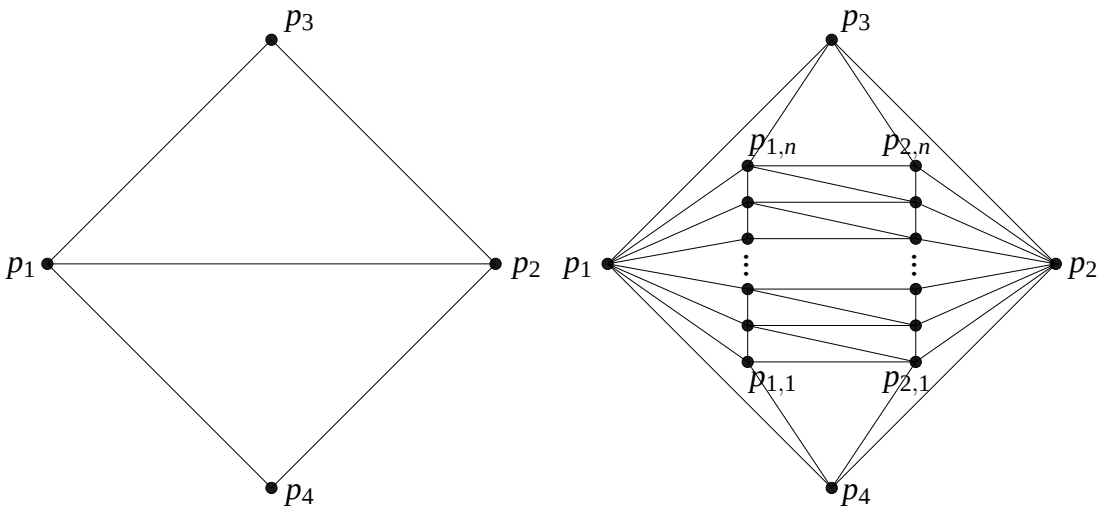

Figure 1.6: Adding edges with the purpose of rounding sharp edges.

3. *Delete the vertices that connect exactly two modified edges. As shown in Figure 1.7, the vertex p_2 will be deleted, and all faces containing it undergo some modification. For $i = 1,\ldots,n-1$, the faces $p_{2,i+1}p_{2,i}p_2$ are replaced by $p_{2,i+1}p_{2,i}p'_{2,i}$, and the faces $p'_{2,i}p'_{2,i+1}p_2$ are replaced by $p'_{2,i}p'_{2,i+1}p_{2,i+1}$. For all other faces that contain the vertex p_2, the vertex p_2 is replaced by $p'_{2,n}$ or $p_{1,2}$ which depends on which sides the face is located to the edge p_1p_2. In detail, if $p_2p_ip_j$, $p_jp_2p_i$ or $p_ip_jp_2$ is a face containing p_2, we will consider the inner product $\langle p_j - p_i, p_2 - p_1\rangle$. If it is positive, p_2 will be replaced by $p'_{2,n}$ in this face; otherwise it will be replaced by $p_{2,1}$.*

Figure 1.8 shows an example of rounding the sharp edges of a cube.

1.6 Numerical examples

We experienced computation times of 10^{-5} seconds per vertex and pose on a PC with 1.0 GHz in computing the oriented envelope, without trimming and smoothing. Depending on the size of the pose cloud, up to 7 % of points with non-unique index in Algorithms 6 and 8 were observed.

§ 1.6.1 Pose clouds of varying smoothness

To show numerical examples, we consider the pose clouds: $\mathscr{A}_k = \alpha^1,\ldots,\alpha^r$ ($k = 1,2,\ldots,5$), where $\alpha^i = \exp(d^i,\overline{d^i})$, and d^i and $\overline{d^i}$ are 3-vectors which are chosen as follows:

1. In $\mathscr{A}_1$, $r = 200$, $(d^i,\overline{d^i})$ are randomly chosen such that $\|d^i\|^2 + \|\overline{d^i}\|^2 \leq 0.2$.

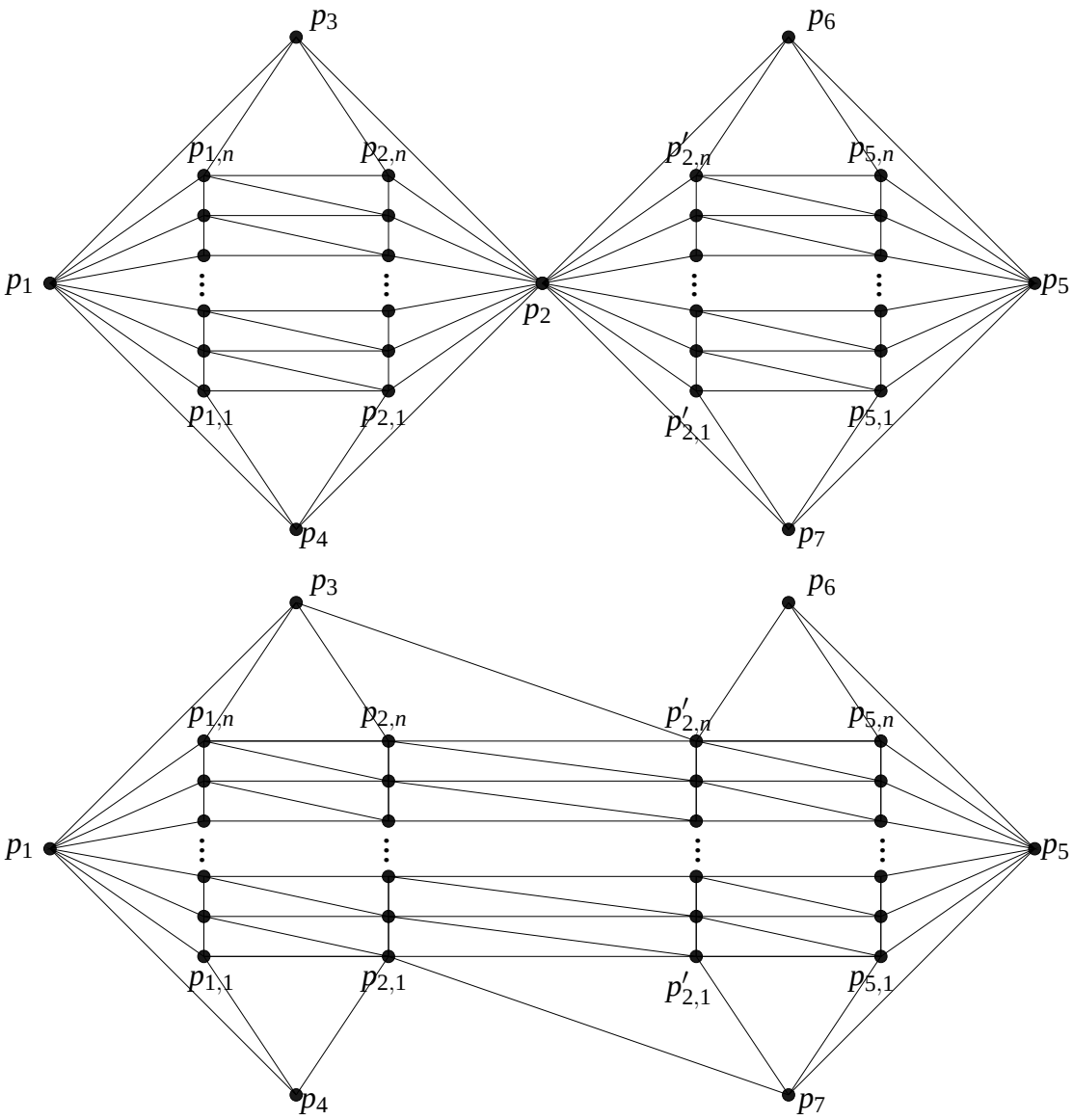

Figure 1.7: Deleting vertices in rounding sharp edges.

2. A_2 is the same as A_1, but $0.1 \leq \|d^i\|^2 + \|\overline{d^i}\|^2 \leq 0.2$.

3. A_3 is the same as A_1, but $\|d^i\| \leq 0.2$, $\|\overline{d^i}\| \leq 0.2$.

4. In A_4, we let $r = 2^6$ and take $(d^i, \overline{d^i})$ as the vertices of the cube $0.2 \cdot [0,1]^6$.

5. In A_5, we let $r = 20^2$ and choose both d^i and $\overline{d^i}$ as one of 20 evenly distributed points on a sphere of radius 0.2 in $\mathbb{R}^3$. These 20 evenly distributed points are, e.g., $\frac{0.2p}{\|p\|}$, where

$$p = (i_1(0,0,3) + i_2(2\sqrt{2},0,-1) + i_3(-\sqrt{2},\sqrt{6},-1) + i_4(-\sqrt{2},-\sqrt{6},-1), \tag{1.36}$$

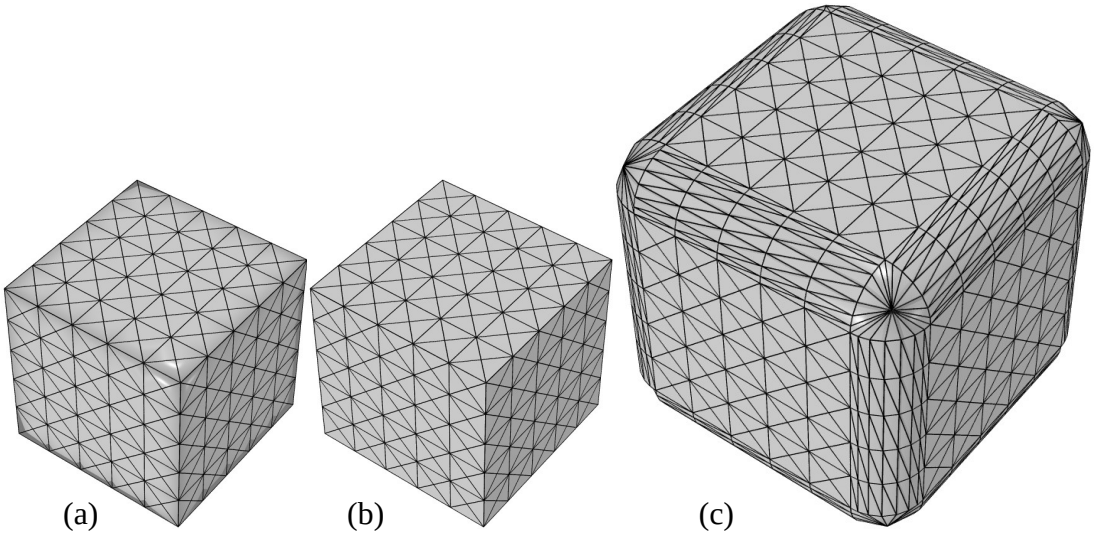

Figure 1.8: rounding the sharp edges of a cube. (a) the original cube; (b) the cube after rounding sharp edges, where only a slight difference in shading is visible; (c) the offset surface of (b), where the vertices p_i with outward unit normal vector n_i are moved to $p_i + 2n_i$.

and $i_1, \ldots, i_4$ are non-negative integers with $i_1 + i_2 + i_3 + i_4 = 3$.

We apply these pose clouds to a 3D model courtesy of Vienna University of Technology and the well known Stanford dragon respectively. The oriented envelopes are computed by Algorithm 10, and Figures 1.9 and 1.10 show these swept volumes.

§ 1.6.2 Swept volumes of vibrating parts

Figure 1.11.a shows the evenly sampled surface of a car part X, which assumes all poses in some cloud $\mathscr{A}$. The motion of the part, i.e., the poses in $\mathscr{A}$, could for example be given by simulating vibration. The result of the action of $\mathscr{A}$ on X is shown in Figures 1.11.b and 1.11.c. Details of the oriented envelope is shown in Figures 1.11.d–i.

The pose cloud $\mathscr{A}$ used in the figure of the simulating vibration does not come from an actual simulation but is designed as below:

$$\mathscr{A} = \{\alpha^i \mid i = 1, 2, \ldots, 200\}, \quad \alpha^i = \exp(d^i, \bar{d^i}), \quad (d^i, \bar{d^i}) = \sum_{j=1}^{8} r_j \sin(\omega_j i) V_j, \quad (1.37)$$

where V_j are eight random unit vectors in $\mathbb{R}^6$, and

$$\omega = (1.12321, 2.2134, 3.3421, 4.4532, 5.5643, 7.75, 8.89, 10.0),$$

$$r = (0.01, 0.006, 0.004, 0.0026, 0.0017, 0.0008, 0.0004, 0.0002).$$

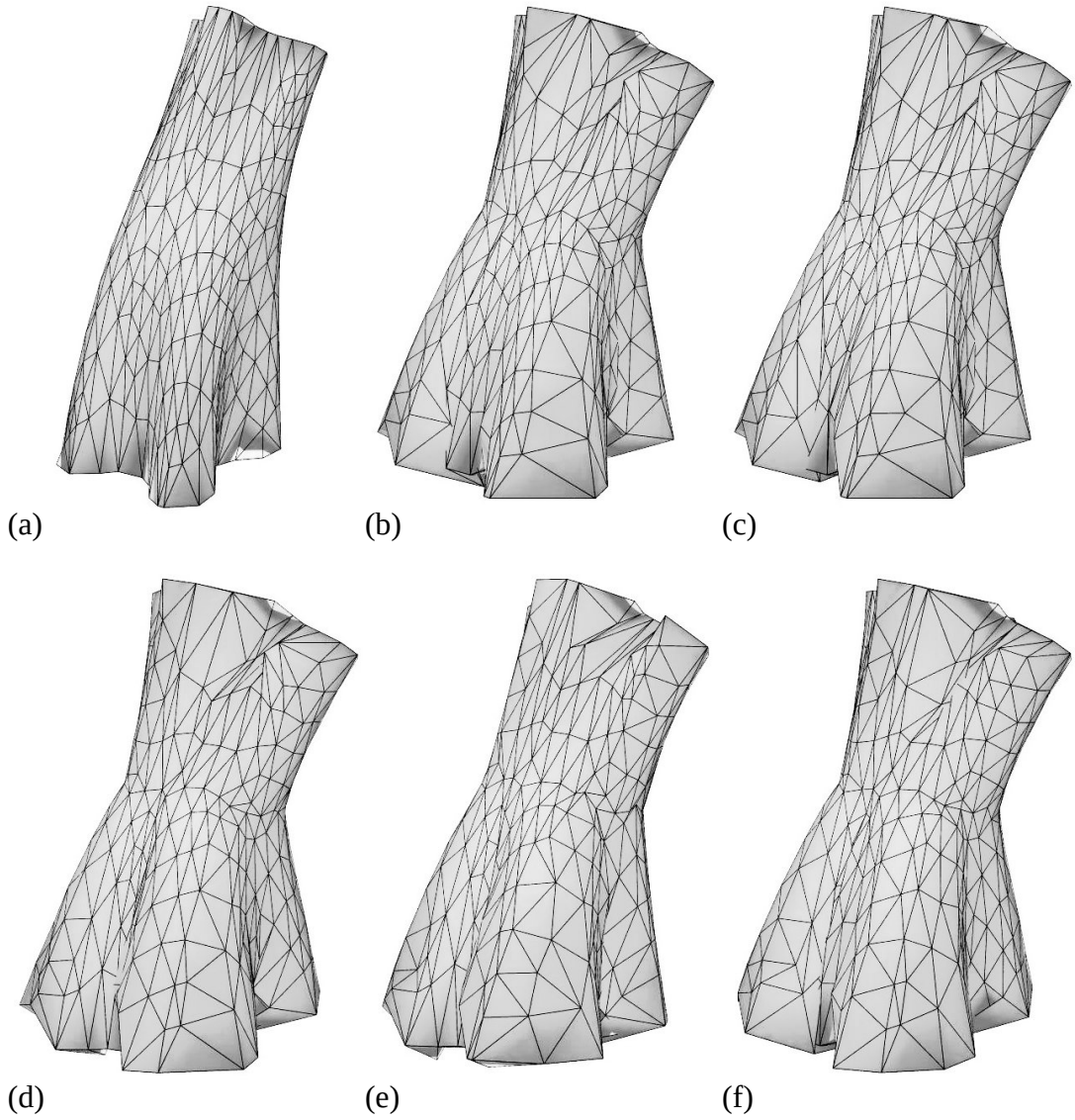

Figure 1.9: (a) A 3D model courtesy of Vienna University of Technology; (b)–(f) Swept volumes of the object corresponding to $\mathscr{A}_1, \ldots, \mathscr{A}_5$ of Section § 1.6.1, respectively.

1.7 Conclusion

We have shown how to compute the swept volume of a solid given by a triangle mesh under the action of a full-dimensional set of poses, which can be thought of either as tolerance zone of an imprecisely defined pose, or as a set of poses obtained by measurements or simulation. The algorithms are based on geometric properties of normal vectors of pose clouds and oriented envelopes. Thus the problem which a priori is difficult and requires searching in high dimensions, is reduced to dimension

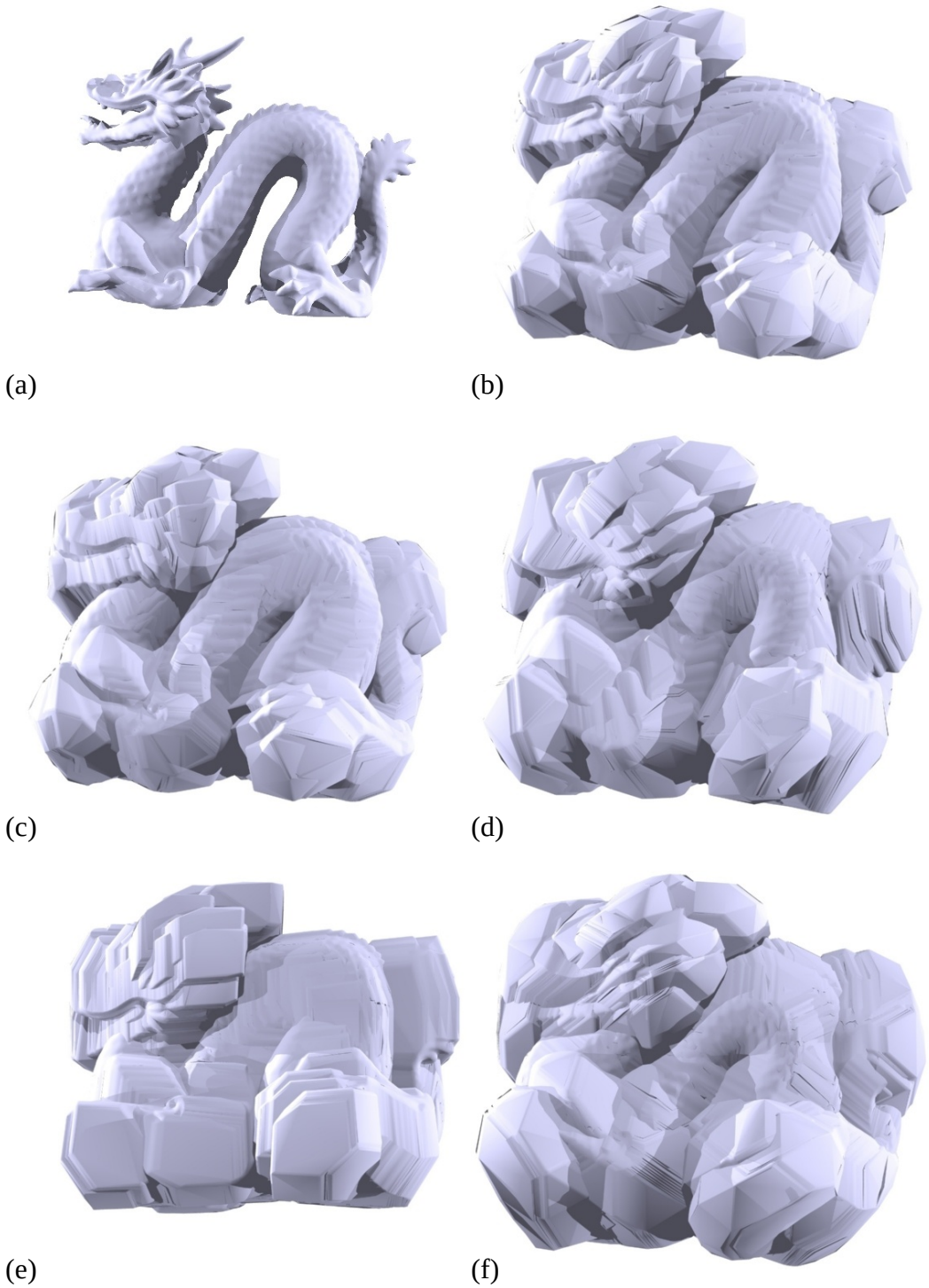

Figure 1.10: (a) The Stanford dragon; (b)–(f) Swept volumes of the Stanford dragon corresponding to $\mathscr{A}_1, \ldots, \mathscr{A}_5$ of Section § 1.6.1, respectively.

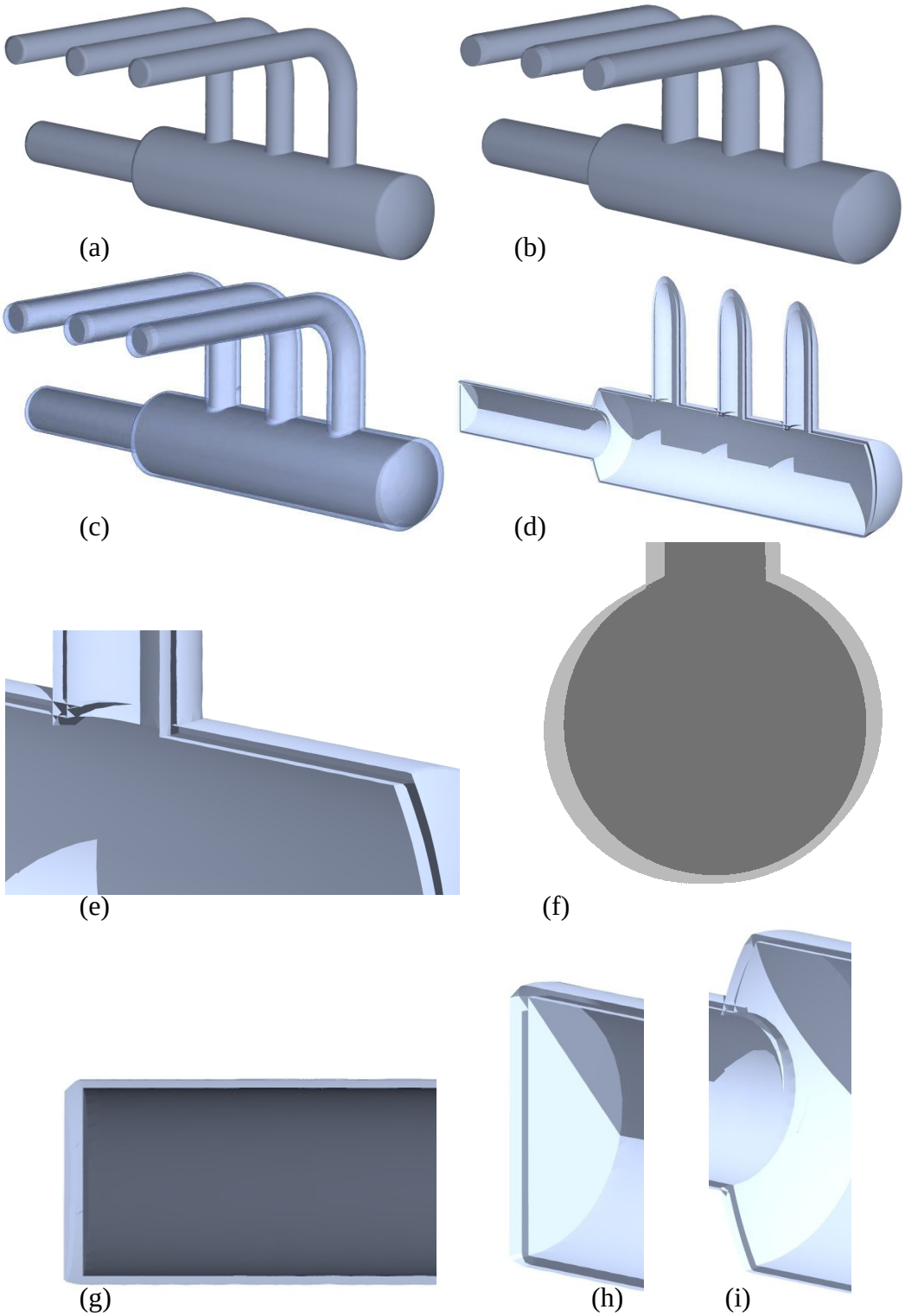

Figure 1.11: (a) Car part courtesy AVL List GmbH. (b) Swept volume for a pose cloud representing vibration. (c) the mixture image of the original and the swept. (d)–(i) Part surface and the oriented envelope. Here trimming is necessary.

two.

Chapter 2

Asymptotic analysis of implicit tolerance problems

2.1 Introduction

Geometric constraint solving means the problems which arise when the location of geometric objects is described via relations between them. Issues important in applications of this concept are *solvability* of constraint problems and their *sensitivity to errors* [21]. Many methods have been proposed for geometric constraint solving: based on dependency graphs [7, 27, 14, 26, 29], rule-based [8, 16, 17, 36] and numerical ones [25, 28], and methods based on symbolic computing [16, 17, 24]. See also the survey article [22].

This chapter is concerned with the propagation of errors through implicit constraints, based on the concept of *tolerance zone* [22, 31, 33, 37]. The present chapter is a sequel of [38], which describes a general analysis of the propagation of tolerance zones through implicit constraints, with a focus on geometric constructions.

We assume that a certain number of geometric objects are given imprecisely – each of them is known to be contained in a certain tolerance zone. Other geometric objects are located via constraints, and we want to give tolerance zones for them. This is done by linearizing the system of constraints and estimating the linearization error. For each configuration, this works only up to a certain maximum size of tolerance zones, dependent on the particular instance of the constraint problem we wish to analyze, on the number of objects and constraints involved, and on the behavior of the constraints' derivatives.

Estimating the linearization error in the way presented here is most efficient if the constraints are quadratic polynomials. The reason for this is that these constraints are reproduced exactly by their second order Taylor expansion. As it is hard to think of geometric relations which are not expressible via quadratic polynomials, this means that for many applications estimating the norms of second derivatives in a certain region

as described in Section § 2.3.3 can be replaced by computing those norms once. A short discussion of the relation of this work and tolerance zones in general to interval arithmetic can be also found in the introductions to [37] and [38]. Most of the material in this chapter is also contained in the technical report [39].

2.2 Preliminaries

We consider two kinds of entities: the *fixed* variables $x = (x_1, \ldots, x_n)$, and the *moving* variables $y = (y_1, \ldots, y_m)$ with $x_i, y_j \in \mathbb{R}$. The *constraints* imposed on x and y are collected in a C^2 function F as follows:

$$F : U \times V \to W : F(x,y) = (F_1(x,y), \ldots, F_m(x,y)) \quad (U = \mathbb{R}^n, V = W = \mathbb{R}^m), \quad (2.1)$$

where each component $F_i(x,y)$ represents a constraint. Solving the constraint problem means finding y for given x such that $F(x,y) = 0$.

We shortly discuss solvability and uniqueness of a solution: Suppose that $F(u,v) = 0$. A *local* solution of the constraint problem which extends the solution (u,v) is a function $G : U \to V$, defined in a connected neighbourhood of u such that $F(x, G(x)) = 0$ for all x where G is defined. It follows from the inverse function theorem that such a local solution exists if $F_y(u,v)$ is nonsingular. If we are interested in only one y_j, we write $y_j = G_j(x)$.

§ 2.2.1 Linear and bilinear mappings: notation

For the convenience of the reader we repeat some facts concerning linear and bilinear operators, their norms, and their relation to the Taylor expansion in Section § 2.2.1— Section § 2.2.4.

We use the symbols U, V, W for linear spaces. $L(U,W)$ and $B(U,V,W)$ denote the spaces of linear mappings from U to W and bilinear mappings from $U \times V$ to W, respectively. We employ the notation "$\alpha \cdot u$" and "$\beta[u,v]$" to indicate that we apply α to u and β to the pair (u,v). "$\alpha(u)$" is a linear mapping which depends on u. For each $\beta \in B(U,V,W)$ there are associated mappings

$$\beta^\phi \in L(U, L(V,W)),\ \beta^\psi \in L(V, L(U,W)),\ \text{with } \beta[u,v] = \beta^\phi(u) \cdot v = \beta^\psi(v) \cdot u. \quad (2.2)$$

Subscripts indicate coefficients of vectors with respect to previously defined bases: $\alpha \in L(U,W)$ and $\beta \in B(U,V,W)$ have the coordinate representations

$$[\alpha \cdot u]_r = \sum_i \alpha_{ri} u_i \qquad \text{and} \qquad \beta[u,v]_r = \sum_{i,j} \beta_{rij} u_i v_j, \quad (2.3)$$

respectively. The *coordinate matrix* of α contains the coefficients α_{ri}. It is elementary that the coordinate matrices of the linear mappings $\beta^{\phi}(u)$ and $\beta^{\psi}(v)$ consist of

$$[\beta^{\phi}(u)]_{rj} = \sum_i u_i \beta_{rij} \qquad \text{and} \qquad [\beta^{\psi}(v)]_{ri} = \sum_j v_j \beta_{rij}, \tag{2.4}$$

respectively.

§ 2.2.2 Taylor expansion of the constraints

Derivatives of the function F of (2.1) with respect to x and y at (u,v) are the linear mappings

$$F_{,x}(u,v) \in L(U,W), \quad F_{,y}(u,v) \in L(V,W) \quad (U=\mathbb{R}^n, V=W=\mathbb{R}^m), \tag{2.5}$$

whose coefficients are given by the partial derivatives $\frac{\partial F_r}{\partial x_i}$ and $\frac{\partial F_r}{\partial y_i}$, respectively. Second derivatives of F are the bilinear mappings

$$F_{,xx} \in B(U,U,W), F_{,xy} \in B(U,V,W), F_{,yy} \in B(V,V,W) \ (U=\mathbb{R}^n, V=W=\mathbb{R}^m), \tag{2.6}$$

whose coefficients are the second partial derivatives $\frac{\partial^2 F_r}{\partial x_i \partial x_j}$, $\frac{\partial^2 F_r}{\partial x_i \partial y_j}$, and $\frac{\partial^2 F_r}{\partial y_i \partial y_j}$ (in that order). Taylor's theorem says that for any $(u,v),(h,k) \in \mathbb{R}^n \times \mathbb{R}^m$ there is $\theta \in [0,1]$ with

$$\begin{aligned} F([{}^{u}_{v}] + [{}^{h}_{k}]) &= F([{}^{u}_{v}]) + F_{,x}([{}^{u}_{v}]) \cdot h + F_{,y}([{}^{u}_{v}]) \cdot k \\ &+ \frac{1}{2} F_{,xx}([{}^{u}_{v}] + \theta[{}^{h}_{k}])[h,h] + F_{,xy}([{}^{u}_{v}] + \theta[{}^{h}_{k}])[h,k] + \frac{1}{2} F_{,yy}([{}^{u}_{v}] + \theta[{}^{h}_{k}])[k,k]. \end{aligned} \tag{2.7}$$

Here we employed column vector notation "$[{}^{u}_{v}]$" for $(u,v) \in \mathbb{R}^n \times \mathbb{R}^m$.

§ 2.2.3 Computing norms of linear and bilinear mappings

We assume that $\alpha \in L(U,W)$, $\beta \in B(U,V,W)$, and that the linear spaces U,V,W are equipped with norms. We are going to use the L^p norms in $p = 1,2,\infty$:

$$\|x\|_p := (\sum |x_i|^p)^{\frac{1}{p}} \quad \text{for} \quad 1 \le p < \infty, \tag{2.8}$$

and $\|x\|_\infty = \max_i |x_i|$. In any case,

$$\|\alpha\|_{L(U,W)} := \sup_{\|u\|_U \le 1} \|\alpha \cdot u\|_W, \quad \|\beta\|_{B(U,V,W)} := \sup_{\|u\|_U, \|v\|_V \le 1} \|\beta[u,v]\|_W. \tag{2.9}$$

For computing norms in $L(U,W)$, see e.g. [19]. In general, if the unit sphere S_U in U is a convex polyhedron with vertices x_i, then for any normed space X and linear mapping $\alpha : U \to X$, we have

$$\|\alpha\|_{L(U,X)} = \max_i \|\alpha \cdot x_i\|_X. \tag{2.10}$$

This applies to the 1-norm and the ∞-norm in U. As to bilinear mappings, it is not difficult to show that

$$\|\beta\|_{B(U,V,W)} = \|\beta^{\phi}\|_{L(U,L(V,W))} = \|\beta^{\Psi}\|_{L(V,L(U,W))}. \tag{2.11}$$

This means that in case either S_V or S_U is a polyhedron, we are able to compute $\|\beta\|_{B(U,V,W)}$. We write $\|\beta\|_{p,q,r}$ in order to indicate that the spaces U,V,W use the p-, q-, and r-norms, respectively.

A case not handled by the polyhedral approach is $\|\beta\|_{2,2,\infty}$, which equals the maximum singular value of the $\dim W$ matrices $(\beta_{rij})_{i=1,\ldots,\dim U}^{j=1,\ldots,\dim V}$. Further, there is the inequality

$$\|\beta\|_{2,2,2} \leq \sqrt{\dim W}\|\beta\|_{2,2,\infty} \tag{2.12}$$

For more details, see also [38].

§ 2.2.4 Norms of derivatives

The three vector spaces U, V, W involved in the definition of F in (2.1) and the second derivatives in (2.6) are assumed to be equipped with norms. $V = W$ as a linear space, but V and W may be different as normed linear spaces. We are going to consider only solutions of the constraint problems where there are upper bounds of the following form

$$\|F_{,xx}(u,v)\| \leq \alpha,\ \|F_{,xy}(u,v)\| \leq \beta,\ \|F_{,yy}(u,v)\| \leq \gamma \quad (\alpha^2+\beta^2+\gamma^2 > 0). \tag{2.13}$$

Upper bounds as required by (2.13) are particularly simple to give if F is a *quadratic* function, because then $F_{,xx}$, $F_{,xy}$, and $F_{,yy}$ depend neither on x nor on y. Later we need the following function:

$$\Delta(s,t) := \frac{1}{2}(\alpha s^2 + 2\beta st + \gamma t^2). \tag{2.14}$$

2.3 Tolerance zones and implicit equations

This section sums up results of [38]. We first discuss local solutions of implicit equations and later apply a linearized local solution to tolerance zones. Theorem 1 below yields an upper bound for the error we make in this process, provided tolerance zones are small enough. The range of validity of Theorem 1 is the subject of Section 2.5 below.

§ 2.3.1 Local solutions

Geometric tolerance analysis means that we are dealing with imprecisely defined geometric objects $p_1, p_2, \ldots$, each of which is contained in its tolerance zone $P_1, P_2, \ldots$.

Geometric objects $q_1, q_2, \ldots$ depend on the p_i's, and we want to find tolerance zones $Q_1, Q_2, \ldots$ for the $q_1, q_2, \ldots$ such that whenever $p_i \in P_i$ for all i, we can be sure that $q_j \in Q_j$ for all j. We treat this problem by introducing coordinates for all geometric entities involved, such that each p_i is represented by a group of fixed variables, and each q_i is given by a group of moving variables:

$$x = (\underbrace{x_1, \ldots, x_{r_1}}_{p_1}, \underbrace{x_{r_1+1}, \ldots, x_{r_1+r_2}}_{p_2}, \ldots, x_n),\ y = (\underbrace{y_1, \ldots, y_{s_1}}_{q_1}, \ldots, y_m). \tag{2.15}$$

If $p_i \in P_i$ for all i, then the vector x, which actually constitutes coordinates for $p_1, p_2, \ldots$, is contained in the set

$$P_1 \times P_2 \times \ldots \in \mathbb{R}^{r_1} \times \mathbb{R}^{r_2} \times \ldots.$$

Suppose $F(u,v) = 0$ as above, such that $x = u, y = v$ represents a particular solution of the constraint problem, then the local solution $y = G(x)$ leads to a tolerance zone $G(P_1 \times P_2 \times \ldots)$ for the vector y. We define the functions $G^{(j)}$ as those coordinates of G, which belong to the geometric object q_j:

$$G(x) = (\underbrace{G_1(x), \ldots, G_{s_1}(x)}_{q_1 = G^{(1)}(x)}, \underbrace{G_{s_1+1}(x), \ldots, G_{s_1+s_2}(x)}_{q_2 = G^{(2)}(x)}, \ldots, G_m(x)). \tag{2.16}$$

Thus a tolerance zone of the geometric entity q_j is given by $G^{(j)}(P_1 \times P_2 \times \ldots)$. It is customary to consider only such tolerance zones P_i which have the topology of a ball. For computations one usually chooses simple shapes, such as convex ones.

As an example, we consider the case $n = 4$, $m = 2$, and

$$F_1(x,y) = (x_1 - y_1)^2 + (x_2 - y_2)^2 - 2900,$$

$$F_2(x,y) = (x_3 - y_1)^2 + (x_4 - y_2)^2 - 4100.$$

A particular solution is

$$(u,v) = (0,0,60,0,20,50).$$

This constraint problem has the following interpretation: The points

$$p_1 = (x_1, x_2), \quad p_2 = (x_3, x_4), \quad q_1 = (y_1, y_2)$$

are constrained by the conditions

$$\|p_1 - q_1\|^2 = 2900 \qquad \text{and} \qquad \|p_2 - q_1\|^2 = 4100.$$

Figure 2.1.a illustrates tolerance zones P_1, P_2, and the tolerance zone $Q_1 = G^{(1)}(P_1 \times P_2)$, where $y = G(x)$ is a local solution of the equation $F(x,y) = 0$ in a neighbourhood of $x = u, y = v$.

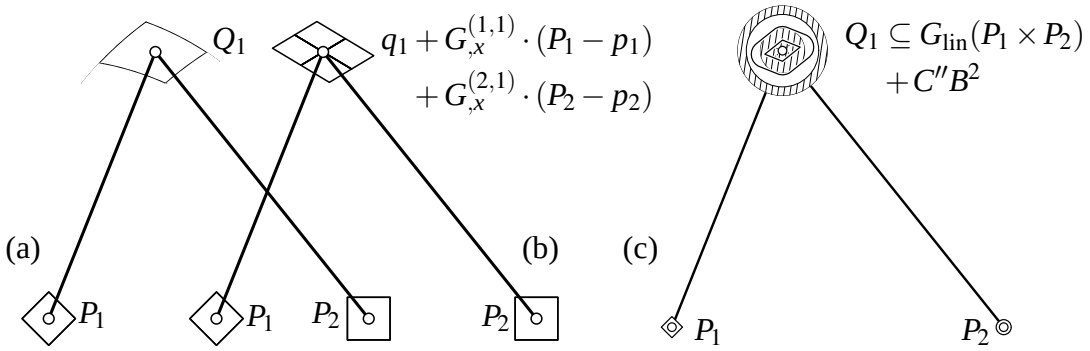

Figure 2.1: (a) Exact and (b) linearized tolerance zones. (c) Upper bound of linearization error.

§ 2.3.2 Linearizing constraints

We linearize the local solution $y = G(x)$ in a neighbourhood of a particular solution u, v with $F(u,v) = 0$:

$$G_{\text{lin}}(u+h) = G(u) + G_{,x}(u) \cdot h, \quad \text{where } G_{,x}(u) = -F_{,y}(u,v)^{-1} F_{,x}(u,v) \in L(U,V). \tag{2.17}$$

The matrix $G_{,x}$ can be partitioned into column groups which correspond to the variables contribute to a particular geometric entity p_i, and into row groups which contribute to a particular entity q_j. Thus we get the following block matrix decomposition with numbers r_i and s_j from (2.15), and a first order approximation for tolerance zones Q_j:

$$G_{,x} = \begin{bmatrix} G_{,x}^{(1,1)} & G_{,x}^{(2,1)} & \cdots \\ G_{,x}^{(1,2)} & G_{,x}^{(2,2)} & \cdots \\ \vdots & \vdots & \ddots \\ \underbrace{}_{r_1} & \underbrace{}_{r_2} & \end{bmatrix} \begin{matrix} \}s_1 \\ \}s_2 \end{matrix} \quad \Longrightarrow \quad \begin{cases} Q_j \approx G_{\text{lin}}^{(j)}(P_1 \times P_2 \times \cdots) \\ \qquad = q_j + \sum_i G_{,x}^{(i,j)} \cdot (P_i - p_i). \end{cases} \tag{2.18}$$

This Minkowski sum of affinely transformed tolerance zones P_i is particularly simple to compute if $s_i \leq 2$ in (2.15) (cf. [18]). We continue the example above, which is illustrated by Figure 2.1: Here

$$G_{,x} = \begin{bmatrix} G_{,x}^{(1,1)} \mid G_{,x}^{(2,1)} \end{bmatrix} = \frac{1}{30} \begin{bmatrix} 10 & 25 & 20 & -25 \\ 8 & 20 & -8 & 10 \end{bmatrix}.$$

The resulting linearized tolerance zone is shown in Figure 2.1.b. Both $G_{,x}^{(1,1)}$ and $G_{,x}^{(2,1)}$ are singular, and $G_{,x}^{(i,1)} \cdot (P_i - p_i)$ is a straight line segment. It follows that we approximate the tolerance zone Q_1 by a parallelogram.

§ 2.3.3 Estimating the linearization error

The *linearization error* is the difference between an exact local solution G and the linearized one, G_{lin}. Following [38], we use function Δ defined in (2.14).

If F is linear, then the norms $\|F_{,xx}\|, \ldots$ are zero and linearization is exact. For our purposes it is essential that $\Delta(s,t)$ is non-zero if $s,t > 0$. Therefore we require that $\alpha^2 + \beta^2 + \gamma^2 > 0$.

Theorem 1. *Consider a solution (u,v) of the constraint problem $F(x,y) = 0$, and assume that $\Delta(s,t)$ is defined according to* (2.14)*. Further assume that there is a local solution G with $v = G(u)$ and the corresponding linearized solution G_{lin}. Choose C, C', C_{max} such that*

$$C_{max} = \frac{\|G_{,x}(u)\|}{\|F_{,y}(u,v)^{-1}\| \cdot \Delta(1, 2\|G_{,x}(u)\|)}, \quad C < C_{max}, \quad C' = \|G_{,x}(u)\| C. \tag{2.19}$$

A perturbation in u causes v to move with $G(u+h) = v+k$. The linearization of this equation is $G_{\text{lin}}(u+h) = v + k_{\text{lin}}$. The linearization error obeys the following inequalities:

$$\|h\| \le C \implies \|k\| < 2C', \quad \|k - k_{\text{lin}}\| \le \|F_{,y}(u,v)^{-1}\| \cdot \Delta(C, 2C') < C'. \tag{2.20}$$

By modifying the proof of Theorem 1 in [38], it is easy to show the following stronger result:

Theorem 2. *Consider a solution (u,v) of the constraint problem $F(x,y) = 0$, and assume that there exist upper bounds α', β' and γ' such that $\forall x \in U, y \in V$,*

$$\|F_{,y}(u,v)^{-1} F_{,xx}(x,y)\| \le \alpha', \quad \|F_{,y}(u,v)^{-1} F_{,xy}(x,y)\| \le \beta', \quad \|F_{,y}(u,v)^{-1} F_{,yy}(x,y)\| \le \gamma'.$$

Define

$$\Delta'(s,t) := \frac{1}{2}(\alpha' s^2 + 2\beta' st + \gamma' t^2).$$

Further assume that there is a local solution G with $v = G(u)$ and the corresponding linearized solution G_{lin}. Choose C, C', C_{max} such that

$$C_{max} = \frac{\|G_{,x}(u)\|}{\Delta'(1, 2\|G_{,x}(u)\|)}, \quad C < C_{max}, \quad C' = \|G_{,x}(u)\| C. \tag{2.21}$$

A perturbation in u causes v to move with $G(u+h) = v+k$. The linearization of this equation is $G_{\text{lin}}(u+h) = v + k_{\text{lin}}$. The linearization error obeys the following inequalities:

$$\|h\| \le C \implies \|k\| < 2C', \quad \|k - k_{\text{lin}}\| \le \Delta'(C, 2C') < C'. \tag{2.22}$$

Proof: From Talor expansion, there is a $\theta \in [0,1]$ such that

$$\begin{aligned} k - k_{\text{lin}} = -\frac{1}{2} F_{,y}(u,v)^{-1} \big(& F_{,xx}(u+\theta h, v+\theta k)[h,h] \\ & + 2F_{,xy}(u+\theta h, v+\theta k)[h,k] + F_{,yy}(u+\theta h, v+\theta k)[k,k] \big). \end{aligned}$$

Then

$$\begin{aligned}\|k-k_{\text{lin}}\| &\le \frac{1}{2}\big(\|F_y(u,v)^{-1}F_{xx}(u+\theta h,v+\theta k)\|\,\|h\|^2\\ &+2\|F_y(u,v)^{-1}F_{xy}(u+\theta h,v+\theta k)\|\,\|h\|\,\|k\|+\|F_y(u,v)^{-1}F_{yy}(u+\theta h,v+\theta k)\|\,\|k\|^2\big)\\ &\le \Delta'(\|h\|,\|k\|). \end{aligned} \tag{2.23}$$

Let $C'' = \Delta'(C,2C')$, then $C'' < C'$ which is equivalent to the condition $C < C_{\max}$.
If $\|k\| < 2C'$, according to (2.23), the linearization error

$$\|k-k_{\text{lin}}\| \le \Delta'(\|h\|,\|k\|) \le \Delta'(C,2C') = C''$$

By the definition of k_{lin}, we have

$$\|k\| \le \|k_{\text{lin}}\| + \|k-k_{\text{lin}}\| \le \|G_x(u)\|\,\|h\| + C'' \le C' + C''.$$

This implies that either $\|k\| \le C' + C''$ or $\|k\| \ge 2C'$. As $C'' < C'$, there is a certain region, bounded by the spheres of radius $C' + C''$ and $2C'$, which contains no vector k. As G was supposed to be a local solution, and the sphere $\|h\| \le C$ is connected, the local value of k must remain inside the sphere of radius $C' + C''$. So

$$\|k\| \le C' + C'' < 2C'$$

□

Similar to Theorem 1, the estimates here can be sharpened a little without much effort: Theorem 2 says that $\|h\| < C$ implies that $\|k_{\text{lin}}\| \le C'$ and $\|k-k_{\text{lin}}\| \le C''$. We get the relation

$$\|k-k_{\text{lin}}\| \le \Delta'(\|h\|,\|k\|) \le \Delta'(C,C'+C'') =: C''' < C''.$$

In case the constraints in F are quadratic, (2.19) has the advantage over (2.21) that the norms $\|F_{xx}\|$ $\|F_{xy}\|$ $\|F_{yy}\|$ have to be computed only once. On the other hand, (2.21) gives a larger value of $C_{\max}$. There is also the following difference: If $F : U \times V \to W$, then $F_y \in L(V,W)$ and $F_y^{-1} \in L(W,V)$. So for (2.21), we compute norms in the following spaces:

$$\begin{aligned} F_y(u,v)^{-1}F_{xx}(x,y) &\in B(U,U,V),\\ F_y(u,v)^{-1}F_{xy}(x,y) &\in B(U,V,V),\\ F_y(u,v)^{-1}F_{yy}(x,y) &\in B(V,V,V). \end{aligned}$$

[38] gives examples which use Theorem 1 in order to give an upper bound for the linearization error. Figure 2.1.c illustrates an offset of the linearized tolerance zone, where the exact tolerance zone Q_1 is known to be contained in.

Theorem 1 gives an answer to the question of maximal size of the tolerance zone of the fixed variables such that a tolerance zone of the corresponding moving variables can be linearization computed with linear analysis plus an estimate for the linearization error. Conversely, assume that the tolerance zone of the moving variables is prescribed as a ball of radius C^*, we have

Theorem 3. *With the assumption in Theorem 1, if*

$$C^* < C^*_{max} := 2\|G_{,x}(u)\|C_{max}, \tag{2.24}$$

then the choice of

$$C = \sqrt{C_{max}\left(\frac{C^*}{\|G_{,x}(u)\|} + \frac{C_{max}}{4}\right)} - \frac{C_{max}}{2} \tag{2.25}$$

ensures that $\|h\| \leq C$ *implies* $\|k\| < C^*$.

Proof: From (2.24) and (2.25) we know that $C < C_{\max}$, according to Theorem 1, if $\|h\| \leq C < C_{\max}$, then

$$\|k\| < C' + \|F_{,y}^{-1}\| \cdot \Delta(C, 2C') = C^*.$$

□

According to Theorem 2, Theorem 3 remains true if we make the substitution

$$\|F_{,y}(u,v)^{-1}\|\dot{\Delta}(s,t) \longrightarrow \Delta'(s,t). \tag{2.26}$$

§ 2.3.4 Balancing the constraint equations

Obviously the local solutions do not change if we multiply some constraints by factors, but the computation of $C_{\max}$ is affected by it. A rule of thumb might be that all variables should have values of the same order of magnitude. The same holds true for the choice of coordinate system, especially the choice of unit length. Some of the coordinates may reflect length, or length squared, or might have no dimension. The coordinate vector of a plane, for instance, contains a unit vector together with a coordinate whose geometric meaning is length. By choosing the unit length appropriately it is easy to achieve any magnitude of that single coefficient. A general answer to the balancing question appears to be difficult.

It is an aim of the following sections to investigate several geometric constructions in Euclidean $\mathbb{R}^3$ in order to gain insight in the behavior of $C_{\max}$ and the norms of derivatives needed when changing the coordinate system.

2.4 Coordinates and relations

This section sums up elementary properties of coordinates for points, oriented lines and oriented planes in Euclidean space.

geometric relation	number and nature of constraints involving more than one geometric entity		number and nature of constraints involving only one geometric entity	
$\operatorname{dist}(p,q)=d$	1	$\|p-q\|^2=d$	0	
$p \in L$	3	$p \times l = \bar{l}$	1	$\|l\|^2=1, \cancel{\langle l,\bar{l}\rangle=0}$
$p \in L$	2	two of $p \times l = \bar{l}$	2	$\|l\|^2=1, \langle l,\bar{l}\rangle=0$
$q=\operatorname{pedal}_L(p)$	4	$q \times l = \bar{l}, \langle p-q,l\rangle = 0$	1	$\|l\|^2=1, \cancel{\langle l,\bar{l}\rangle=0}$
$\overrightarrow{\operatorname{dist}}(p,U)=d$	1	$u_0+\langle u,p\rangle = d$	1	$\|u\|^2=1$
$p \in U$	1	$u_0+\langle u,p\rangle = 0$	1	$\|u\|^2=1$
$\sphericalangle(G,H)=\theta$	1	$\langle g,h\rangle = \cos\theta$	4	$\|g\|^2=1, \|h\|^2=1,$ $\langle g,\bar{g}\rangle=0, \langle h,\bar{h}\rangle=0$
$G \parallel H$	3	$g=\pm h,$	3	$\|g\|^2=1, \cancel{\|h\|^2=1},$ $\langle g,\bar{g}\rangle=0, \langle h,\bar{h}\rangle=0$
$G \cap H \neq \{\}$	1	$\langle g,\bar{h}\rangle + \langle \bar{g},h\rangle = 0$	4	$\|g\|^2=1, \|h\|^2=1,$ $\langle g,\bar{g}\rangle=0, \langle h,\bar{h}\rangle=0$
$L \subset U$	3	$u \times \bar{l} = u_0 l$	3	$\|u\|^2 = \|l\|^2=1, \cancel{\langle l,\bar{l}\rangle=0}$
$L \perp U$	3	$u=\pm l$	2	$\|u\|^2=1, \cancel{\|l\|^2=1}, \langle l,\bar{l}\rangle=0$
$U \parallel V$	3	$u=\pm v$	1	$\|u\|^2=1, \cancel{\|v\|^2=1}$

Table 2.1: Relations between points p,q, lines $L=(l,\bar{l})$, $G=(g,\bar{g})$, $H=(h,\bar{h})$, and planes $U=(u_0,u)$, $V=(v_0,v)$. (cf. Section § 2.4.2).

§ 2.4.1 Coordinates for geometric objects

A *point* $(x_1,x_2,x_3) \in \mathbb{R}^3$ naturally is given the coordinates x_1,x_2,x_3. The *plane* with equation $\langle u,x\rangle + u_0 = 0$ such that $u=(u_1,u_2,u_3)$ has the coordinates (u_0,u_1,u_2,u_3). We normalize the equation such that $u_1^2+u_2^2+u_3^2=\langle u,u\rangle = 1$. Actually such coordinates represent an oriented plane, i.e., a plane together with a side of the plane where the normal vector u points to. A *line* parallel to the vector $l=(l_1,l_2,l_3)$ with $l_1^2+l_2^2+l_3^2=1$ is uniquely characterized by the moment vector $\bar{l}=x \times l$, if x is a point on the line, and the line is reconstructed as the solution set of the three equations $x \times l = \bar{l}$, if vectors l and $\bar{l}$ with $\langle l,\bar{l}\rangle = 0$ are given [32]. Thus we coordinatize the set of straight lines in $\mathbb{R}^3$ by the six coordinates $(l,\bar{l})=(l_1,\ldots,l_6)$ with the side conditions $\langle l,l\rangle = 1$ and $\langle l,\bar{l}\rangle = 0$. Actually any such coordinate vector means an oriented line, and $(-l, -\bar{l})$ means the same line, but equipped with the reverse orientation. We will not always mention that lines and planes are oriented.

§ 2.4.2 Relations between geometric objects

We summarize relations between geometric objects in Tables 2.1 and 2.2. We use the symbols p, q for points, $L = (l, \bar{l})$, $G = (g, \bar{g})$, $H = (h, \bar{h})$ for lines, and $U = (u_0, u)$, $V = (v_0, v)$ for planes. First comes a relation which involves points only: the distance constraint. Next are relations between a point and a line. The incidence relation $p \in L$ either uses only two out of the three equations $\bar{l} = p \times l$, or the condition that $\langle l, \bar{l} \rangle = 0$ has to be dropped. This is indicated by the canceling stroke in the right hand column.

We further consider the case that q is the pedal point of p on L, which means that $q \in L$ and the line $p \vee q$ is orthogonal to L. For the pedal point we give two formulas: One in Table 2.1, and another on in Table 2.2, which introduces as a new variable the distance of p's pedal point q from the origin's pedal point $l \times \bar{l}$. The oriented distance of points on a line, denoted by the symbol $\overrightarrow{\mathrm{dist}}_L(p, q)$, is negative, if the vector $\overrightarrow{pq}$ does not point in the same direction as l.

Next come relations between points and planes, which are straightforward. Relations between lines include parallelity, distance of parallel lines, and distance of skew lines G, H. The latter constraint can be made quadratic by introducing both sine and cosine of the angle $\sphericalangle(G, H)$ as new variables.

Relations between a line and a plane are orthogonality (two cases), parallelity and incidence ($L \subset U$). A relation between planes given here is parallelity. As the line given as intersection of two planes has coordinates proportional to $(u \times v, u_0 v - v_0 u)$, also this results in a quadratic relation.

In Table 2.2, we introduce auxiliary variables (called λ or d) into relations, which either keep the symmetry in deleting equations and then make the equation easier, or make equations quadratic. For instance, we consider the pedal point in a line again, as represented in Table 2.2. After introducing a new variable $\lambda = \langle l, p \rangle$, we do not have to delete any equations. The four other relations in that table would not be quadratic if no auxiliary variables were introduced. It is easy to add more relations to these tables.

§ 2.4.3 Changing the coordinate system

It is an aim of this chapter to study the influence of translation, rotation, and scaling of the underlying coordinate system on the local tolerance analysis via Theorem 1. The choice of a different unit length (i.e., a scaling of the coordinate system with a factor $s > 0$), translation by $t \in \mathbb{R}^3$, and rotation by a matrix $A \in \mathrm{SO}_3$ transform coordinates according to

$$p \longrightarrow sp, \qquad (l, \bar{l}) \longrightarrow (l, s\bar{l}), \qquad (u_0, u) \longrightarrow (su_0, u). \tag{2.27}$$

$$p \longrightarrow p + t, \qquad (l, \bar{l}) \longrightarrow (l, \bar{l} + t \times l), \qquad (u_0, u) \longrightarrow (u_0 - \langle u, t \rangle, u). \tag{2.28}$$

$$p \longrightarrow Ap, \qquad (l, \bar{l}), \longrightarrow (Al, A\bar{l}) \qquad (u_0, u) \longrightarrow (u_0, Au). \tag{2.29}$$

The value $C_{\max}$ as computed by Theorems 1 or 2 means the maximum size of tolerance

geometric relation		number and nature of constraints involving more than one geometric entity		number and nature of constraints involving only one geometric entity
$q = \mathrm{pedal}_L(p)$ $\quad\big[\lambda = \overrightarrow{\mathrm{dist}}_L(p,q)\big]$	4	$\langle l, \underline{p}\rangle = \lambda,$ $l \times \underline{l} + \lambda l = q$	2	$\|l\|^2{=}1, \langle l, \underline{l}\rangle{=}0$
$q = \mathrm{pedal}_U(p)$ $\quad\big[\lambda = \overrightarrow{\mathrm{dist}}_U(p,q)\big]$	4	$u_0 + \langle q, u\rangle = 0$ $p - q = \lambda u,$	1	$\|u\|^2{=}1$
$G \parallel H$ $\quad \mathrm{dist}(G,H) = d$	4	$g = \pm h, \|\bar{g} \mp \bar{h}\|^2 = d^2$	3	$\|g\|^2{=}1, \cancel{\|h\|^2{=}1},$ $\langle g, \bar{g}\rangle{=}0, \langle h, \bar{h}\rangle{=}0$
$\mathrm{dist}(G,H) = d$ $\quad\big[\lambda_2 = \cos\sphericalangle(G,H)\big]$	2	$\langle g, \underline{h}\rangle = \lambda_2,$ $\langle g, \underline{h}\rangle + \langle \bar{g}, h\rangle = d\lambda_1$	5	$\|g\|^2{=}\|h\|^2{=}\lambda_1^2 + \lambda_2^2{=}1,$ $\langle g, \bar{g}\rangle{=}0, \langle g, \underline{h}\rangle{=}0$
$L = U \cap V$	6	$\lambda(l,l) = (u \times v, u_0 v - v_0 u)$	3	$\|l\|^2{=}1, \cancel{\langle l, l\rangle = 0},$ $\|u\|^2{=}1, \|v\|^2{=}1$

Table 2.2: Relations becoming quadratic with new variables (cf. Section § 2.4.2).

zone of the fixed variables "x" around a local solution $x = u, y = v$ of the constraint problem $F(x,y) = 0$. When changing the unit length so that coordinates of points get multiplied by a factor $s > 0$, $C_{\max}$ usually will change.

If the fixed variables consist only of points, then an optimal method for local tolerance analysis would result in $C_{\max}$ getting multiplied by s. If the different parts of x as described by (2.15) have also other meanings, such a simple statement is no longer possible. For lines and planes, for instance, not all coordinates are scaled. While it would be nice if $C_{\max}$ would get bigger if all coordinates are multiplied by s, we cannot expect this to be the case.

As all three type of geometric entities considered in detail in this chapter contain at least one coordinate which is scaled with s, we do the following: We scale with s according to (2.27), and have a look at $\frac{C_{\max}}{s}$, which in the case of points means the size of tolerance zone with respect to the coordinate system before scaling.

2.5 Examples

In this section, we collect constraints useful in geometric constraint solving problems and show the influence of translation, rotation, and scaling on the value of $C_{\max}$ computed via Theorem 1. In the detailed computations included in the text, we use 1-norm in the fixed variable space and 2-norm in the moving variable space. Other norms are illustrated in data tables only. When investigating the influence of translations and

$\|\cdot\|_U$	$\|\cdot\|_V$	$\|F_y^{-1}F_{xx}\|$	$\|F_y^{-1}F_{xy}\|$	$\|F_y^{-1}F_{yy}\|$	$\|G_x\|$	$\frac{C_{\max}}{s}$	$\frac{C^*_{max}}{s}$
∞	∞	0.00	4.00	0.00	18.05	1.25	45.13
∞	1	0.00	3.00	0.00	45.26	1.67	150.87
∞	2	0.00	2.61	0.00	23.93	1.92	91.83
1	∞	0.00	2.00	0.00	8.16	2.50	40.80
1	1	0.00	2.00	0.00	18.16	2.50	90.80
1	2	0.00	1.62	0.00	10.80	3.09	66.73
2	∞	0.00	2.46	0.00	10.10	2.03	41.03
2	1	0.00	2.83	0.00	24.45	1.77	86.44
2	2	0.00	2.83	0.00	12.64	1.77	44.69

Table 2.3: Experimental values for various norms and the values $C_{\max}$ and C^*_{max} according to the constraint problem of Section § 2.5.1, where $s = 0.1$.

rotations we select the translation vectors $t(\tau)$ and rotation matrices $A(\phi)$ as

$$t(\tau) = \begin{bmatrix} \tau \\ \tau \\ \tau \end{bmatrix}, \quad A(\phi) = \begin{bmatrix} 1 & 0 & 0 \\ 0 & \cos\phi & -\sin\phi \\ 0 & \sin\phi & \cos\phi \end{bmatrix}.$$

§ 2.5.1 The pedal point in a plane

Consider points $p_1 = (x_1, x_2, x_3)$, $q_1 = (y_1, y_2, y_3)$, and a plane $U = (x_4, \ldots, x_7)$. Formally, we let $p_2 = U$. We consider the constraints $F(x,y) = 0$ defined by the relation $q_1 = \text{pedal}_U(p_1)$ according to Table 2.1. The auxiliary variable λ is identified with y_4, so we get

$$F(x,y) = \begin{bmatrix} x_4 + x_5y_1 + x_6y_2 + x_7y_3 \\ x_1 - y_4x_5 - y_1 \\ x_2 - y_4x_6 - y_2 \\ x_3 - y_4x_7 - y_3 \end{bmatrix} \Longrightarrow F_y = \begin{bmatrix} x_5 & x_6 & x_7 & 0 \\ -1 & 0 & 0 & -x_5 \\ 0 & -1 & 0 & -x_6 \\ 0 & 0 & -1 & -x_7 \end{bmatrix} \tag{2.30}$$

Besides, $F_{xx} = 0$ and $F_{yy} = 0$, so, $C_{\max}(u,v) = (2\|F_y^{-1}F_{xy}\|)^{-1}$. In view of (2.27), $C_{\max}$ does not depend on the choice of unit length. A logarithmic diagram of $\frac{C_{\max}}{s}$ is given in Figure 2.2.d. For the particular solution

$$x = (50, 28.9, 81.6, 0, 0, 0, 1) \qquad \text{and} \qquad y = (50, 28.9, 0, 81.6),$$

data are shown in Table 2.3. Other experimental data are shown in Figure 2.2.

§ 2.5.2 The pedal point in a line

Consider the geometric relation $q_1 = \text{pedal}_L(p_1)$, where $p_1 = (x_1, x_2, x_3)$ is a fixed point, $q_1 = (y_1, y_2, y_3)$ is a moving point, $L = (x_4, \ldots, x_9)$ is a line. According to Table

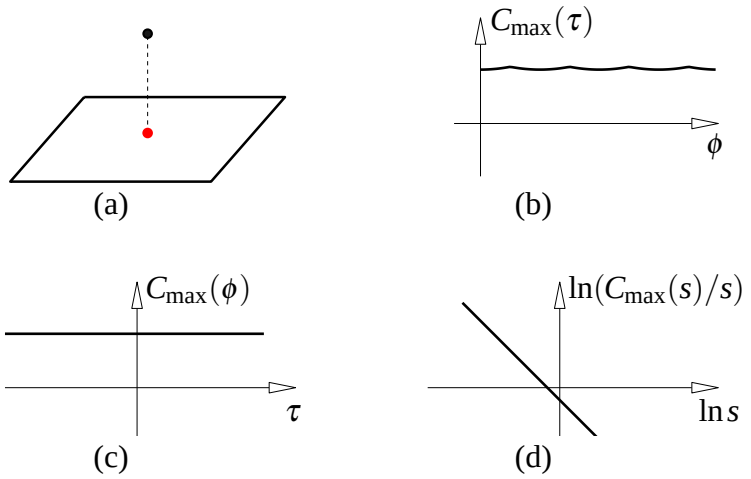

Figure 2.2: The change of $C_{\max}$ over coordinate transformations in the constraint problem of Section § 2.5.1. (a) The pedal point in a plane. (b) Diagram of the change of $C_{\max}$ over the rotation angle ϕ while rotating the coordinate system. (c) the same for translating the coordinate system. (d) Logarithmic diagram of $\frac{C_{\max}}{s}$ over a scaling factor s.

2.2, we add a variable $\lambda = y_4$. We get the following constraint problem $F(x,y) = 0$, where

$$F(x,y) = \begin{bmatrix} x_4x_1 + x_5x_2 + x_6x_3 - y_4 \\ x_5x_9 - x_6x_8 + y_4x_4 - y_1 \\ x_6x_7 - x_4x_9 + y_4x_5 - y_2 \\ x_4x_8 - x_5x_7 + y_4x_6 - y_3 \end{bmatrix}. \tag{2.31}$$

Formally, we let $L = p_2$. As a particular solution, we consider

$$p_1 = (100,100,100), \quad L = \frac{\sqrt{3}}{3}(-1,1,1,0,-100,100),$$

$$q_1 = \frac{1}{3}(100,200,200), \quad \text{and} \quad \lambda = y_4 = \frac{100\sqrt{6}}{3}.$$

Experimental data are shown in Table 2.4.

When scaling with a factor $s > 0$, F_y does not depend on s. So the bilinear mappings $B_1 := F_y^{-1}F_{xx}$ and $B_2 := F_y^{-1}F_{xy}$ are constant. F_{yy} is zero. G_x expands to

$$\begin{bmatrix} -x_4^2 & -x_4x_5 & -x_4x_6 & (-x_4x_1 - y_4)s & (-x_4x_2 - x_9)s & (-x_4x_3 + x_8)s & 0 & x_6 & -x_5 \\ -x_4x_5 & -x_5^2 & -x_5x_6 & (-x_5x_1 + x_9)s & (-x_5x_2 - y_4)s & (-x_5x_3 - x_7)s & -x_6 & 0 & -x_4 \\ -x_4x_6 & -x_5x_6 & -x_6^2 & (-x_6x_1 - x_8)s & (-x_6x_2 + x_7)s & (-x_6x_3 - y_4)s & x_5 & -x_4 & 0 \\ -x_4 & -x_5 & -x_6 & -x_1s & -x_2s & -x_3s & 0 & 0 & 0 \end{bmatrix}.$$

It is obvious that both $M_0 := \lim_{s\to 0} G_x$ and $\lim_{s\to\infty} \frac{G_x}{s}$ depend only on x. Thus we get the following expressions for $C_{\max}$:

$$C_{\max} = \frac{2\|G_x\|}{\|B_1\| + 4\|B_2\|\|G_x\|},$$

$\|\cdot\|_U$	$\|\cdot\|_V$	$\|F_{,y}^{-1}F_{,xx}\|$	$\|F_{,y}^{-1}F_{,xy}\|$	$\|F_{,y}^{-1}F_{,yy}\|$	$\|G_{,x}\|$	$\frac{C_{\max}}{s}$	$\frac{C^*_{max}}{s}$
∞	∞	7.46	1.00	0.00	31.73	4.72	299.70
∞	1	24.39	3.00	0.00	76.86	1.62	249.59
∞	2	12.63	1.73	0.00	43.82	2.77	242.92
1	∞	1.00	1.00	0.00	13.94	4.91	136.93
1	1	2.73	1.00	0.00	29.71	4.89	290.44
1	2	1.41	1.00	0.00	18.10	4.90	177.53
2	∞	1.15	1.00	0.00	17.45	4.92	171.68
2	1	4.62	2.00	0.00	43.87	2.47	216.49
2	2	2.31	2.00	0.00	25.07	2.47	123.94

Table 2.4: Experimental values for various norms and the values $C_{\max}$ and C^*_{max} according to the constraint problem of Section § 2.5.2, where $s = 0.1$.

$\|\cdot\|_U$	$\|\cdot\|_V$	$\|F_{,y}^{-1}F_{,xx}\|$	$\|F_{,y}^{-1}F_{,xy}\|$	$\|F_{,y}^{-1}F_{,yy}\|$	$\|G_{,x}\|$	$\frac{C_{\max}}{s}$	$\frac{C^*_{max}}{s}$
∞	∞	28.28	129.10	6.00	39.80	1.39	108.13
∞	1	28.28	39.11	4.20	44.91	2.19	197.07
∞	2	28.28	56.37	4.90	39.93	1.98	158.34
1	∞	14.14	20.00	6.00	14.14	4.76	134.56
1	1	14.14	14.14	4.20	14.14	6.78	191.66
1	2	14.14	14.21	4.90	14.14	5.97	168.87
2	∞	14.14	43.89	6.00	20.20	3.03	122.23
2	1	84.85	34.64	4.20	26.36	3.42	180.36
2	2	34.64	49.23	4.90	20.21	3.36	135.93

Table 2.5: Experimental values for various norms and the values $C_{\max}$ and C^*_{max} according to the constraint problem of Section § 2.5.3, where $s = 0.001$.

and

$$\lim_{s\to 0} C_{\max} = \frac{2\|M_0\|}{\|B_1\| + 4\|M_0\|\|B_2\|}, \quad \lim_{s\to\infty} C_{\max} = \frac{1}{2\|B_2\|}. \tag{2.32}$$

It follows that the graph of $\eta = \ln\frac{C_{\max}}{s}$ over $\xi = \ln s$ has asymptotes of the form $\eta = -\xi + \ln C$ for both $s \to 0$ and $s \to \infty$, where $\ln C$ is the logarithm of either of the two values in (2.32). Experimental data for the change of $C_{\max}$ when changing the coordinate system is also shown in Figure 2.3.

§ 2.5.3 The distance of skew lines

Consider the following constraint problem: The line $G = (g, \bar{g})$ and the point p are fixed, and $H = (h, \bar{h})$ is a moving line which is incident with p. Further, $\text{dist}(G, H) = d$

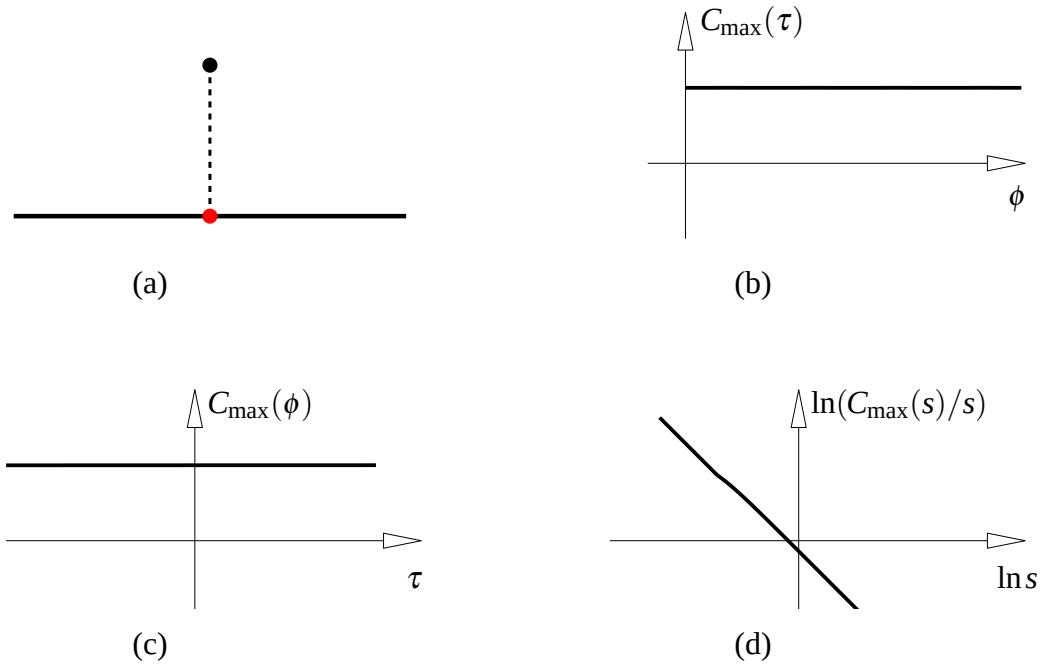

Figure 2.3: (a) The pedal point in a line. (b)–(d) analogous to Figure 2.2, but for the constraint problem of Section § 2.5.2.

and $\sphericalangle(G,H) = \theta$, where d and θ are fixed. This is not quite the constraint problem "dist$(G,H) = d$" of Table 2.2, because there the angle was expressed in terms of the auxiliary variables $\lambda_1 = \sin\theta$, $\lambda_2 = \cos\theta$. As this example shows, it is possible to take the constraints with exactly the variables as listed in the tables above, but it is certainly better from the viewpoint of problem size and magnitude of $C_{\max}$ that the number of variables is low. In this special case we have the 6 equations

$$\bar{h} = p \times h \text{ (3 Equations)}, \quad \|h\|^2 = 1, \quad \langle g,h\rangle = \cos\theta, \quad \langle g,\bar{h}\rangle + \langle \bar{g},h\rangle = d\sin\theta.$$

for the 6 variables $(h,\bar{h})$. Let $G = (x_1,\ldots,x_6)$, $p = (x_7,x_8,x_9)$, $d = x_{10}$, $\lambda_1 = x_{11}$ and $\lambda_2 = x_{12}$. We get

$$F(x,y) = \begin{bmatrix} y_4 + x_9y_2 - x_8y_3 \\ y_5 + x_7y_3 - x_9y_1 \\ y_6 + x_8y_1 - x_7y_2 \\ y_1^2 + y_2^2 + y_3^2 - 1 \\ x_1y_1 + x_2y_2 + x_3y_3 - x_{11} \\ x_1y_4 + x_2y_5 + x_3y_6 + x_4y_1 + x_5y_2 + x_6y_3 - x_{10}x_{12} \end{bmatrix}, \tag{2.33}$$

$$F_{,y} = \begin{bmatrix} 0 & x_9 & -x_8 & 1 & 0 & 0 \\ -x_9 & 0 & x_7 & 0 & 1 & 0 \\ x_8 & -x_7 & 0 & 0 & 0 & 1 \\ 2y_1 & 2y_2 & 2y_3 & 0 & 0 & 0 \\ x_1 & x_2 & x_3 & 0 & 0 & 0 \\ x_4 & x_5 & x_6 & x_1 & x_2 & x_3 \end{bmatrix},$$

$$F_{,x} = \begin{bmatrix} 0 & 0 & 0 & 0 & 0 & 0 & 0 & -y_3 & y_2 & 0 & 0 & 0 \\ 0 & 0 & 0 & 0 & 0 & 0 & y_3 & 0 & -y_1 & 0 & 0 & 0 \\ 0 & 0 & 0 & 0 & 0 & 0 & -y_2 & y_1 & 0 & 0 & 0 & 0 \\ 0 & 0 & 0 & 0 & 0 & 0 & 0 & 0 & 0 & 0 & 0 & 0 \\ y_1 & y_2 & y_3 & 0 & 0 & 0 & 0 & 0 & 0 & 0 & -1 & 0 \\ y_4 & y_5 & y_6 & y_1 & y_2 & y_3 & 0 & 0 & 0 & -x_{12} & 0 & -x_{10} \end{bmatrix},$$

$$F_{r,xx} = 0_{12\times 12} (r = 1, \ldots, 5), \quad F_{4,xy} = 0_{12\times 6}, \quad F_{r,yy} = 0_{6\times 6} (r = 1,2,3,5,6),$$

$$F_{6,xx} = \begin{bmatrix} 0_{9\times 9} & 0_{9\times 3} \\ 0_{3\times 9} & K \end{bmatrix}, \quad F_{r,xy} = \begin{bmatrix} 0_{6\times 3} & 0_{6\times 3} \\ K_r & 0_{3\times 3} \\ 0_{3\times 3} & 0_{3\times 3} \end{bmatrix} \quad (r = 1,2,3),$$

$$F_{5,xy} = \begin{bmatrix} E_3 & 0_{3\times 3} \\ 0_{9\times 3} & 0_{9\times 3} \end{bmatrix}, \quad F_{6,xy} = \begin{bmatrix} 0_{3\times 3} & E_3 \\ E_3 & 0_{3\times 3} \\ 0_{6\times 3} & 0_{6\times 3} \end{bmatrix}, \quad F_{4,yy} = \begin{bmatrix} 2E_3 & 0_{3\times 3} \\ 0_{3\times 3} & 0_{3\times 3} \end{bmatrix},$$

where

$$K = \begin{bmatrix} 0 & 0 & -1 \\ 0 & 0 & 0 \\ -1 & 0 & 0 \end{bmatrix}, \quad K_1 = \begin{bmatrix} 0 & 0 & 0 \\ 0 & 0 & -1 \\ 0 & 1 & 0 \end{bmatrix}, \quad K_2 = \begin{bmatrix} 0 & 0 & 1 \\ 0 & 0 & 0 \\ -1 & 0 & 0 \end{bmatrix}, \quad K_3 = \begin{bmatrix} 0 & -1 & 0 \\ 1 & 0 & 0 \\ 0 & 0 & 0 \end{bmatrix}.$$

The particular solution chosen here is $G = \frac{\sqrt{2}}{2}(1,-1,0,0,0,-100)$, $p = (0,0,100)$, $d = 100$, $\theta = \frac{\pi}{4}$, $H = (1,0,0,0,100,0)$. Table 2.5 shows experimental data for norms and $C_{\max}$. When scaling with a factor $s > 0$, the variables $x_4, \ldots, x_{10}, y_4, y_5, y_6$ are scaled by s, while the others keep unchanged. We get

$$F_{,y}(s) = \frac{1}{2} \begin{bmatrix} 0 & 200s & 0 & 2 & 0 & 0 \\ -200s & 0 & 0 & 0 & 2 & 0 \\ 0 & 0 & 0 & 0 & 0 & 2 \\ 4 & 0 & 0 & 0 & 0 & 0 \\ \sqrt{2} & -\sqrt{2} & 0 & 0 & 0 & 0 \\ 0 & 0 & -100\sqrt{2}s & \sqrt{2} & -\sqrt{2} & 0 \end{bmatrix},$$

$$F_y^{-1}(s)=\frac{1}{100s}\begin{bmatrix} 0 & 0 & 0 & 50s & 0 & 0\\ 0 & 0 & 0 & 50s & -100\sqrt{2}s & 0\\ 1 & -1 & 0 & -100s & 100\sqrt{2}s & -\sqrt{2}\\ 100s & 0 & 0 & -5000s^2 & 10000\sqrt{2}s^2 & 0\\ 0 & 100s & 0 & 5000s^2 & 0 & 0\\ 0 & 0 & 100s & 0 & 0 & 0 \end{bmatrix}$$

$$F_{,x}(s)=\begin{bmatrix} 0 & 0 & 0 & 0 & 0 & 0 & 0 & 0 & 0 & 0 & 0 & 0\\ 0 & 0 & 0 & 0 & 0 & 0 & 0 & 0 & -1 & 0 & 0 & 0\\ 0 & 0 & 0 & 0 & 0 & 0 & 0 & 1 & 0 & 0 & 0 & 0\\ 0 & 0 & 0 & 0 & 0 & 0 & 0 & 0 & 0 & 0 & 0 & 0\\ 1 & 0 & 0 & 0 & 0 & 0 & 0 & 0 & 0 & 0 & -1 & 0\\ 0 & 100s & 0 & 1 & 0 & 0 & 0 & 0 & 0 & -\frac{\sqrt{2}}{2} & 0 & -100s \end{bmatrix},$$

$$G_{,x}(s)=\begin{bmatrix} 0 & 0 & 0 & 0 & 0 & 0 & 0 & 0 & 0 & 0 & 0 & 0\\ -\sqrt{2} & 0 & 0 & 0 & 0 & 0 & 0 & 0 & 0 & 0 & \sqrt{2} & 0\\ \sqrt{2} & -\sqrt{2} & 0 & \frac{-\sqrt{2}}{100s} & 0 & 0 & 0 & 0 & \frac{1}{100s} & \frac{1}{100s} & -\sqrt{2} & \sqrt{2}\\ 100\sqrt{2}s & 0 & 0 & 0 & 0 & 0 & 0 & 0 & 0 & 0 & -100\sqrt{2}s & 0\\ 0 & 0 & 0 & 0 & 0 & 0 & 0 & 0 & -1 & 0 & 0 & 0\\ 0 & 0 & 0 & 0 & 0 & 0 & 0 & 1 & 0 & 0 & 0 & 0 \end{bmatrix}.$$

We compute the bilinear mappings $F_y^{-1}F_{,xx}$, $F_y^{-1}F_{,xy}$, $F_y^{-1}F_{,yy}$:

$$[F_y^{-1}F_{,xx}(s)]_r=0_{12\times 12}\quad (r\neq 3),\quad [F_y^{-1}F_{,xx}(s)]_3=\frac{-\sqrt{2}}{100s}F_{6,xx},$$

$$[F_y^{-1}F_{,xy}(s)]_1=0_{12\times 9},\quad [F_y^{-1}F_{,xy}(s)]_2=-\sqrt{2}F_{5,xy},$$

$$[F_y^{-1}F_{,xy}(s)]_5=F_{2,xy},\quad [F_y^{-1}F_{,xy}(s)]_6=F_{3,xy};$$

$$[F_y^{-1}F_{,xy}(s)]_3=\frac{1}{100s}\begin{bmatrix} 100\sqrt{2}sE_3 & -\sqrt{2}E_3\\ -\sqrt{2}E_3 & 0_{3\times 3}\\ K_1-K_2 & 0_{3\times 3}\\ 0_{3\times 3} & 0_{3\times 3}\end{bmatrix},\quad [F_y^{-1}F_{,xy}(s)]_4=\begin{bmatrix} 100\sqrt{2}sE_3 & 0_{3\times 3}\\ 0_{3\times 3} & 0_{3\times 3}\\ K_1 & 0_{3\times 3}\\ 0_{3\times 3} & 0_{3\times 3}\end{bmatrix};$$

$$[F_y^{-1}F_{,yy}(s)]_1=[F_y^{-1}F_{,yy}(s)]_2=\begin{bmatrix} E_3 & 0_{3\times 3}\\ 0_{3\times 3} & 0_{3\times 3}\end{bmatrix},\quad [F_y^{-1}F_{,yy}(s)]_3=\begin{bmatrix} -2E_3 & 0_{3\times 3}\\ 0_{3\times 3} & 0_{3\times 3}\end{bmatrix},$$

$$[F_y^{-1}F_{,yy}(s)]_4=\begin{bmatrix} -100sE_3 & 0_{3\times 3}\\ 0_{3\times 3} & 0_{3\times 3}\end{bmatrix},[F_y^{-1}F_{,yy}(s)]_5=\begin{bmatrix} 100sE_3 & 0_{3\times 3}\\ 0_{3\times 3} & 0_{3\times 3}\end{bmatrix},[F_y^{-1}F_{,yy}(s)]_6=0_{6\times 6}.$$

$\|\cdot\|_U$	$\|\cdot\|_V$	$\|F_y^{-1}F_{,xx}\|$	$\|F_y^{-1}F_{,xy}\|$	$\|F_y^{-1}F_{,yy}\|$	$\|G_{,x}\|$	$\frac{C_{\max}}{s}$	$\frac{C^*_{max}}{s}$
∞	∞	0.00	28.57	2.98	15.22	6.76	205.67
∞	1	0.00	31.43	1.21	33.51	6.94	465.17
∞	2	0.00	24.74	2.44	21.45	6.49	278.52
1	∞	0.00	7.14	2.98	7.07	17.70	250.31
1	1	0.00	8.47	1.21	8.39	26.84	450.25
1	2	0.00	7.16	2.44	7.11	20.42	290.35
2	∞	0.00	14.25	2.98	10.03	11.32	226.95
2	1	0.00	18.35	1.21	18.94	12.11	458.54
2	2	0.00	24.62	2.44	10.06	10.17	204.77

Table 2.6: Experimental values for various norms and the values $C_{\max}$ and C^*_{max} according to the constraint problem of Section § 2.5.4 (first variant), where $s = 0.001$.

Hence we have the following limits:

$$\begin{aligned} A_0 &= \lim_{s\to 0}(sG_{,x}(s)), & A_\infty &= \lim_{s\to\infty}\tfrac{G_{,x}(s)}{s};\\ B_0 &= \lim_{s\to 0}(sF_y^{-1}F_{,xx}(s)), & B_\infty &= \lim_{s\to\infty}(F_y^{-1}F_{,xx}(s));\\ C_0 &= \lim_{s\to 0}(sF_y^{-1}F_{,xy}(s)), & C_\infty &= \lim_{s\to\infty}\tfrac{F_y^{-1}F_{,xy}(s)}{s};\\ D_0 &= \lim_{s\to 0}(F_y^{-1}F_{,yy}(s)), & D_\infty &= \lim_{s\to\infty}\tfrac{F_y^{-1}F_{,yy}(s)}{s}; \end{aligned} \tag{2.34}$$

By definition, we have

$$\lim_{s\to 0}\frac{C_{\max}(s)}{s} = \frac{1}{2(\|C_0\| + \|A_0\|\|D_0\|)}, \quad \lim_{s\to\infty}(s^2 C_{\max}(s)) = \frac{1}{2\|A_\infty\|\|D_\infty\|}. \tag{2.35}$$

Thus the graph of $\eta = \ln\frac{C_{\max}}{s}$ over $\xi = \ln s$ has the asymptotes

$$\eta = -\ln[2(\|C_0\| + \|A_0\|\|D_0\|)]$$

as $\xi \to -\infty$ and

$$\eta = -3\xi - \ln(2\|A_\infty\|\|D_\infty\|)$$

as $\xi \to \infty$. They intersect at $\xi = \ln s_0$, where

$$s_0^3 = \frac{\|C_0\| + \|A_0\|\|D_0\|}{\|A_\infty\|\|D_\infty\|}.$$

This is illustrated in Figure 2.4.

Further, Figure 2.4 shows the behavior of $C_{\max}$ if the origin is moved or the coordinate system is rotated. It is apparent that the choice of origin is important, and that $C_{\max}$ is only marginally influenced by the choice of s, provided $s < s_0$.

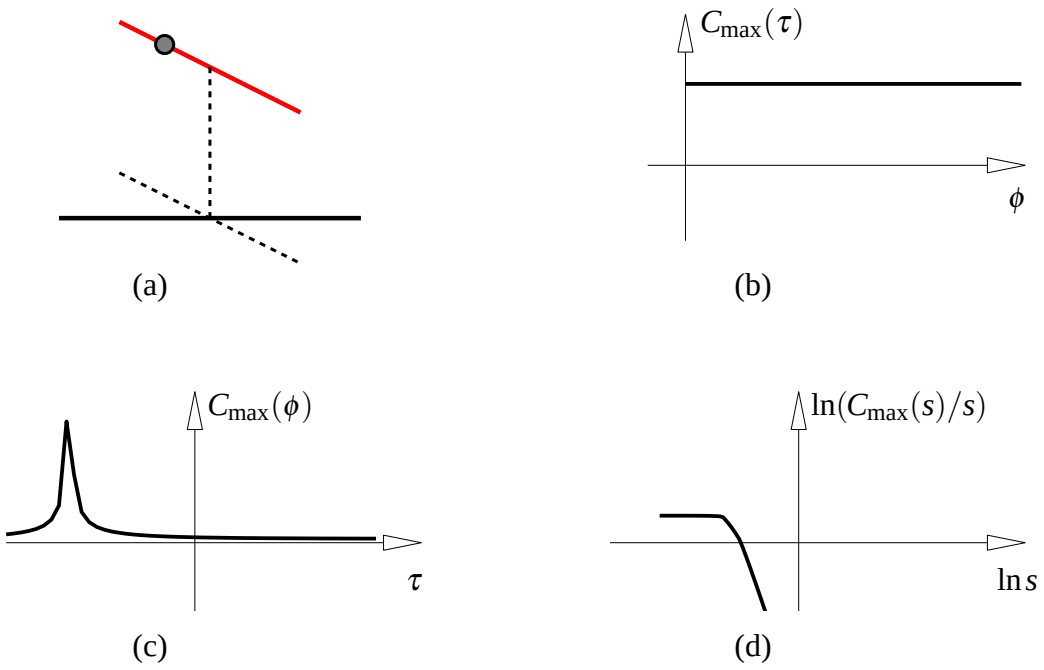

Figure 2.4: (a) A line passes through a fixed point and has fixed distance and angle to another line. (b)–(d) analogous to Figure 2.2, but for the constraint problem of Section § 2.5.3.

§ 2.5.4 The line spanned by two points

We consider two points $p_1 = (x_1, x_2, x_3)$, $p_2 = (x_4, x_5, x_6)$ as fixed variables, and the coordinates of the line $L = (l, \bar{l}) = (y_1, \ldots, y_6)$ spanned by them as moving variables. Table 2.1 contains two different ways of expressing the condition that $p_i \in L$. Because the four equations $\bar{l} = p_i \times l$ plus $\langle l, \bar{l} \rangle = 0$ are not independent, each incidence condition can use only three of them. For reasons of symmetry, it is preferable that we drop $\langle l, \bar{l} \rangle = 0$, but we can do that only once — for the other incidence constraint, one of the three equations of $\bar{l} = p_i \times l$ has to go also. Thus we get the following six equations for $y_1, \ldots, y_6$:

$$F(x,y) = \begin{bmatrix} y_1^2 + y_2^2 + y_3^2 - 1 \\ y_3 x_2 - y_2 x_3 - y_4 \\ y_1 x_3 - y_3 x_1 - y_5 \\ y_2 x_1 - y_1 x_2 - y_6 \\ y_3 x_5 - y_2 x_6 - y_4 \\ y_1 x_6 - y_3 x_4 - y_5 \end{bmatrix} = 0. \tag{2.36}$$

The particular solution for which we display experimental data in Table 2.6 and Figure 2.5,b–d is

$$p_1 = (40, 30, 70), \quad p_2 = (30, 40, -70), \quad L = \frac{\sqrt{22}}{33}(-\frac{1}{2}, \frac{1}{2}, -7, -245, 245, 35).$$

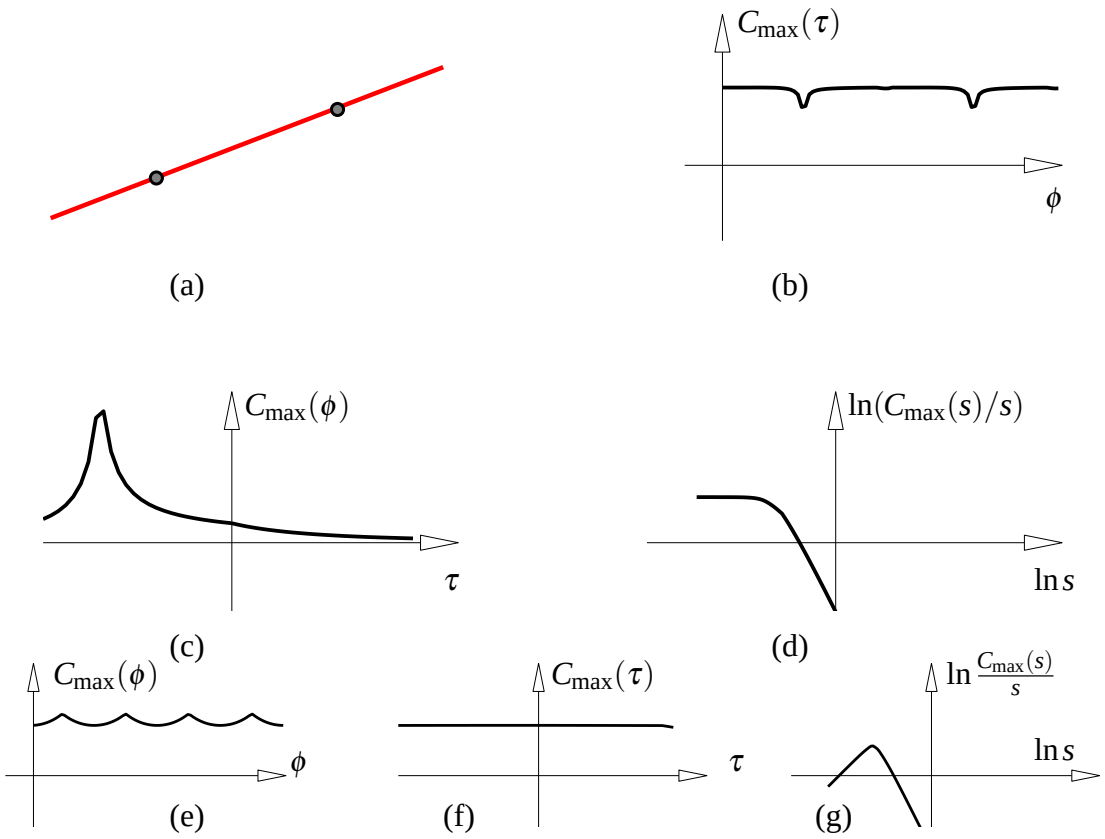

Figure 2.5: (a) A line spanned by two points. (b)–(d) analogous to Figure 2.2, but for the constraint problem of Section § 2.5.4. (e)–(g) analogous to (b)–(d) but with the second variant.

It is elementary to compute the following derivatives:

$$F_{,y} = \begin{bmatrix} 2y_1 & 2y_2 & 2y_3 & 0 & 0 & 0 \\ 0 & -x_3 & x_2 & -1 & 0 & 0 \\ x_3 & 0 & -x_1 & 0 & -1 & 0 \\ -x_2 & x_1 & 0 & 0 & 0 & -1 \\ 0 & -x_6 & x_5 & -1 & 0 & 0 \\ x_6 & 0 & -x_4 & 0 & -1 & 0 \end{bmatrix}, \qquad F_{,x} = \begin{bmatrix} 0 & 0 & 0 & 0 & 0 & 0 \\ 0 & y_3 & -y_2 & 0 & 0 & 0 \\ -y_3 & 0 & y_1 & 0 & 0 & 0 \\ y_2 & -y_1 & 0 & 0 & 0 & 0 \\ 0 & 0 & 0 & 0 & y_3 & -y_2 \\ 0 & 0 & 0 & -y_3 & 0 & y_1 \end{bmatrix},$$

Further, $F_{,xx} = 0$, $F_{1,xy} = 0$, $F_{r,yy} = 0$ for $r = 2, \ldots, 6$, $F_{r,xy} = \begin{bmatrix} K_r & 0_{3\times3} \\ 0_{3\times3} & 0_{3\times3} \end{bmatrix}$ for $r = 2,3,4$, $F_{r,xy} = \begin{bmatrix} 0_{3\times3} & 0_{3\times3} \\ K_{r-3} & 0_{3\times3} \end{bmatrix}$ for $r = 5,6$, and $F_{1,yy} = \begin{bmatrix} 2E_3 & 0_{3\times3} \\ 0_{3\times3} & 0_{3\times3} \end{bmatrix}$, where we have used the abbreviations

$$K_2 = \begin{bmatrix} 0 & 0 & 0 \\ 0 & 0 & 1 \\ 0 & -1 & 0 \end{bmatrix}, \quad K_3 = \begin{bmatrix} 0 & 0 & -1 \\ 0 & 0 & 0 \\ 1 & 0 & 0 \end{bmatrix}, \quad K_4 = \begin{bmatrix} 0 & 1 & 0 \\ -1 & 0 & 0 \\ 0 & 0 & 0 \end{bmatrix}.$$

We scale the coordinates with a factor $s > 0$. For this particular solution,

$$F_{,y}(s) = \frac{1}{33}\begin{bmatrix} -\sqrt{22} & \sqrt{22} & -14\sqrt{22} & 0 & 0 & 0 \\ 0 & -2310s & 990s & -33 & 0 & 0 \\ 2310s & 0 & -1320s & 0 & -33 & 0 \\ -990s & 1320s & 0 & 0 & 0 & -33 \\ 0 & 2310s & 1320s & -33 & 0 & 0 \\ -2310s & 0 & -990s & 0 & -33 & 0 \end{bmatrix},$$

$$F_{,y}^{-1}(s) = \frac{1}{27720s}\begin{bmatrix} -210\sqrt{22}s & -1 & 197 & 0 & 1 & -197 \\ 210\sqrt{22}s & -197 & 1 & 0 & 197 & -1 \\ 2940\sqrt{22}s & -14 & -14 & 0 & 14 & 14 \\ -102900s^2 & -14350s & -490s & 0 & -13370s & 490s \\ 102900\sqrt{22}s^2 & 490s & -13370s & 0 & -490s & -14350s \\ 14700\sqrt{22}s^2 & -7850s & -5870s & -27720s & 7850s & 5870s \end{bmatrix},$$

$$F_{,x}(s) = \frac{\sqrt{22}}{66}\begin{bmatrix} 0 & 0 & 0 & 0 & 0 & 0 \\ 0 & -14 & -1 & 0 & 0 & 0 \\ 14 & 0 & -1 & 0 & 0 & 0 \\ 1 & 1 & 0 & 0 & 0 & 0 \\ 0 & 0 & 0 & 0 & -14 & -1 \\ 0 & 0 & 0 & 14 & 0 & -1 \end{bmatrix},$$

$$G_{,x}(s) = \frac{\sqrt{22}}{130680s}\begin{bmatrix} 197 & 1 & -14 & -197 & -1 & 14 \\ 1 & 197 & 14 & -1 & -197 & -14 \\ -14 & 14 & 2 & 14 & -14 & -2 \\ -490s & 14350s & 1060s & 490s & 13370s & 920s \\ -13370s & -490s & 920s & -14350s & 490s & 106s \\ -7850s & 5870s & 980s & 5870s & -7850s & -980s \end{bmatrix},$$

$$[F_{,y}^{-1}F_{,xy}(s)]_1 = \frac{1}{27720s}\begin{bmatrix} -K_2 + 197K_3 & 0_{3\times 3} \\ K_2 - 197K_3 & 0_{3\times 3} \end{bmatrix}, [F_{,y}^{-1}F_{,xy}(s)]_2 = \frac{1}{27720s}\begin{bmatrix} -197K_2 + K_3 & 0_{3\times 3} \\ -197K_2 - K_3 & 0_{3\times 3} \end{bmatrix},$$

$$[F_{,y}^{-1}F_{,xy}(s)]_3 = \frac{1}{1980s}\begin{bmatrix} -K_2 - K_3 & 0_{3\times 3} \\ K_2 + K_3 & 0_{3\times 3} \end{bmatrix}, \quad [F_{,y}^{-1}F_{,xy}(s)]_4 = \frac{1}{396}\begin{bmatrix} -205K_2 - 7K_3 & 0_{3\times 3} \\ -191K_2 + 7K_3 & 0_{3\times 3} \end{bmatrix},$$

$$[F_{,y}^{-1}F_{,xy}(s)]_5 = \frac{1}{396}\begin{bmatrix} 7K_2 - 191K_3 & 0_{3\times 3} \\ -7K_2 - 205K_3 & 0_{3\times 3} \end{bmatrix},$$

$$[F_{,y}^{-1}F_{,xy}(s)]_6 = \frac{1}{2772}\begin{bmatrix} -785K_2 - 587K_3 - 2772K_4 & 0_{3\times 3} \\ 785K_2 + 587K_3 & 0_{3\times 3} \end{bmatrix},$$

$$[F_{,y}^{-1}F_{,yy}(s)]_1 = \begin{bmatrix} -\frac{\sqrt{22}}{66}E_3 & 0_{3\times3} \\ 0_{3\times3} & 0_{3\times3} \end{bmatrix}, \quad [F_{,y}^{-1}F_{,yy}(s)]_2 = \begin{bmatrix} \frac{\sqrt{22}}{66}E_3 & 0_{3\times3} \\ 0_{3\times3} & 0_{3\times3} \end{bmatrix},$$

$$[F_{,y}^{-1}F_{,yy}(s)]_3 = \begin{bmatrix} -\frac{7}{33}\sqrt{22}E_3 & 0_{3\times3} \\ 0_{3\times3} & 0_{3\times3} \end{bmatrix}, \quad [F_{,y}^{-1}F_{,yy}(s)]_4 = \begin{bmatrix} -\frac{245}{33}\sqrt{22}sE_3 & 0_{3\times3} \\ 0_{3\times3} & 0_{3\times3} \end{bmatrix},$$

$$[F_{,y}^{-1}F_{,yy}(s)]_5 = \begin{bmatrix} \frac{245}{33}\sqrt{22}sE_3 & 0_{3\times3} \\ 0_{3\times3} & 0_{3\times3} \end{bmatrix}, \quad [F_{,y}^{-1}F_{,yy}(s)]_6 = \begin{bmatrix} \frac{35}{33}\sqrt{22}sE_3 & 0_{3\times3} \\ 0_{3\times3} & 0_{3\times3} \end{bmatrix}.$$

We consider the limits

$$B_0 = \lim_{s\to0}(sG_{,x}(s)), \qquad C_0 = \lim_{s\to0}(sF_{,y}^{-1}F_{,xy}(s)), \qquad D_0 = \lim_{s\to0}(F_{,y}^{-1}F_{,yy}(s)), \tag{2.37}$$

$$B_\infty = \lim_{s\to\infty}(G_{,x}(s)), \qquad C_\infty = \lim_{s\to\infty}(F_{,y}^{-1}F_{,xy}(s)), \qquad D_\infty = \lim_{s\to\infty}\frac{F_{,y}^{-1}F_{,yy}(s)}{s}.$$

Theorem 1 now shows that

$$\lim_{s\to0}\frac{C_{\max}(s)}{s} = \frac{1}{2(\|C_0\| + \|B_0\|\|D_0\|)}, \quad \lim_{s\to\infty}(sC_{\max}(s)) = \frac{1}{2\|B_\infty\|\|D_\infty\|}. \tag{2.38}$$

Thus the graph of $\eta = \ln\frac{C_{\max}}{s}$ over $\xi = \ln s$ has the asymptotes

$$\eta = -\ln[2(\|C_0\| + \|B_0\|\|D_0\|)]$$

as $\xi \to -\infty$ and

$$\eta = -2\xi - \ln(2\|B_\infty\|\|D_\infty\|)$$

as $\xi \to \infty$. They intersect at $\xi = \ln s_0$, where

$$s_0^2 = \frac{\|C_0\| + \|B_0\|\|D_0\|}{\|B_\infty\|\|D_\infty\|}.$$

This is illustrated in Figure 2.5.d.

By introducing the oriented distance $d = \overrightarrow{\text{dist}}_L(p_1, p_2)$ of the points p_1 and p_2, we get a set of equations different from the previous one: $\|l\|^2 = 1$, $\bar{l} = p_1 \times l$ and $p_2 = p_1 + dl$. Experimental data are shown in Table 2.7 and Figures 2.5,d–f. The limit case of scaling in the constraint is similar to that of Section § 2.5.9 and we don't include the details here. We notice the following facts: Introduction of an auxiliary variable did not diminish the size of $C_{\max}$ overmuch, and it did improve the behavior with respect to translations. However, it is apparently more important to choose the right scaling factor s than it was with the first variant.

$\|\cdot\|_U$	$\|\cdot\|_V$	$\|F_{,y}^{-1}F_{,xx}\|$	$\|F_{,y}^{-1}F_{,xy}\|$	$\|F_{,y}^{-1}F_{,yy}\|$	$\|G_{,x}\|$	$\frac{C_{\max}}{s}$	$\frac{C^*_{max}}{s}$
∞	∞	0.00	2.00	4.43	2.98	6.45	38.47
∞	1	0.00	2.00	2.34	9.25	4.14	76.63
∞	2	0.00	1.73	3.77	4.66	5.08	47.31
1	∞	0.00	1.00	4.43	1.39	13.74	38.09
1	1	0.00	1.00	2.34	2.34	15.11	70.81
1	2	0.00	1.00	3.77	1.50	14.73	44.16
2	∞	0.00	1.41	4.43	1.97	9.69	38.10
2	1	0.00	2.65	2.34	4.33	7.67	66.39
2	2	0.00	2.65	3.77	2.03	9.51	38.64

Table 2.7: Experimental values for various norms and the values $C_{\max}$ and C^*_{max} according to the constraint problem of Section § 2.5.4 (second variant), where $s = 0.0051$.

$\|\cdot\|_U$	$\|\cdot\|_V$	$\|F_{,y}^{-1}F_{,xx}\|$	$\|F_{,y}^{-1}F_{,xy}\|$	$\|F_{,y}^{-1}F_{,yy}\|$	$\|G_{,x}\|$	$\frac{C_{\max}}{s}$	$\frac{C^*_{max}}{s}$
∞	∞	0.00	4.00	1.73	2.31	6.25	28.87
∞	1	0.00	3.00	2.31	5.20	3.33	34.64
∞	2	0.00	2.89	1.15	2.89	8.04	46.41
1	∞	0.00	0.67	1.73	0.38	37.50	28.87
1	1	0.00	1.67	2.31	0.96	12.86	24.74
1	2	0.00	0.88	1.15	0.51	34.02	34.64
2	∞	0.00	1.73	1.73	1.00	14.43	28.87
2	1	0.00	1.81	2.31	1.81	8.35	30.22
2	2	0.00	1.63	1.15	1.00	17.94	35.87

Table 2.8: Experimental values for various norms and the values $C_{\max}$ and C^*_{max} according to the constraint problem of Section § 2.5.5, where $s = 0.01$.

§ 2.5.5 The plane spanned by three points

Consider the three points $p_1 = (x_1, x_2, x_3)$, $p_2 = (x_4, x_5, x_6)$, $p_3 = (x_7, x_8, x_9)$ as fixed variables and the coordinates of the plane $U = (u_0, u) = (y_1, \ldots, y_4)$ as moving variables. The condition that $p_1, p_2, p_3 \in U$ is expressed by the three constraints $\langle p_i, u\rangle + u_0 = 0$ together with the normalization $\|u\|^2 = 1$. Experimental data for the particular solution $p_1 = (100, 0, 0)$, $p_2 = (0, 100, 0)$, $p_3 = (0, 0, 100)$, and $U = \frac{\sqrt{3}}{3}(-100, 1, 1, 1)$ are shown in Table 2.8 and Figure 2.6.

We demonstrate the influence of the choice of unit length via the following detailed computations. Obviously, $F_{,xx} = 0$, so

$$C_{\max} = \frac{1}{2(\|F_{,y}^{-1}F_{,xy}\| + \|G_{,x}\|\|F_{,y}^{-1}F_{,yy}\|)}.$$

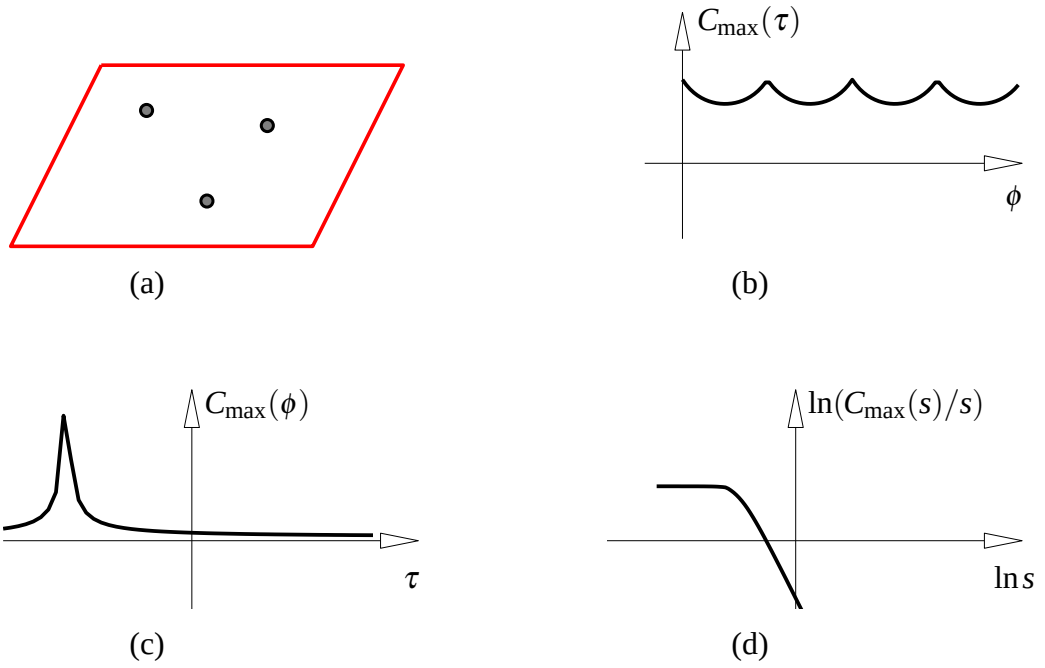

Figure 2.6: (a) A plane spanned by three points. (b)–(d) analogous to Figure 2.2, but for the constraint problem of Section § 2.5.5.

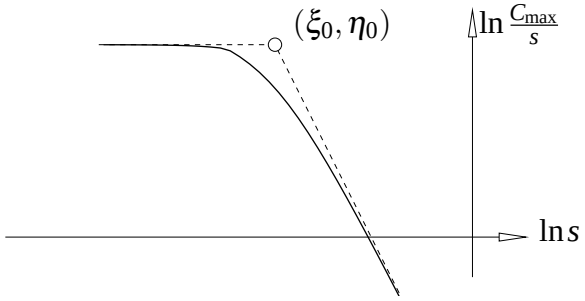

Figure 2.7: Detail of Figure 2.6.d (asymptotes).

We have

$$F(x,y) = \begin{bmatrix} y_2^2 + y_3^2 + y_4^2 - 1 \\ y_1 + y_2 x_1 + y_3 x_2 + y_4 x_3 \\ y_1 + y_2 x_4 + y_3 x_5 + y_4 x_6 \\ y_1 + y_2 x_7 + y_3 x_8 + y_4 x_9 \end{bmatrix},$$

$$F_{,y} = \begin{bmatrix} 0 & 2y_2 & 2y_3 & 2y_4 \\ 1 & x_1 & x_2 & x_3 \\ 1 & x_4 & x_5 & x_6 \\ 1 & x_7 & x_8 & x_9 \end{bmatrix}, \quad F_{,x} = \begin{bmatrix} 0_{1\times 3} & 0_{1\times 3} & 0_{1\times 3} \\ M & 0_{1\times 3} & 0_{1\times 3} \\ 0_{1\times 3} & M & 0_{1\times 3} \\ 0_{1\times 3} & 0_{1\times 3} & M \end{bmatrix}.$$

$F_{,y}^{-1} = \frac{1}{m}(n_{ij})_{4\times 4}$, where $M = [y_2, y_3, y_4]$, $m = \det(F_{,y})$,

$$n_{11} = \begin{vmatrix} x_1 & x_2 & x_3 \\ x_4 & x_5 & x_6 \\ x_7 & x_8 & x_9 \end{vmatrix}, \; n_{12} = -2\begin{vmatrix} y_2 & y_3 & y_4 \\ x_4 & x_5 & x_6 \\ x_7 & x_8 & x_9 \end{vmatrix}, \; n_{13} = 2\begin{vmatrix} y_2 & y_3 & y_4 \\ x_1 & x_2 & x_3 \\ x_7 & x_8 & x_9 \end{vmatrix}, \; n_{14} = -2\begin{vmatrix} y_2 & y_3 & y_4 \\ x_1 & x_2 & x_3 \\ x_4 & x_5 & x_6 \end{vmatrix},$$

$$n_{21} = -\begin{vmatrix} 1 & x_2 & x_3 \\ 1 & x_5 & x_6 \\ 1 & x_8 & x_9 \end{vmatrix}, \quad n_{22} = 2\begin{vmatrix} 0 & y_3 & y_4 \\ 1 & x_5 & x_6 \\ 1 & x_8 & x_9 \end{vmatrix}, \quad n_{23} = -2\begin{vmatrix} 0 & y_3 & y_4 \\ 1 & x_2 & x_3 \\ 1 & x_8 & x_9 \end{vmatrix}, \quad n_{24} = 2\begin{vmatrix} 0 & y_3 & y_4 \\ 1 & x_2 & x_3 \\ 1 & x_5 & x_6 \end{vmatrix},$$

$$n_{31} = \begin{vmatrix} 1 & x_1 & x_3 \\ 1 & x_4 & x_6 \\ 1 & x_7 & x_9 \end{vmatrix}, \quad n_{32} = -2\begin{vmatrix} 0 & y_2 & y_4 \\ 1 & x_4 & x_6 \\ 1 & x_7 & x_9 \end{vmatrix}, \quad n_{33} = 2\begin{vmatrix} 0 & y_2 & y_4 \\ 1 & x_1 & x_3 \\ 1 & x_7 & x_9 \end{vmatrix}, \quad n_{34} = -2\begin{vmatrix} 0 & y_2 & y_4 \\ 1 & x_1 & x_3 \\ 1 & x_4 & x_6 \end{vmatrix},$$

$$n_{41} = -\begin{vmatrix} 1 & x_1 & x_2 \\ 1 & x_4 & x_5 \\ 1 & x_7 & x_8 \end{vmatrix}, \quad n_{42} = 2\begin{vmatrix} 0 & y_2 & y_3 \\ 1 & x_4 & x_5 \\ 1 & x_7 & x_8 \end{vmatrix}, \quad n_{43} = -2\begin{vmatrix} 0 & y_2 & y_3 \\ 1 & x_1 & x_2 \\ 1 & x_7 & x_8 \end{vmatrix}, \quad n_{44} = 2\begin{vmatrix} 0 & y_2 & y_3 \\ 1 & x_1 & x_2 \\ 1 & x_4 & x_5 \end{vmatrix}.$$

Further, the coordinate matrices $[F_{,xy}]_{rij}$ for $r = 1,2,3,4$ are given in block matrix form as

$$F_{1,xy} = 0_{9\times 4},\; F_{2,xy} = \begin{bmatrix} N \\ 0_{6\times 4} \end{bmatrix},\; F_{3,xy} = \begin{bmatrix} 0_{3\times 4} \\ N \\ 0_{3\times 4} \end{bmatrix},\; F_{4,xy} = \begin{bmatrix} 0_{6\times 4} \\ N \end{bmatrix}, \text{where } N = \begin{bmatrix} 0_{3\times 1} & E_3 \end{bmatrix}.$$

So the four components of $F_{,y}^{-1}F_{,xy}$ have the form

$$[F_{,y}^{-1}F_{,xy}]_r = \frac{1}{m}\begin{bmatrix} n_{r2}N \\ n_{r3}N \\ n_{r4}N \end{bmatrix} \quad (r = 1,2,3,4).$$

The coordinate matrices $[F_{,yy}]_{1ij} = 2\text{diag}(0,1,1,1)$ and $[F_{,yy}]_{rij} = 0_{4\times 4}$ $(r \neq 1)$, so the four components of $F_{,y}^{-1}F_{,yy}$ have the form

$$[F_{,y}^{-1}F_{,yy}]_r = 2\frac{n_{r1}}{m}\text{diag}(0,1,1,1) \quad (r = 1,2,3,4).$$

We get the following expression for $G_{,x}$:

$$G_{,x} = \frac{1}{m}\begin{bmatrix} n_{12}M & n_{13}M & n_{14}M \\ n_{22}M & n_{23}M & n_{24}M \\ n_{32}M & n_{33}M & n_{34}M \\ n_{42}M & n_{43}M & n_{44}M \end{bmatrix}.$$

Now introduce scaling with s, i.e.,

$$(x_1,\ldots,x_9) \mapsto (sx_1,\ldots,sx_9) \quad \text{and} \quad (y_1,\ldots,y_4) \mapsto (sy_1,y_2,y_3,y_4)$$

according to (2.27). We write $F_{,y}^{-1}F_{,xy}(s)$, $F_{,y}^{-1}F_{,yy}(s)$, $G_{,x}(s)$ in order to indicate that there is a dependence on s. We see that:

$$[F_{,y}^{-1}F_{,xy}(s)]_1 = \frac{1}{m}\begin{bmatrix} n_{12}N \\ n_{13}N \\ n_{14}N \end{bmatrix}, \quad [F_{,y}^{-1}F_{,xy}(s)]_r = \frac{1}{sm}\begin{bmatrix} n_{r2}N \\ n_{r3}N \\ n_{r4}N \end{bmatrix} (r = 2,3,4).$$

$$[F_{,y}^{-1}F_{,yy}(s)]_1 = 2\frac{sn_{11}}{m}\mathrm{diag}(0,1,1,1),$$

$$[F_{,y}^{-1}F_{,yy}(s)]_r = 2\frac{n_{r1}}{m}\mathrm{diag}(0,1,1,1) \quad (r \neq 1).$$

$$G_{,x}(s) = \frac{1}{sm}\begin{bmatrix} sn_{12}M & sn_{13}M & sn_{14}M \\ n_{22}M & n_{23}M & n_{24}M \\ n_{32}M & n_{33}M & n_{34}M \\ n_{42}M & n_{43}M & n_{44}M \end{bmatrix}.$$

We consider the limit of $F_{,y}^{-1}F_{,xy}(s)$, $F_{,y}^{-1}F_{,yy}(s)$ and $G_{,x}(s)$ as $s \to 0$ and $s \to \infty$, and introduce the following notation:

$$B_0 := \lim_{s\to 0}(sG_{,x}(s)) = \frac{1}{m}\begin{bmatrix} 0_{1\times 3} & 0_{1\times 3} & 0_{1\times 3} \\ n_{22}M & n_{23}M & n_{24}M \\ n_{32}M & n_{33}M & n_{34}M \\ n_{42}M & n_{43}M & n_{44}M \end{bmatrix};$$

$$B_\infty := \lim_{s\to\infty} G_{,x}(s) = \frac{1}{m}\begin{bmatrix} n_{12}M & n_{13}M & n_{14}M \\ 0_{3\times 3} & 0_{3\times 3} & 0_{3\times 3} \end{bmatrix};$$

$$\begin{aligned}
&C_0 := \lim_{s\to 0}(sF_{,y}^{-1}F_{,xy}(s)): && [C_0]_1 = 0_{9\times 4}, \quad [C_0]_r = [F_{,y}^{-1}F_{,xy}(1)]_r && (r = 2,3,4);\\
&C_\infty := \lim_{s\to\infty} F_{,y}^{-1}F_{,xy}(s): && [C_\infty]_1 = [F_{,y}^{-1}F_{,xy}(1)]_1, \quad [C_\infty]_r = 0_{4\times 4} && (r = 2,3,4);\\
&D_0 := lim_{s\to 0}F_{,y}^{-1}F_{,yy}(s): && [D_0]_1 = 0_{4\times 4}, \quad [D_0]_r = [F_{,y}^{-1}F_{,yy}(1)]_r && (r = 2,3,4);\\
&D_\infty := \lim_{s\to\infty}(\frac{1}{s}F_{,y}^{-1}F_{,yy}(s)): && [D_\infty]_1 = [F_{,y}^{-1}F_{,yy}(1)]_1, \quad [D_\infty]_r = 0_{4\times 4} && (r = 2,3,4).
\end{aligned}$$

Then the limits are given by

$$\lim_{s\to 0}\frac{C_{\max}(s)}{s} = \frac{1}{2(\|C_0\| + \|B_0\|\|D_0\|)}, \quad \lim_{s\to\infty}(sC_{\max}(s)) = \frac{1}{2\|B_\infty\|\|D_\infty\|}. \qquad (2.39)$$

The graph of $\eta = \ln\frac{C_{\max}}{s}$ over $\xi = \ln s$ has exactly the same behavior as the respective graph in Section § 2.5.4 (first variant), as is also illustrated by Figure 2.7.

$\|\cdot\|_U$	$\|\cdot\|_V$	$\|F_y^{-1}F_{xx}\|$	$\|F_y^{-1}F_{xy}\|$	$\|F_y^{-1}F_{yy}\|$	$\|G_x\|$	$\frac{C_{\max}}{s}$	$\frac{C^*_{max}}{s}$
∞	∞	0.00	4.75	0.00	3.38	10.53	71.24
∞	1	0.00	4.75	0.00	6.89	10.53	145.15
∞	2	0.00	4.00	0.00	4.21	12.49	105.13
1	∞	0.00	1.30	0.00	1.30	38.42	100.00
1	1	0.00	2.14	0.00	2.14	23.33	100.00
1	2	0.00	1.30	0.00	1.30	38.42	100.00
2	∞	0.00	2.22	0.00	1.70	22.55	76.56
2	1	0.00	2.82	0.00	3.21	17.70	113.48
2	2	0.00	2.57	0.00	1.89	19.44	73.52

Table 2.9: Experimental values for various norms and the values $C_{\max}$ and C^*_{max} according to the constraint problem of Section § 2.5.6, where $s = 0.01$.

$\|\cdot\|_U$	$\|\cdot\|_V$	$\|F_y^{-1}F_{xx}\|$	$\|F_y^{-1}F_{xy}\|$	$\|F_y^{-1}F_{yy}\|$	$\|G_x\|$	$\frac{C_{\max}}{s}$	$\frac{C^*_{max}}{s}$
∞	∞	5.66	0.00	5.66	3.27	26.44	172.73
∞	1	20.01	0.00	2.43	7.53	26.38	397.47
∞	2	8.53	0.00	4.17	3.70	31.23	231.04
1	∞	1.06	0.00	5.66	0.82	101.14	165.16
1	1	1.82	0.00	2.43	1.84	106.21	390.23
1	2	1.06	0.00	4.17	1.06	106.95	226.86
2	∞	1.06	0.00	5.66	1.41	61.07	172.72
2	1	7.44	0.00	2.43	3.21	59.66	383.45
2	2	2.81	0.00	4.17	1.41	78.12	221.07

Table 2.10: Experimental values for various norms and the values $C_{\max}$ and C^*_{max} according to the constraint problem of Section § 2.5.7, where $s = 0.001$.

§ 2.5.6 Intersection of line and plane

The intersection point $q_1 = (y_1, y_2, y_3)$ of a line $L = (l, \overline{l})$ and a plane $U = (u_0, u)$ is computed via the first of the two incidence conditions $q_1 \in L$ and the incidence condition $q_1 \in U$ mentioned in Table 2.1. As $F_{xx} = 0$, $F_{yy} = 0$, and F_y is scale-invariant, also $C_{\max}$ is scale-invariant.

For the particular solution

$$L = \frac{\sqrt{83}}{83}(3, -5, 7, 350, -350, -400),$$

$$U = (0, 0, 0, -1), \quad \text{and} \quad q_1 = (50, 50, 0),$$

experimental data are shown by Table 2.9 and Figure 2.8.

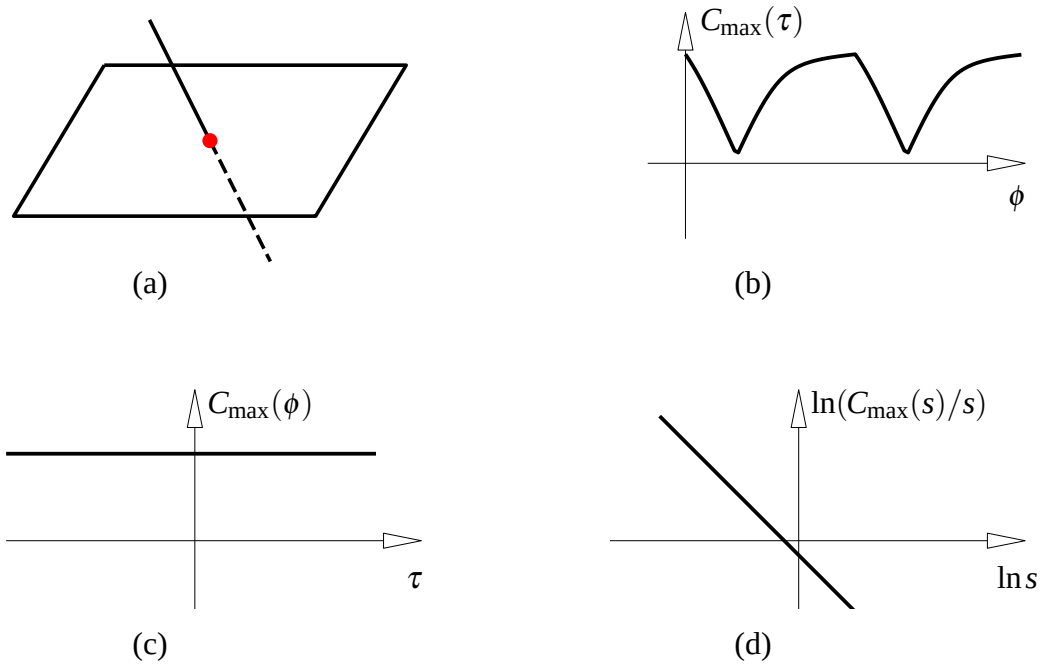

Figure 2.8: (a) Intersection of a line and a plane. (b)–(d) analogous to Figure 2.2, but for the constraint problem of Section § 2.5.6.

§ 2.5.7 Intersection of two planes

We consider the intersection line $L = (l, \overline{l}) = (y_1, \ldots, y_6)$ of two planes $U = (u_0, u) = (x_1, \ldots, x_4)$ and $V = (v_0, v) = (x_5, \ldots, x_8)$, where the planes are fixed and the line is moving. The constraints $F(x,y) = 0$ is defined by the relation $L = U \cap V$ according to Table 2.2. By introducing the auxiliary variable $\lambda = y_7$, we get

$$F(x,y) = \begin{bmatrix} y_1^2 + y_2^2 + y_3^2 - 1 \\ x_3x_8 - x_4x_7 - y_1y_7 \\ x_4x_6 - x_2x_8 - y_2y_7 \\ x_2x_7 - x_3x_6 - y_3y_7 \\ x_1x_6 - x_2x_5 - y_4y_7 \\ x_1x_7 - x_3x_5 - y_5y_7 \\ x_1x_8 - x_4x_5 - y_6y_7 \end{bmatrix} \Longrightarrow F_y = \begin{bmatrix} 2y_1 & 2y_2 & 2y_3 & 0 & 0 & 0 & 0 \\ -y_7 & 0 & 0 & 0 & 0 & 0 & -y_1 \\ 0 & -y_7 & 0 & 0 & 0 & 0 & -y_2 \\ 0 & 0 & -y_7 & 0 & 0 & 0 & -y_3 \\ 0 & 0 & 0 & -y_7 & 0 & 0 & -y_4 \\ 0 & 0 & 0 & 0 & -y_7 & 0 & -y_5 \\ 0 & 0 & 0 & 0 & 0 & -y_7 & -y_6 \end{bmatrix}, \quad (2.40)$$

$$F_x = \begin{bmatrix} 0 & 0 & 0 & 0 & 0 & 0 & 0 & 0 \\ 0 & 0 & x_8 & -x_7 & 0 & 0 & -x_4 & x_3 \\ 0 & -x_8 & 0 & x_6 & 0 & x_4 & 0 & -x_2 \\ 0 & x_7 & -x_6 & 0 & 0 & -x_3 & x_2 & 0 \\ x_6 & -x_5 & 0 & 0 & -x_2 & x_1 & 0 & 0 \\ x_7 & 0 & -x_5 & 0 & -x_3 & 0 & x_1 & 0 \\ x_8 & 0 & 0 & -x_5 & -x_4 & 0 & 0 & x_1 \end{bmatrix},$$

$$F_y^{-1}=\frac{-1}{2y_7}\begin{bmatrix} -y_1y_7 & 2(1-y_1^2) & -2y_1y_2 & -2y_1y_3 & 0 & 0 & 0 \\ -y_2y_7 & -2y_1y_2 & 2(1-y_2^2) & -2y_2y_3 & 0 & 0 & 0 \\ -y_3y_7 & -2y_1y_3 & -2y_2y_3 & 2(1-y_3^2) & 0 & 0 & 0 \\ -y_4y_7 & -2y_1y_4 & -2y_2y_4 & -2y_3y_4 & 2 & 0 & 0 \\ -y_5y_7 & -2y_1y_5 & -2y_2y_5 & -2y_3y_5 & 0 & 2 & 0 \\ -y_6y_7 & -2y_1y_6 & -2y_2y_6 & -2y_3y_6 & 0 & 0 & 2 \\ y_7^2 & 2y_1y_7 & 2y_2y_7 & 2y_3y_7 & 0 & 0 & 0 \end{bmatrix},$$

$$G_{,x}=\begin{bmatrix} 0 & R_1y_1 & x_8+R_2y_1 & -x_7+R_3y_1 & 0 & R_4y_1 & -x_4+R_5y_1 & x_3+R_6y_1 \\ 0 & -x_8+R_1y_2 & R_2y_2 & R_3y_2 & 0 & x_4+R_4y_2 & R_5y_2 & -x_2+R_6y_2 \\ 0 & x_7+R_1y_3 & -x_6+R_2y_3 & R_3y_3 & 0 & -x_3+R_4y_3 & x_2+R_5y_3 & R_6y_3 \\ x_6 & -x_5+R_1y_4 & R_2y_4 & R_3y_4 & -x_2 & x_1+R_4y_4 & R_5y_4 & R_6y_4 \\ x_7 & R_1y_5 & -x_5+R_2y_5 & R_3y_5 & -x_3 & R_4y_5 & x_1+R_5y_5 & R_6y_5 \\ x_8 & R_1y_6 & R_2y_6 & -x_5+R_3y_6 & -x_4 & R_4y_6 & R_5y_6 & x_1+R_6y_6 \\ 0 & -R_1y_7 & -R_2y_7 & -R_3y_7 & 0 & -R_4y_7 & -R_5y_7 & -R_6y_7 \end{bmatrix}.$$

Here we have used the abbreviations

$$R_1=x_8y_2-x_7y_3, \qquad R_2=x_6y_3-x_8y_1, \qquad R_3=x_7y_1-x_6y_2,$$
$$R_4=x_3y_3-x_4y_2, \qquad R_5=x_4y_1-x_2y_3, \qquad R_6=x_2y_2-x_3y_1.$$

Further,

$$[F_y^{-1}F_{,xx}]_r=\frac{1}{y_7}\begin{bmatrix} 0_{4\times4} & -M_r \\ M_r & 0_{4\times4} \end{bmatrix}(r=1,\ldots,7), \quad \text{where } M_1=\begin{bmatrix} 0 & 0 & 0 & 0 \\ 0 & 0 & -y_1y_3 & y_1y_2 \\ 0 & y_1y_3 & 0 & 1-y_1^2 \\ 0 & -y_1y_2 & y_1^2-1 & 0 \end{bmatrix},$$

$$M_2=\begin{bmatrix} 0 & 0 & 0 & 0 \\ 0 & 0 & -y_2y_3 & y_1(y_2^2-1) \\ 0 & y_2y_3 & 0 & -y_1y_2 \\ 0 & y_1(1-y_2^2) & y_1y_2 & 0 \end{bmatrix}, \quad M_3=\begin{bmatrix} 0 & 0 & 0 & 0 \\ 0 & 0 & 1-y_3^2 & y_1y_2y_3 \\ 0 & y_3^2-1 & 0 & -y_1y_3 \\ 0 & -y_1y_2y_3 & y_1y_3 & 0 \end{bmatrix},$$

$$M_4=\begin{bmatrix} 0 & 1 & 0 & 0 \\ -1 & 0 & -y_3y_4 & y_2y_4 \\ 0 & y_3y_4 & 0 & -y_1y_4 \\ 0 & -y_2y_4 & y_1y_4 & 0 \end{bmatrix}, \quad M_5=\begin{bmatrix} 0 & 0 & 1 & 0 \\ 0 & 0 & -y_3y_5 & y_2y_5 \\ -1 & y_3y_5 & 0 & -y_1y_5 \\ 0 & -y_2y_5 & y_1y_5 & 0 \end{bmatrix},$$

$$M_6=\begin{bmatrix} 0 & 0 & 0 & 1 \\ 0 & 0 & -y_3y_6 & y_2y_6 \\ 0 & y_3y_6 & 0 & -y_1y_6 \\ -1 & -y_2y_6 & y_1y_6 & 0 \end{bmatrix}, \quad M_7=y_7\begin{bmatrix} 0 & 0 & 0 & 0 \\ 0 & 0 & y_3 & -y_2 \\ 0 & -y_3 & 0 & y_1 \\ 0 & y_2 & -y_1 & 0 \end{bmatrix}.$$

As to $F_{,y}^{-1}F_{,yy}$, we have

$$[F_{,y}^{-1}F_{,yy}]_r = \frac{1}{y_7}\begin{bmatrix} \mathrm{diag}(y_r y_7, y_r y_7, y_r y_7, 0, 0, 0) & N_r \\ N_r^T & 0 \end{bmatrix} \quad (r = 1, \ldots, 6),$$
$$[F_{,y}^{-1}F_{,yy}]_7 = \begin{bmatrix} \mathrm{diag}(-y_7, -y_7, -y_7, 0, 0, 0) & N_7 \\ N_7^T & 0 \end{bmatrix},$$

where

$$[N_1, \ldots, N_7] = \begin{bmatrix} 1-y_1^2 & -y_1y_2 & -y_1y_3 & -y_1y_4 & -y_1y_5 & -y_1y_6 & y_1 \\ -y_1y_2 & 1-y_2^2 & -y_2y_3 & -y_2y_4 & -y_2y_5 & -y_2y_6 & y_2 \\ -y_1y_3 & -y_2y_3 & 1-y_3^2 & -y_3y_4 & -y_3y_5 & -y_3y_6 & y_3 \\ 0 & 0 & 0 & 1 & 0 & 0 & 0 \\ 0 & 0 & 0 & 0 & 1 & 0 & 0 \\ 0 & 0 & 0 & 0 & 0 & 1 & 0 \end{bmatrix}.$$

$F_{,xy}$ is zero.
When scaling with a factor $s > 0$, coordinates transform according to

$$(x_1, x_5, y_4, y_5, y_6) \mapsto s(x_1, x_5, y_4, y_5, y_6).$$

All other variables are independent on s. We consider the limit case. We can compute the following matrices

$$B_0 = \lim_{s\to 0} G_{,x}(s); \qquad B_\infty = \lim_{s\to\infty} \frac{G_{,x}(s)}{s};$$
$$C_0 = \lim_{s\to 0} F_{,y}^{-1}F_{,xx}(s); \qquad C_\infty = \lim_{s\to\infty} \frac{F_{,y}^{-1}F_{,xx}(s)}{s};$$
$$D_0 = \lim_{s\to 0} F_{,y}^{-1}F_{,yy}(s); \qquad D_\infty = \lim_{s\to\infty} \frac{F_{,y}^{-1}F_{,yy}(s)}{s}.$$

From

$$C_{\max}(s) = \frac{2\|G_{,x}(s)\|}{\|F_{,y}^{-1}F_{,xx}(s)\| + 4\|F_{,y}^{-1}F_{,yy}(s)\|\|G_{,x}(s)\|^2}$$

we get

$$\lim_{s\to 0} C_{\max}(s) = \frac{2\|B_0\|}{\|C_0\| + 4\|B_0\|^2\|D_0\|}, \quad \lim_{s\to\infty}(s^2 C_{\max}(s)) = \frac{1}{2\|B_\infty\|\|D_\infty\|}.$$

Thus the graph of $\eta = \ln\frac{C_{\max}}{s}$ over $\xi = \ln s$ has the asymptotes

$$\eta = -\xi + \ln(2\|B_0\|) - \ln(\|C_0\| + 4\|B_0\|^2\|D_0\|)$$

as $\xi \to -\infty$ and

$$\eta = -3\xi - \ln(2\|B_\infty\|\|D_\infty\|)$$

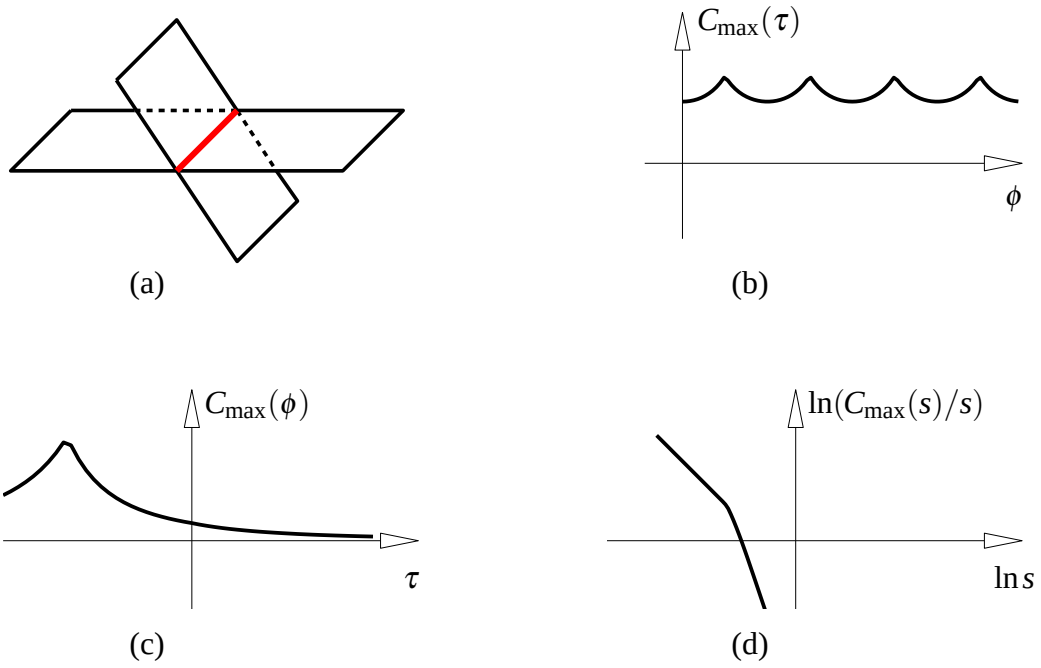

Figure 2.9: (a) Intersection of two planes. (b)–(d) analogous to Figure 2.2, but for the constraint problem of Section § 2.5.7.

as $\xi \to \infty$. They intersect at $\xi = \ln s_0$, where

$$s_0^2 = \frac{\|C_0\| + 4\|B_0\|^2\|D_0\|}{4\|B_0\|\|B_\infty\|\|D_\infty\|}.$$

Experimental data for the particular solution

$$U = \frac{\sqrt{3}}{3}(100,-1,-1,-1), \quad V = \frac{\sqrt{3}}{3}(100,-1,-1,1),$$

$$L = \frac{\sqrt{2}}{2}(-1,1,0,0,0,100), \quad \text{and} \quad \lambda = \frac{2}{3}\sqrt{2}$$

are shown in Table 2.10 and Figure 2.9.

§ 2.5.8 Frameworks

A *framework* is a constraint system where all variables are points and the only constraints either are distances $\|p_i - p_j\|^2 = d_{ij}^2$ involving a fixed and a moving variable, or distances of the form $\|q_i - q_j\|^2 = d_{ij}^2$, involving moving variables. The interested reader is referred e.g. to [3, 4], where the the matrix F_y (the *rigidity matrix*) is the topic of investigations concerning the generic rigidity and flexibility of frameworks.

$\|\cdot\|_U$	$\|\cdot\|_V$	$\|F_{,y}^{-1}F_{,xx}\|$	$\|F_{,y}^{-1}F_{,xy}\|$	$\|F_{,y}^{-1}F_{,yy}\|$	$\|G_{,x}\|$	$\frac{C_{\max}}{s}$	$\frac{C^*_{max}}{s}$
∞	∞	0.09	0.09	0.03	5.00	2.04	20.45
∞	1	0.15	0.05	0.03	7.00	1.88	26.38
∞	2	0.10	0.06	0.02	5.20	3.28	34.13
1	∞	0.01	0.01	0.03	1.00	11.76	23.53
1	1	0.02	0.02	0.03	2.00	6.06	24.24
1	2	0.01	0.01	0.02	1.41	12.15	34.38
2	∞	0.01	0.03	0.03	2.25	5.04	22.62
2	1	0.03	0.03	0.03	3.32	3.79	25.17
2	2	0.02	0.03	0.02	2.33	6.92	32.29

Table 2.11: Experimental values for various norms and the values $C_{\max}$ and C^*_{max} according to the constraint problem of Section § 2.5.8, where $s = 1$.

$\|\cdot\|_U$	$\|\cdot\|_V$	$\|F_{,y}^{-1}F_{,xx}\|$	$\|F_{,y}^{-1}F_{,xy}\|$	$\|F_{,y}^{-1}F_{,yy}\|$	$\|G_{,x}\|$	$\frac{C_{\max}}{s}$	$\frac{C^*_{max}}{s}$
∞	∞	0.00	0.00	4.43	2.98	7.42	44.29
∞	1	0.00	0.00	1.85	8.04	6.58	105.72
∞	2	0.00	0.00	2.85	4.53	7.58	68.75
1	∞	0.00	0.00	4.43	1.39	15.97	44.29
1	1	0.00	0.00	1.85	1.56	33.82	105.72
1	2	0.00	0.00	2.85	1.39	24.70	68.75
2	∞	0.00	0.00	4.43	1.97	11.27	44.29
2	1	0.00	0.00	1.85	3.64	14.53	105.72
2	2	0.00	0.00	2.85	1.97	17.44	68.75

Table 2.12: Experimental values for various norms and the values $C_{\max}$ and C^*_{max} according to the constraint problem of Section § 2.5.9, where $s = 0.0051$.

With these distance constraints, we have

$$F_{,y}(s)=sF_{,y}(1),\ F_{,x}(s)=sF_{,x}(1),\ F_{,yy}(s)=F_{,yy}(1),\ F_{,xx}(s)=F_{,xx}(1),\ F_{,xy}(s)=F_{,xy}(1).$$

It is now obvious that $G_{,x}(s) = G_{,x}(1)$ and that $\frac{C_{\max}(s)}{s}$ does not depend on the scaling factor s.

We consider the simple problem that a point q_1 is given by its three distances $d_i^2 = \|q_1 - p_i\|^2$ from points p_1, p_2, p_3. The particular solution

$$p_1 = (100,0,0), \quad p_2 = (0,100,0), \quad p_3 = (0,0,100)$$

for $d_1 = d_2 = 100$ and $d_3 = 100\sqrt{3}$ is illustrated in Figure 2.10 and Table 2.11.

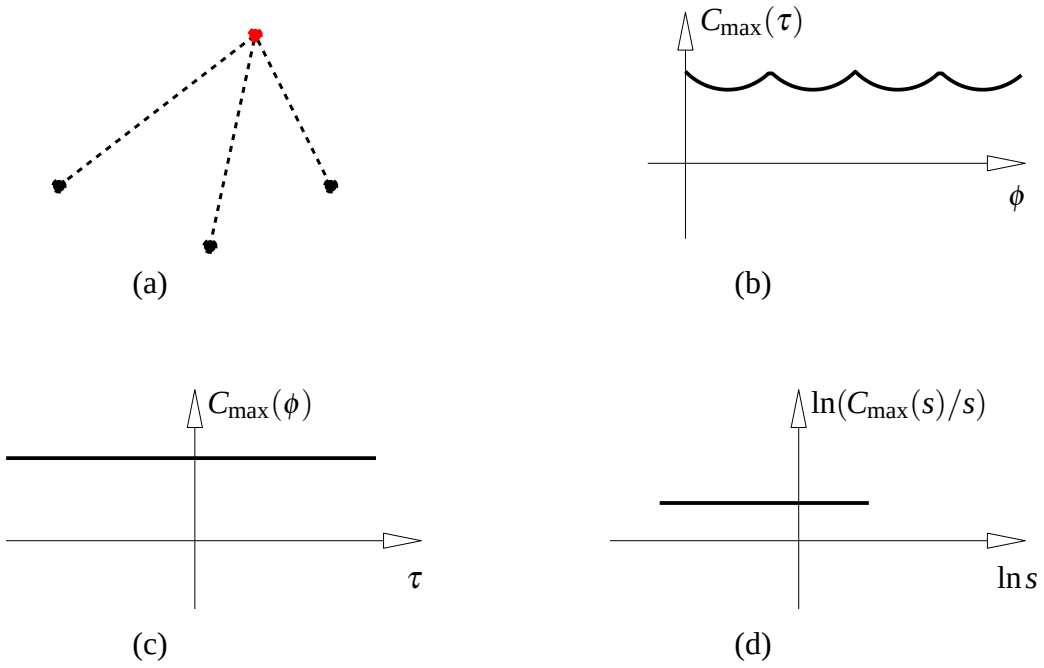

Figure 2.10: (a) A point has fixed distances from three fixed points. (b)–(d) analogous to Figure 2.2, but for the constraint problem of Section § 2.5.8.

§ 2.5.9 Two points determine a unit vector

This is a constraint problem not contained in the tables above. We have the fixed variables $p_1 = (x_1, x_2, x_3)$, $p_2 = (x_4, x_5, x_6)$ and the moving variables $q_1 = (y_1, y_2, y_3) \in \mathbb{R}^3$, $y_4 \in \mathbb{R}$ with the constraints $\|q_1\|^2 = 1$, $p_1 - p_2 = y_4 q_1$ (y_4 is the distance of p_1 from p_2).

The particular solution

$$p_1 = (40, 30, 70), \quad p_2 = (30, 40, -70), \quad q_1 = \frac{p_2 - p_1}{y_4}, \quad y_4 = \|p_2 - p_1\|$$

is illustrated in Table 2.12 and Figure 2.11.

We have $F_{,xx} = 0$ and $F_{,xy} = 0$, so we get

$$C_{\max}(s) = \frac{1}{2\|G_{,x}(s)\|\|F_{,y}^{-1} F_{,yy}(s)\|}.$$

An elementary computation shows that

$$G_{,x}(s) = \frac{1}{s y_4} \begin{bmatrix} \widetilde{G}(s) \\ \widetilde{g}(s) \end{bmatrix}$$

where

$$\widetilde{g}(s) = y_4 \begin{bmatrix} s y_1 & s y_2 & s y_3 & -s y_1 & -s y_2 & -s y_3 \end{bmatrix}$$

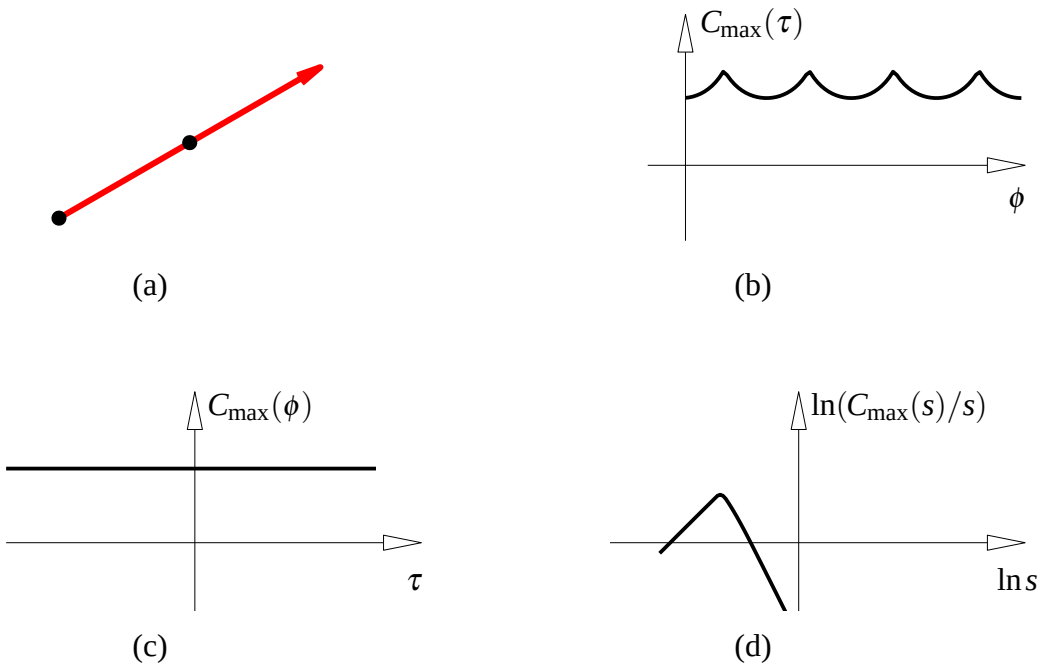

Figure 2.11: (a) An unit vector spanned by two points. (b)–(d) analogous to Figure 2.2, but for the constraint problem of Section § 2.5.9.

and

$$\widetilde{G}(s) = \begin{bmatrix} 1-y_1^2 & -y_1y_2 & -y_1y_3 & y_1^2-1 & y_1y_2 & y_1y_3 \\ -y_1y_2 & 1-y_2^2 & -y_2y_3 & y_1y_2 & y_2^2-1 & y_2y_3 \\ -y_1y_3 & -y_2y_3 & 1-y_3^2 & y_1y_3 & y_2y_3 & y_3^2-1 \end{bmatrix}.$$

We define

$$\widetilde{M}(v_1,v_2,v_3,v_4) = \begin{bmatrix} v_1 & & & v_2 \\ & v_1 & & v_3 \\ & & v_1 & v_4 \\ v_2 & v_3 & v_4 & \end{bmatrix}$$

and get $F_{,y}^{-1}F_{yy}(s) = \frac{1}{sy_4}B_s$, where $B_s \in B(\mathbb{R}^4,\mathbb{R}^4,\mathbb{R}^4)$ has the following coordinates:

$$[B_s]_1 = \widetilde{M}(sy_4y_1, 1-y_1^2, -y_2y_1, -y_1y_3), \quad [B_s]_2 = \widetilde{M}(sy_4y_2, -y_2y_1, 1-y_2^2, -y_3y_2),$$
$$[B_s]_3 = \widetilde{M}(sy_4y_3, -y_1y_3, -y_3y_2, 1-y_3^2), \quad [B_s]_4 = \widetilde{M}(-s^2y_4^2y_3, sy_4y_1, sy_4y_2, sy_4y_3).$$

Limits for $s \to 0$ and $s \to \infty$ are the following:

$$L_0 := \lim_{s\to 0} sG_{,x}(s) = \frac{1}{y_4}\begin{bmatrix} \widetilde{G}(s) \\ \hline 0_{1\times 6} \end{bmatrix},$$
$$L_\infty := \lim_{s\to\infty} G_{,x}(s) = \left[\begin{array}{cccccc} & & O_{3\times 6} & & & \\ \hline y_1 & y_2 & y_3 & -y_1 & -y_2 & -y_3 \end{array}\right].$$

Further,

$$\lim_{s\to 0} sF_{,y}^{-1}F_{yy}(s) = \frac{1}{y_4}\overline{B}_0,$$

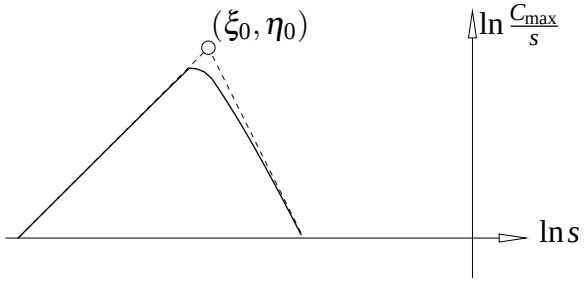

Figure 2.12: Detail of Figure 2.11.d (asymptotes).

where $\overline{B}_0$ has the following coordinates:

$$[\overline{B}_0]_1 = \widetilde{M}(0, 1-y_1^2, -y_2y_1, -y_1y_3), \quad [\overline{B}_0]_2 = \widetilde{M}(0, -y_2y_1, 1-y_2^2, -y_3y_2),$$
$$[\overline{B}_0]_3 = \widetilde{M}(0, -y_1y_3, -y_3y_2, 1-y_3^2), \quad [\overline{B}_0]_4 = 0_{4\times 4}.$$

The limit $\lim_{s\to\infty} \frac{1}{s} F_y^{-1} F_{yy}(s)$ is denoted by $\overline{B}_\infty$ and expands to

$$[\overline{B}_\infty]_r = 0_{4\times 4} \text{ for } r = 1,2,3; \quad [\overline{B}_\infty]_4 = \operatorname{diag}(-y_4, -y_4, -y_4, 0).$$

Thus

$$\lim_{s\to 0}\Big(\frac{1}{s^2} C_{\max}(s)\Big) = \frac{1}{2\|L_0\|\|\overline{B}_0\|}, \quad \lim_{s\to\infty}\big(sC_{\max}(s)\big) = \frac{1}{2\|L_\infty\|\|\overline{B}_\infty\|}. \tag{2.41}$$

The graph of $\eta = \ln \frac{C_{\max}(s)}{s}$ over $\xi = \ln s$ has the asymptotes

$$\eta = \xi - \ln(2\|L_0\|\|\overline{B}_0\|) \qquad (\xi \to -\infty),$$
$$\eta = -2\xi - \ln(2\|L_\infty\|\|\overline{B}_\infty\|) \qquad (\xi \to \infty).$$

They intersect in the point

$$(\xi_0, \eta_0) = \frac{1}{3}\Big(\ln \frac{\|L_0\|\|\overline{B}_0\|}{\|L_\infty\|\|\overline{B}_\infty\|}, -\ln(8\|L_0\|^2\|\overline{B}_0\|^2\|L_\infty\|\|\overline{B}_\infty\|)\Big). \tag{2.42}$$

We have $\xi_0 = \ln s_0$, where

$$s_0^3 = \frac{\|L_0\|\,\|\overline{B}_0\|}{\|L_\infty\|\,\|\overline{B}_\infty\|}.$$

This is illustrated in Figure 2.12.

2.6 Scalar coordinates

There are all kinds of coordinates such as Cartesian coordinates, homogeneous coordinates, Plücker coordinates and the normalized form of them. All they have their

entity	S-coordinate	normalized homogeneous coordinate	transformation
2D-line	(u_0,u_1,u_2) with $u_0^2=u_1^2+u_2^2$	(v_0,v_1,v_2) with $v_1^2+v_2^2=1$	$u_0=v_0$ $u_i=v_0v_i$ $(i=1,2)$
3D-plane	(u_0,u_1,u_2,u_3) with $u_0^2=u_1^2+u_2^2+u_3^2$	(v_0,v_1,v_2,v_3) with $v_1^2+v_2^2+v_3^2=1$	$u_0=v_0$ $u_i=v_0v_i$ $(i=1,2,3)$

Table 2.13: S-coordinates and normalized homogeneous coordinates of 2D-lines and 3D-planes

S-coordinate	normalized Plücker coordinate
$(g,\bar{g})$ with $\|g\| = \|\bar{g}\|, \quad \langle g,\bar{g}\rangle = 0$	$(m,\bar{m})$ with $\|m\| = 1, \quad \langle m,\bar{m}\rangle = 0$
transformation: $g = \|\bar{m}\|\, m, \qquad \bar{g} = \bar{m}$	

Table 2.14: S-coordinate and normalized Plücker coordinate of 3D-line

advantages and disadvantages in dealing with different situations. For instance, homogeneous coordinates enable uniform computations involving both infinite and finite objects. However, they do not behave nicely with respect to the unit length, and also have many problems in dealing with the distance between geometric entities. Here we construct another kind of coordinates for lines and planes in Euclidean space such that all components of the coordinate are proportional to the distance of the entity from the origin. We call them scalar coordinates or simply S-coordinates, as the magnitude of their components are invariant or proportional with respect to scaling or the choice of unit length.

§ 2.6.1 S-coordinates of lines and planes

Ordinary Cartesian coordinates for a point are already proportional to the distance of the point from the origin, so we keep using them for points.

For a line in $\mathbb{R}^2$ or a plane in $\mathbb{R}^3$, we use its distance from the origin as the first component of the S-coordinate, and the coordinates of the pedal point of the origin on it multiplied by -1 as the others. (See Table 2.13).

For a line in $\mathbb{R}^3$, we construct the S-coordinate from its the normalized Plücker coordinate, as shown in Table 2.14. If $(g,\bar{g})$ is the S-coordinate of a line in $\mathbb{R}^3$, $\bar{g}$ is the moment vector of a unit force in the line with respect to the origin, and g is a direction vector of the line such that $\|g\| = \|\bar{g}\|$. $\|\bar{g}\|$ equals the distance of the origin from the line.

geometric relation	number and nature of constraints involving more than one geometric entity		number and nature of constraints involving only one geometric entity	
$\mathrm{dist}(p,q)=d$	1	$\|p-q\|^2=d$	0	
$p \in L$	3	$p \times l = \|\bar{l}\|\bar{l}$	1	$\|l\|^2=\|\underline{l}\|^2, \cancel{\langle l,\bar{l}\rangle=0}$
$p \in L$	2	two of $p \times \underline{l} = \|\bar{l}\|\bar{l}$	2	$\|l\|^2=\|\underline{l}\|^2, \langle l,\underline{l}\rangle=0$
$q=\mathrm{pedal}_L(p)$	4	$q \times l = \|\bar{l}\|\bar{l}, \langle p-q,l\rangle=0$	1	$\|l\|^2=\|l\|^2, \cancel{\langle l,l\rangle=0}$
$\overrightarrow{\mathrm{dist}}(p,U)=d$	1	$u_0^2+\langle u,p\rangle=u_0 d$	1	$\|u\|^2=u_0^2$
$p \in U$	1	$u_0^2+\langle u,p\rangle=0$	1	$\|u\|^2=u_0^2$
$\sphericalangle(G,H)=\theta$	1	$\langle g,h\rangle=\|\bar{g}\|\|\bar{h}\|\cos\theta$	4	$\|g\|^2=\|\bar{g}\|^2, \|\underline{h}\|^2=\|\bar{h}\|^2, \langle g,\bar{g}\rangle=0, \langle h,h\rangle=0$
$G \parallel H$	3	$\|\bar{h}\|g=\pm\|\bar{g}\|h,$	3	$\|g\|^2=\|\bar{g}\|^2, \cancel{\|\underline{h}\|^2=\|\bar{h}\|^2}, \langle g,\bar{g}\rangle=0, \langle h,h\rangle=0$
$G \cap H \neq \{\}$	1	$\|\bar{h}\|\langle g,\bar{h}\rangle+\|\bar{g}\|\langle\bar{g},h\rangle=0$	4	$\|g\|^2=\|\bar{g}\|^2, \|\underline{h}\|^2=\|\bar{h}\|^2, \langle g,\bar{g}\rangle=0, \langle h,h\rangle=0$
$L \subset U$	3	$\|\bar{l}\|u \times \bar{l}=u_0^2 l$	2	$\|u\|^2=u_0^2, \|l\|^2=\|\bar{l}\|^2, \cancel{\langle l,l\rangle=0}$
$L \perp U$	3	$\|\bar{l}\|u=\pm u_0 l$	2	$\|u\|^2=u_0^2, \cancel{\|l\|^2=\|\bar{l}\|^2}, \langle l,l\rangle=0$
$U \parallel V$	3	$v_0 u=\pm u_0 v$	1	$\|u\|^2=u_0^2, \cancel{\|v\|^2=v_0^2}$

Table 2.15: Relations between points p,q, lines $L=(l,\bar{l})$, $G=(g,\bar{g})$, $H=(h,\bar{h})$, and planes $U=(u_0,u)$, $V=(v_0,v)$ with S-coordinates. (cf. Section § 2.6.2).

§ 2.6.2 Expressing geometric relations by S-coordinates

To express geometric relations by S-coordinates, we only need to replace the unit normal vectors such as u, v, l, g, and h in the geometric relations with the ordinary coordinates by $\frac{u}{u_0}$, $\frac{v}{v_0}$, $\frac{l}{\|l\|}$, $\frac{g}{\|g\|}$, and $\frac{h}{\|h\|}$ respectively. Analogous to Section § 2.4.2, we summarize the geometric relations with S-coordinates in Tables 2.15 and 2.16.

§ 2.6.3 Transformation of the scalar coordinate system

The transformation formulas for scalar coordinates can be derived easily from those of (2.27), (2.28) and (2.29). With the symbols as in Section § 2.4.3, we have

$$p \longrightarrow sp, \qquad (l,\bar{l}) \longrightarrow s(l,\bar{l}), \qquad (u_0,u) \longrightarrow s(u_0,u) \tag{2.43}$$

geometric relation	number and nature of constraints involving more than one geometric entity		number and nature of constraints involving only one geometric entity	
$q=\text{pedal}_L(p)$ $\left[\lambda=\frac{1}{\|l\|}\langle l,p\rangle\right]$	4	$\langle l,p\rangle=\lambda\|\bar{l}\|$, $l\times l+\lambda l=q\|\bar{l}\|$	2	$\|l\|^2=\|\bar{l}\|^2, \langle l,\bar{l}\rangle=0$
$q=\text{pedal}_U(p)$ $\left[\lambda=\overrightarrow{\text{dist}}(p,U)\right]$	4	$u_0^2+\langle q,u\rangle=0$ $u_0(p-q)=\lambda u$,	1	$\|u\|^2=u_0^2$
$G \parallel H$ $\text{dist}(G,H)=d$	4	$\|\bar{h}\|g=\pm\|\bar{g}\|h$, $\|\bar{g}\mp h\|^2=d^2$	3	$\|g\|^2=\|\bar{g}\|^2, \cancel{\|h\|^2=\|\bar{h}\|^2}$ $\langle g,\bar{g}\rangle=0, \langle h,h\rangle=0$
$\text{dist}(G,H)=d$ $\left[\lambda_2=\cos\sphericalangle(G,H)\right]$	3	$\langle g,h\rangle=\lambda_2\|\bar{g}\|\|\bar{h}\|$, $\|h\|\langle g,\bar{h}\rangle+\|\bar{g}\|\langle\bar{g},h\rangle=d\lambda_1\|\bar{g}\|\|\bar{h}\|$, $\lambda_1^2+\lambda_2^2=1$	4	$\|g\|^2=\|\bar{g}\|^2, \|h\|^2=\|\bar{h}\|^2$ $\langle g,\bar{g}\rangle=0, \langle g,\bar{h}\rangle=0$
$L=U\cap V$	6	$\lambda(l,\bar{l})=(u\times v, u_0^2v-v_0^2u)$	3	$\|l\|^2=\|\bar{l}\|^2, \cancel{\langle l,\bar{l}\rangle=0}$, $\|u\|^2=u_0^2, \|v\|^2=v_0^2$

Table 2.16: Relations becoming quadratic with new variables with S-coordinates. (cf. Section § 2.6.2).

$$p\longrightarrow p+t,\qquad (l,\bar{l})\longrightarrow\frac{(\left\|t\times l+\|\bar{l}\|\bar{l}\right\|l,\ \|\bar{l}\|t\times l+\|\bar{l}\|^2\bar{l})}{\|\bar{l}\|^2},$$
$$(u_0,u)\longrightarrow(1-\frac{\langle u,t\rangle}{u_0^2})(u_0,u) \tag{2.44}$$

$$p\longrightarrow Ap,\qquad (l,\bar{l})\longrightarrow(\frac{\|A\bar{l}\|Al}{\|\bar{l}\|},A\bar{l}),\qquad (u_0,u)\longrightarrow(u_0,Au) \tag{2.45}$$

Obviously, $C_{\max}$ of Theorem 1 is expected to be multiplied by s as well in case of choosing a different unit length.

§ 2.6.4 Geometric constraint problems with S-coordinates

Here we consider some of the examples in Section 2.5 again, but we use S-coordinates in order to see how $C_{\max}$ is influenced by scaling.

$\|\cdot\|_U$	$\|\cdot\|_V$	$\|F_y^{-1}F_{,xx}\|$	$\|F_y^{-1}F_{,xy}\|$	$\|F_y^{-1}F_{,yy}\|$	$\|G_{,x}\|$	$\frac{C_{\max}}{s}$	$\frac{C^*_{max}}{s}$
∞	∞	0.00	7.18	26.16	1.41	1.13	3.20
∞	1	0.00	10.12	9.66	5.31	0.81	8.65
∞	2	0.00	6.05	10.64	2.45	1.56	7.63
1	∞	0.00	2.59	26.16	0.52	3.11	3.21
1	1	0.00	3.82	9.66	1.86	2.30	8.53
1	2	0.00	2.19	10.64	0.83	4.55	7.53
2	∞	0.00	3.64	26.16	0.71	2.26	3.19
2	1	0.00	6.48	9.66	3.24	1.32	8.58
2	2	0.00	5.98	10.64	1.22	2.63	6.45

Table 2.17: Experimental values for various norms and the values $C_{\max}$ and C^*_{max} according to the constraint problem of Constructing a 3D-line with S-coordinate form two points, where $s = 0.01$.

Example 1. The line spanned by two points

We consider the example of Section § 2.5.4 again, this time using S-coordinates. A new free variable $y_7 = \|\overline{l}\|$ is introduced. The particular solution here is

$$L = (-3.518, 3.518, -49.25, -34.8, 34.82, 4.975) \quad \text{and} \quad d = 49.497.$$

From Table 2.15 we get the constraint problem $F(x,y) = 0$, where

$$F(x,y) = \begin{bmatrix} y_1^2 + y_2^2 + y_3^2 - y_7^2 \\ y_4^2 + y_5^2 + y_6^2 - y_7^2 \\ y_3x_2 - y_2x_3 - y_4y_7 \\ y_1x_3 - y_3x_1 - y_5y_7 \\ y_2x_1 - y_1x_2 - y_6y_7 \\ y_3x_5 - y_2x_6 - y_4y_7 \\ y_1x_6 - y_3x_4 - y_5y_7 \end{bmatrix}. \tag{2.46}$$

We select the unit length $s = 1$. Table 2.17 shows $\frac{C_{\max}}{s}$ and $\frac{C^*_{max}}{s}$, computed with different norms.

Here, $F_{,xx} = 0$, $F_{,xy}$ and $F_{,yy}$ are constant with respect to s,

$$F_{,x}(s) = sF_{,x}(1), F_y^{-1}(s) = \frac{1}{s}F_y^{-1}(1), G_{,x}(s) = F_y^{-1}(s)F_{,x}(s) = F_y^{-1}(1)F_{,x}(1) = G_{,x}(1).$$

It follows that

$$C_{\max}(s) = \frac{1}{\|F_y^{-1}(s)F_{,xy}\| + 2\|F_y^{-1}(s)F_{,yy}\|\|G_{,x}(s)\|}$$

$$= \frac{s}{\|F_y^{-1}(1)F_{,xy}\| + 2\|F_y^{-1}(1)F_{,yy}\|\|G_{,x}(1)\|},$$

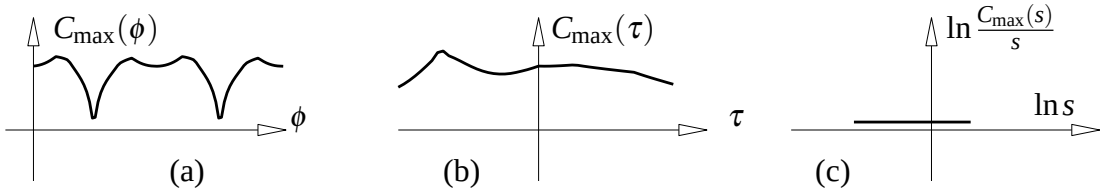

Figure 2.13: The change of $C_{\max}$ over coordinate transformations in the constraint problem of Example § 2.6.4 in Section § 2.6.4. (a) Diagram of the change of $C_{\max}$ over the rotation angle ϕ while rotating the coordinate system. (b) the same for translating the coordinate system. (c) Logarithmic diagram of $\frac{C_{\max}}{s}$ over a scaling factor s.

$\|\cdot\|_U$	$\|\cdot\|_V$	$\|F_{,y}^{-1}F_{,xx}\|$	$\|F_{,y}^{-1}F_{,xy}\|$	$\|F_{,y}^{-1}F_{,yy}\|$	$\|G_{,x}\|$	$\frac{C_{\max}}{s}$	$\frac{C^*_{max}}{s}$
∞	∞	0.00	5.20	6.93	1.73	2.91	10.07
∞	1	0.00	4.73	7.73	4.73	1.21	11.45
∞	2	0.00	4.24	4.00	2.45	3.56	17.45
1	∞	0.00	0.67	6.93	0.22	22.66	10.07
1	1	0.00	2.24	7.73	0.75	6.23	9.32
1	2	0.00	1.15	4.00	0.38	18.56	14.29
2	∞	0.00	1.73	6.93	0.58	8.72	10.07
2	1	0.00	2.83	7.73	1.63	3.24	10.57
2	2	0.00	2.00	4.00	0.81	9.49	15.51

Table 2.18: Experimental values for various norms and the values $C_{\max}$ and C^*_{max} according to the constraint problem of Constructing a 3D-plane with S-coordinate form three points, where $s = 0.01$.

and $\frac{C_{\max}(s)}{s}$ does not depend on s. See Figure 2.13.

Example 2. The plane spanned by three points

We continue to consider the example in Section § 2.5.5. In terms of S-coordinates, the particular solution of the plane is changed to

$$U = (-57.7, 33.3394, 33.3394, 33.3394).$$

According to Table 2.15, the constraints read

$$F(x,y) = \begin{bmatrix} y_2^2 + y_3^2 + y_4^2 - y_1^2 \\ y_1^2 + x_1 y_2 + x_2 y_3 + x_3 y_4 \\ y_1^2 + x_4 y_2 + x_5 y_3 + x_6 y_4 \\ y_1^2 + x_7 y_2 + x_8 y_3 + x_9 y_4 \end{bmatrix} = 0. \tag{2.47}$$

We select the unit length $s = 1$. Table 2.18 shows $\frac{C_{\max}}{s}$ and $\frac{C^*_{max}}{s}$, computed using different norms.

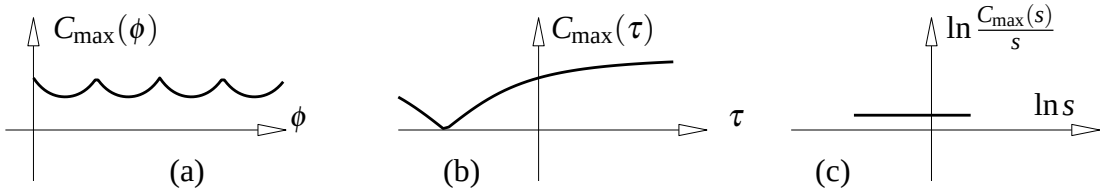

Figure 2.14: (a)–(c) analogous to Figure 2.13, but for the constraint problem of Example § 2.6.4 in Section § 2.6.4.

$\|\cdot\|_U$	$\|\cdot\|_V$	$\|F_{,y}^{-1}F_{,xx}\|$	$\|F_{,y}^{-1}F_{,xy}\|$	$\|F_{,y}^{-1}F_{,yy}\|$	$\|G_{,x}\|$	$\frac{C_{\max}}{s}$	$\frac{C^*_{max}}{s}$
∞	∞	14.57	21.18	2.86	13.25	0.84	22.33
∞	1	29.20	11.12	7.73	21.54	0.28	12.10
∞	2	16.97	11.70	5.71	14.23	0.54	15.25
1	∞	6.00	4.06	2.86	3.46	3.47	24.07
1	1	7.73	4.35	7.73	4.70	1.22	11.43
1	2	6.03	3.53	5.71	3.48	2.10	14.59
2	∞	6.00	7.75	2.86	5.08	2.22	22.52
2	1	24.00	7.57	7.73	8.39	0.68	11.47
2	2	12.00	8.31	5.71	5.38	1.26	13.59

Table 2.19: Experimental values for various norms and the values $C_{\max}$ and C^*_{max} according to the constraint problem of Constructing the intersection of a 3D-line and a 3D-plane with S-coordinate, where $s = 0.01$.

Here, $F_{,xx} = 0$, $F_{,xy}$ and $F_{,yy}$ do not depend on s, $F_x(s) = sF_x(1)$, $F_{,y}^{-1}(s) = \frac{1}{s}F_{,y}^{-1}(1)$, $G_{,x}(s) = F_{,y}^{-1}(s)F_x(s) = F_{,y}^{-1}(1)F_x(1) = G_{,x}(1)$. So

$$\begin{aligned} C_{\max}(s) &= \frac{1}{\|F_{,y}^{-1}(s)F_{,xy}\| + 2\|F_{,y}^{-1}(s)F_{,yy}\|\|G_{,x}(s)\|} \\ &= \frac{s}{\|F_{,y}^{-1}(1)F_{,xy}\| + 2\|F_{,y}^{-1}(1)F_{,yy}\|\|G_{,x}(1)\|}. \end{aligned}$$

We see that $\frac{C_{\max}(s)}{s}$ is constant. See Figure 2.14.

Example 3. The intersection of a line and a plane

We continue the example in Section § 2.5.6. When using S-coordinates, the particular solution is given by

$$L = (l, \overline{l}) = (-3.518, 3.518, -49.25, -34.8, 34.82, 4.975)$$

and

$$U = (u_0, u) = (-57.7, 33.3394, 33.3394, 33.3394).$$

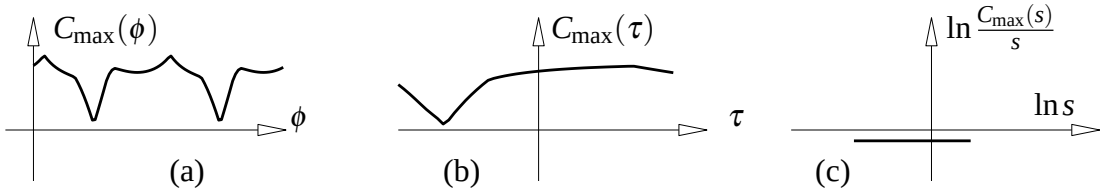

Figure 2.15: (a)–(c) analogous to Figure 2.13, but for the constraint problem of Example § 2.6.4 in Section § 2.6.4.

A new free variable $y_4 = \|\bar{l}\|$ is introduced. For the particular solution $y_4 = 49.497$. From Table 2.15, we have

$$F(x,y) = \begin{bmatrix} x_7^2 + x_8 y_1 + x_9 y_2 + x_{10} y_3 \\ x_4^2 + x_5^2 + x_6^2 - y_4^2 \\ x_3 y_2 - x_2 y_3 - x_4 y_4 \\ x_1 y_3 - x_3 y_1 - x_5 y_4 \end{bmatrix}. \tag{2.48}$$

We select the unit length $s = 1$. Table 2.19 shows that $\frac{C_{\max}}{s}$ and $\frac{C^*_{max}}{s}$ with respect to different norms.

$F_{,xx}$, $F_{,xy}$ and $F_{,yy}$ are independent of s, and $F_x(s) = sF_x(1)$, $F_{,y}^{-1}(s) = \frac{1}{s}F_{,y}^{-1}(1)$, $G_{,x}(s) = F_{,y}^{-1}(s)F_x(s) = F_{,y}^{-1}(1)F_x(1) = G_{,x}(1)$. Thus,

$$\begin{aligned} C_{\max}(s) &= \frac{2\|G_{,x}(1)\|}{\|\frac{1}{s}F_{,y}^{-1}(1)F_{,xx}\| + 2\|\frac{1}{s}F_{,y}^{-1}(1)F_{,xy}\|\|G_{,x}(1)\| + 4\|\frac{1}{s}F_{,y}^{-1}(1)F_{,yy}\|\|G_{,x}(1)\|^2} \\ &= sC_{\max}(1), \end{aligned}$$

We see that $\frac{C_{\max}(s)}{s}$ does not depend on s. This is illustrated by Figure 2.15.

Bibliography

[1] K. Abdel-Malek, Blackmore D., and K. Joy. Swept volumes: Foundations, perspectives, and applications. *Internat. J. Shape Modeling*. to appear. URL *http://www.engineering.uiowa.edu/∼amalek*.

[2] P. K. Agarwal, E. Flato, and D. Halperin. Polygon decomposition for efficient construction of Minkowski sums. *Comput. Geom. Theory Appl.*, 21:39–61, 2002.

[3] L. Asimov and B. Roth. The rigidity of graphs. *Trans. Amer. Math. Soc.*, 245:171–190, 1978.

[4] L. Asimov and B. Roth. The rigidity of graphs II. *J. Math. Anal. Appl.*, 68:171–190, 1979.

[5] D. Blackmore and M.C. Leu. Analysis of swept volumes via lie groups and differential equations. *Int. J. Robotics Res.*, 11:516–537, 1992.

[6] O. Bottema and B. Roth. *Theoretical Kinematics*. North–Holland, 1979.

[7] W. Bouma, I. Fudos, C. Hoffmann, J. Cai, and R. Paige. Geometric constraint solver. *Computer-Aided Design*, 27:487–501, 1995.

[8] B. Bruederlin. Using geometric rewriting rules for solving geometric problems symbolically. *Theoret. Comput. Sci.*, 116:291–303, 1993.

[9] E. Ezra, D. Halperin, and M. Sharir. Speeding up the incremental construction of the union of geometric objects in practice. In R. Möhring and R. Raman, editors, *Algorithms — ESA 2002*, pages 473–484. Springer, 2002.

[10] R. T. Farouki, H. P. Moon, and B. Ravani. Algorithms for Minkowski products and implicitly-defined complex sets. *Adv. Comp. Math.*, 13:199–229, 2000.

[11] R. T. Farouki, H. P. Moon, and B. Ravani. Minkowski geometric algebra of complex sets. *Geom. Dedicata*, 85:283–315, 2001.

[12] R. T. Farouki and H. Pottmann. Exact Minkowski products of *N* complex disks. *Reliable Computing*, 8:43–66, 2002.

[13] E. Flato and D. Halperin. Robust and efficient construction of planar Minkowski sums. In *Abstracts 16th Europ. Workshop Comput. Geom.*, pages 85–88, 2000. URL *http://www.cs.bgu.ac.il/∼cg2000/PS/16.ps*.

[14] I. Fudos and C. Hoffmann. A graph-constructive approach to solving systems of geometric constraints. *ACM Transactions on Graphics*, 16:179–216, 1997.

[15] Varadhan G. and Manocha D. Accurate Minkowski sum approximation of polyhedral models. In *Pacific Conference on Computer Graphics and Applications*, pages 392–401. IEEE Computer Society, 2004.

[16] X. S. Gao and S. C. Chou. Solving geometric constraint systems. I. A global propagation approach. *Computer-Aided Design*, 30:47–54, 1998.

[17] X. S. Gao and S. C. Chou. Solving geometric constraint systems. II. A symbolic approach and decision of rc-constructibility. *Computer-Aided Design*, 30:115–122, 1998.

[18] P. Ghosh. A unified computational framework for Minkowski operations. *Computers & Graphics*, 17:357–378, 1993.

[19] N. Higham. *Accuracy and Stability of Numerical Algorithms*, chapter Matrix Norms. Soc. Industrial and Appl. Math, 1996.

[20] S. Hirsch and D. Halperin. Hybrid motion planning: Coordinating two discs moving along polygonal obstacles in the plane. In J.-D Boissonnat et al., editors, *Algorithmic Foundations of Robotics V*, pages 225–241. Springer Verlag, 2003.

[21] C. Hoffmann. Robustness in geometric computations. *J. Comput. Information Sc. Engrg.*, 1:143–156, 2001.

[22] C. Hoffmann and P. J. Vermeer. Geometric constraint solving in R^2 and R^3. In D. Z. Du and F. Huang, editors, *Computing in Euclidean Geometry*, pages 266–298. World Scientific, 1995.

[23] Y..J. Kim, Varadhan G., M.C. Lin, and D. Manocha. Fast swept volume approximation of complex polyhedral models. *Computer-Aided Design*, 36:1013–1027, 2004.

[24] K. Kondo. Algebraic method for manipulation of dimensional relationships in geometric models. *Computer-Aided Design*, 24:141–147, 1992.

[25] H. Lamure and D. Michelucci. Solving geometric constraints by homotopy. *IEEE Trans. Vis. Comp. Graph.*, 2:28–34, 1996.

[26] J. Y. Lee and K. Kim. A 2-D geometric constraint solver using DOF-based graph reduction. *Computer-Aided Design*, 30:883–896, 1998.

[27] K.-Y. Lee, O-H. Kwon, J.-Y. Lee, and T.W. Kim. A hybrid approach to geometric constraint solving with graph analysis and reduction. *Adv. Eng. Software*, 34:103–113, 2003.

[28] Y.-T. Li, S.-M. Hu, and J.-G. Sun. A constructive approach to solving 3-D geometric constraint systems using dependence analysis. *Computer-Aided Design*, 34:97–108, 2002.

[29] R. Light and D. Gossard. Modification of geometric models through variational geometry. *Computer-Aided Design*, 14:209–214, 1982.

[30] J. Milnor. *Topology from the Differentiable Viewpoint*. The University Press of Virginia, 1965.

[31] H. Pottmann, B. Odehnal, M. Peternell, J. Wallner, and R.A. Haddou. On optimal tolerancing in Computer-Aided Design. In R. Martin and W. Wang, editors, *Geometric Modeling and Processing 2000*, pages 347–363. IEEE Computer Society, 2000.

[32] H. Pottmann and J. Wallner. *Computational Line Geometry*. Springer, 2001.

[33] A. Requicha. Towards a theory of geometric tolerancing. *Int. J. Robotics Res.*, 2:45–60, 1983.

[34] H.-P. Schröcker and J. Wallner. Curvatures and tolerances in the Euclidean motion group. *Results Math.*, 47:132–146, 2005.

[35] H. Shaul and D. Halperin. Improved construction of vertical decompositions of three-dimensional arrangements. In *Proc. 18th annual Symposium on Computational geometry*, pages 283–292. ACM Press, 2002.

[36] A. Verroust, F. Schonek, and D. Roller. Rule-oriented method for parameterized computer-aided design. *Computer-Aided Design*, 24:531–540, 1992.

[37] J. Wallner, R. Krasauskas, and H. Pottmann. Error propagation in geometric constructions. *Computer-Aided Design*, 32:631–641, 2000.

[38] J. Wallner, H.-P. Schröcker, and S.-M. Hu. Tolerances in geometric constraint problems. *Reliable Computing*, 11:235–251, 2005.

[39] J. Wallner and Q.-M. Yang. Asymptotic analysis of implicit tolerance problems. Technical Report 138, Institute of Discrete Mathematics and Geometry, Vienna University of technology, 2005. URL *http://www.geometrie.tuwien.ac.at/wallner/impl2.pdf*.

[40] J. Wallner and Q.-M. Yang. Swept volumes of many poses. In *SGP 2005: Third Eurographics Symposium on Geometry processing*, pages 161–170. Eurographics Association, 2005.